MULTI-TARGET TRACKING ALGORITHMS FOR CLUTTERED ENVIRONMENTS

A Dissertation

Submitted to the Faculty

of

Purdue University

by

Dohyeung Kim

In Partial Fulfillment of the

Requirements for the Degree

of

Doctor of Philosophy

December 2019

Purdue University

West Lafayette, Indiana

THE PURDUE UNIVERSITY GRADUATE SCHOOL
STATEMENT OF DISSERTATION APPROVAL

Dr. Inseok Hwang, Chair

School of Aeronautics and Astronautics

Dr. Dengfeng Sun

School of Aeronautics and Astronautics

Dr. Jianghai Hu

School of Electrical and Computer Engineering

Dr. Shaoshuai Mou

School of Aeronautics and Astronautics

Approved by:

Dr. Weinong Chen

Head of the School Graduate Program

To my wife Youngkyoung Kim and my son Seungwon Kim.

ACKNOWLEDGMENTS

I am deeply grateful to many people who were formative in the development of my research as this thesis would not have been possible without their help. First and foremost, I would like to express my sincere gratitude to my adviser, Professor Inseok Hwang, for skillfully guiding and supporting my PhD study and related research. He has provided structure, organization, and inspiration, to help overcome many difficulties and challenges in my research. I am also grateful to my other thesis committee members, Professor Dengfeng Sun, Professor Jianghai Hu, and Professor Shaoshuai Mou for their time and advice on my thesis and research work.

My sincere gratitude goes to my former advisers in Hanyang University, Professor Taek-Lyul Song and Professor Darko Musicki, for their valuable suggestions and guidance. They were instrumental in preparing for my studies in the United States of America.

Additionally, I greatly appreciate the support from my former and current lab mates, Cheolhyeon Kwon, Kwangyeon Kim, Shubhankar Gupta, Jayaprakash Suraj Nandiganahalli, Chiyu Zhang, Dawei Sun, and Jooyoung Lee. I want to express my special gratitude to my mentors during my first year at Purdue, Cheolhyeon Kwon and Kwangyeon Kim. They spent countless hours helping me form an effective and rigid style in studying, doing research and writing.

Last but not least, I want to thank my wife Youngkyoug, my son Seungwon, my parents, and my wife's parents for their sincere support, love, and encouragement. This dissertation is devoted to all of you!

TABLE OF CONTENTS

Page

LIST OF TABLES

LIST OF FIGURES

Figure Page

ABBREVIATIONS

CT	coordinated turn
CV	constant velocity
EKF	extended Kalman filter
FAT	feature-aided tracking
FISST	finite set statistics
GM-CPHD	Gaussian mixture cardinalized probability hypothesis density
GM-PHD	Gaussian mixture probability hypothesis density
IMMF	interacting multiple model filter
IPHD	improved probability hypothesis density
ISR	intelligence, surveillance and reconnaissance
JIPDAF	joint integrated probabilistic data association filter
JMS	jump Markov system
JPDAF	joint probabilistic data association filter
JPDAF-AI	joint probabilistic data association filter - amplitude information
JPDAF-TKSDFI	joint probabilistic data association filter with target kinematic-state-dependent feature information
KF	Kalman filter
MHT	multiple hypothesis tracking
MTT	multi-target tracking
NDS	normalized distance squared
NNF	nearest neighbor filter
OSPA	optimal sub-pattern assignment
PDAF	probabilistic data association filter
PDAF-AI	probabilistic data association filter - amplitude information

pdf	probability density function
PHD	probability hypothesis density
PNNF	probabilistic nearest neighbor filter
PSNF	probabilistic strongest neighbor filter
RCS	radar cross section
RFS	random finite set
RGM-PHD	refined Gaussian mixture probability hypothesis density
SD-JMS	state-dependent jump Markov system
SNF	strongest neighbor filter
SNR	signal-to-noise ratio
TDA	target dimensions with aspect-angle
TDD	target dimensions with distance
TKSD	target kinematic-state-dependent
VS-MM	variable structure multiple model
VTS	vessel traffic service

ABSTRACT

Kim, Dohyeung Ph.D., Purdue University, December 2019. Multi-Target Tracking Algorithms for Cluttered Environments. Major Professor: Inseok Hwang.

MTT is the problem to simultaneously estimate the number of targets and their states or trajectories. Numerous techniques have been developed for over 50 years, with a multitude of applications in many fields of study; however, there are two most widely used approaches to MTT: i) data association-based traditional algorithms; and ii) FISST-based data association free Bayesian multi-target filtering algorithms. Most data association-based traditional filters mainly use a statistical or simple model of the feature without explicitly considering the correlation between the target behavior and feature characteristics. The inaccurate model of the feature can lead to divergence of the estimation error or the loss of a target in heavily cluttered and/or low SNR environments. Furthermore, the FISST-based data association free Bayesian multi-target filters can lose estimates of targets frequently in harsh environments mainly attributed to insufficient consideration of uncertainties not only measurement origin but also target's maneuvers.

To address these problems, three main approaches are proposed in this research work: i) new feature models (e.g., target dimensions) dependent on the target behavior (i.e., distance between the sensor and the target, and aspect-angle between the longitudinal axis of the target and the axis of sensor line of sight); ii) new GM-PHD filter which explicitly considers the uncertainty in the measurement origin; and iii) new GM-PHD filter and tracker with JMS models. The effectiveness of the analytical findings is demonstrated and validated with illustrative target tracking examples and real data collected from the surveillance radar.

1. INTRODUCTION

1.1 Background and Motivation

MTT has a long history spanning more than 50 years. Due to the evolution of computing and sensing technologies during the last two decades, the field of MTT is rapidly expanding and many current algorithms in MTT and associated track filtering have been used in applications in diverse disciplines, including, air traffic control, ISR, space applications, and autonomous vehicles. MTT has challenges including estimating the state of an unknown and time-varying number of targets in the presence of measurement noise, uncertainties in target maneuvers, and clutter [1–4]. In addition to process and measurement noises in the dynamic and measurement models, respectively, one has to deal with much more complex sources of uncertainty such as the measurement origin uncertainty, data association, clutter, missed-detection, and appearance and disappearance of targets.

To address the problems, data association-based traditional algorithms have been proposed and widely used in many tracking systems [4–16]. For the last decade, the FISST-based data association free Bayesian multi-target filtering algorithms without the measurement-to-track association have gained significant popularity in the tracking community. However, the target tracking algorithms have uncertainty in terms of the system models and the measurement origin, which can lead to divergence of the estimation error or the missed estimate of a target.

The complex nature of the correlation between the kinematics and feature states, states of a target, and measurements make designing proper system models and considering the measurement origin uncertainty quite challenging tasks. Some of the main challenges are described as follows.

First, the data association-based traditional algorithms utilize not only the kinematic of a target but also the feature (e.g., amplitude, RCS, or dimensions) of measurement signal to decide which measurement is generated from a target [9,10]. However, most data association-based traditional filters mainly use a statistical or simple model of the feature without explicitly considering the correlation between the target behavior and feature characteristics. Inaccurate model of the feature could lead to divergence of the estimation error or the loss of a target in heavily cluttered and/or low SNR environments.

Second, FISST-based data association free Bayesian multi-target filtering algorithms, such as the well-known GM-PHD filter, are a promising solution to the MTT problem, which successfully integrates target detection, tracking, and identification. Despite its wide applicability and computational efficiency, existing GM-PHD filter can lose the estimates of the targets frequently in heavily cluttered and/or low SNR environments. This is mainly attributed to insufficient consideration of uncertainties of whether a measurement is from a target or not in the GM-PHD filter. At each time step, the GM-PHD filter generates new Gaussian components corresponding to individual measurements which have the same estimate error covariances regardless of whether the measurement is from a target or not, so that it can lose the estimates of targets when the clutter density is high and/or the detection probability is low.

Another challenge occurs when states of targets are subject to abrupt changes due to internal or external conditions (e.g., acceleration of a target in surveillance systems can abruptly change due its aggressive maneuvers). Rapid change in the trajectory of the maneuvering target can cause the existing GM-PHD filter and tracker to lose the estimate of the maneuvering target frequently due to the target's maneuver uncertainty. The estimate of the GM-PHD filter with abrupt state changes is quite challenging because the GM-PHD filter should be able to detect the abrupt changes in a timely manner and appropriately adjust the estimates of GM-PHD filter to compensate for the changes. Furthermore, in the GM-PHD algorithm, it is quite challenging to provide not only the state estimates of maneuvering targets at each time step, but also their identities (or labels) due to the complexity of the label assignment. These challenges necessitate the development of an adaptive GM-PHD approach, which can perform the state jump detection and provide the trajectories of targets in a systematic manner.

1.2 Objectives and Contributions

The contribution of this thesis is theoretical development of new state estimation algorithms that overcome the aforementioned challenges in complex MTT.

The first objective of this thesis is to develop new feature models that can explicitly consider the correlation between kinematics and feature of a target. To achieve this goal, we first develop new feature models (e.g., target dimensions) dependent on the target behavior (i.e., distance between the sensor and target, and the aspect-angle between the longitudinal axis of the target and the axis of sensor line of sight) via rigorous mathematical derivations. With the feature models developed, we then propose a data association filter which can facilitate the feature models dependent on the target kinematics to reduce the misassociations.

The second objective of this thesis is to develop a new state estimation algorithm that can explicitly consider the measurement origin uncertainty. To mathematically describe the measurement origin uncertainty, a new covariance update equation of a Gaussian component is introduced. This equation computes the estimate error covariance of a newly generated Gaussian component corresponding to each measurement conditioned on the uncertainty in the measurement origin, i.e. whether: 1) measurement is clutter; 2) measurement is originated from a target; and 3) there is no measurement.

Third objective of this thesis is to develop a multiple model GM-PHD filter with state-dependent mode transition probabilities which are represented as Gaussian probability density functions, and a new multi-target tracker based on the GM-PHD filter with JMS models, referred to as the GM-PHD tracker with JMS models, which provides both the state estimates of maneuvering targets and their identities (or labels).

1.3 Outline of Thesis

The rest of the thesis is organized as follows: In Chapter 2, kinematic and feature models of a target and the data association algorithm based on the JPDAF framework integrated with the target dynamic model-based feature are presented. In Chapter 3, the proposed GM-PHD filter that explicitly accounts for the measurement origin uncertainty for the FISST-based filter. Chapter 4 proposes a new GM-PHD filter with SD-JMS models and a new GM-PHD tracker with JMS models. Finally, a summary of the thesis and future research direction is presented in Chapter 5. The appendices provide the detailed proofs of the Lemmas developed to support the proposed approaches in this research.

2. DYNAMIC MODEL-BASED FEATURE AIDED DATA ASSOCIATION FILTER IN TARGET TRACKING

This chapter discusses feature models dependent on the kinematic models of a target to improve the performance of the data association-based filters. In Section 2.1, the motivation and literature review for this problem are presented. In Section 2.2, kinematic and feature models of a target are mathematically formulated. A target dynamic model-based feature, integrated into the data association algorithm based on the JPDAF framework is presented in Section 2.3. In Section 2.4, the performance of the proposed feature models and the proposed data association algorithm is demonstrated via comparison with the existing feature model and the well-known JPDAF-AI algorithms, respectively.

2.1 Background and Motivation

Target tracking in a noisy environment necessitates data association to distinguish the true target measurement from clutter. If the clutter or false measurements are used for tracking targets, the resulting tracks could be diverged, merged, or swapped, causing the loss of crucial information for tracking the targets [1,2]. Therefore, a number of data association algorithms have been proposed to assign proper measurements to the tracks.

To estimate the accurate target state in a noisy environment including clutter or spurious measurements, the distance between the expected output of the target's dynamic propagation model and the measurement is used in most data association algorithms such as the NNF, PNNF, PDAF, and MHT [3,5–8]. On the other hand, the SNF and PSNF use the feature (e.g., amplitude, RCS, or dimensions) of measurement signal to decide which measurement is generated from a target [9, 10]. To increase the performance of the data association algorithms in heavily cluttered and/or low SNR environments, the PDAF-AI and JPDAF-AI that exploit both the distance and the amplitude information were proposed for tracking a single target and multiple targets, respectively [11, 12].

The conventional data association algorithms using amplitude information, however, are based on the restrictive assumption that a measurement with high amplitude is originated from a target, while those with smaller amplitude are from clutter. However, in some target tracking scenarios, the amplitude of false measurements could be stronger than that of the target to deceive the position of the target. For example, Figure 2.1(a) shows that a fighter jet launches an anti-missile system or flares to distract the target tracking system with an infrared sensor. In this case, the temperatures of flares are much higher (2,500 degrees Celsius) than that of the fighter (1,200 degrees Celsius) [17, 18]. As a result, the target tracking system on the missile is likely to lock on a false measurement instead of the fighter. Furthermore, the conventional data association algorithms utilize a single statistical model for representing the amplitudes of multiple targets. However, the signals for individual targets could have different amplitudes based on the RCSs which are determined by the target dimensions, the distance between the target and a radar, and the aspect-angle between the heading and the line of sight of the target. For instance, Figure 2.1(b) shows the image of a port surveilled by a radar, where the signals from an oil tanker and a tugboat have quite different RCSs due to their dimensions.

In general, the RCS consists of a constant RCS dependent on the dimensions of a target and RCS fluctuation due to noise in radar measurements when the target does not move [19, 20]. The RCS fluctuation can be expressed in terms of stochastic models but it is difficult to compute the constant RCS since it changes corresponding to the motion of a target relative to a radar. However, the constant RCS can be estimated, and the estimated constant RCS is used in the FAT approaches to reduce the divergence of the estimation error or loss of a target [21–24]. Despite the promising capability of the estimated constant RCS, the existing FAT approaches model the

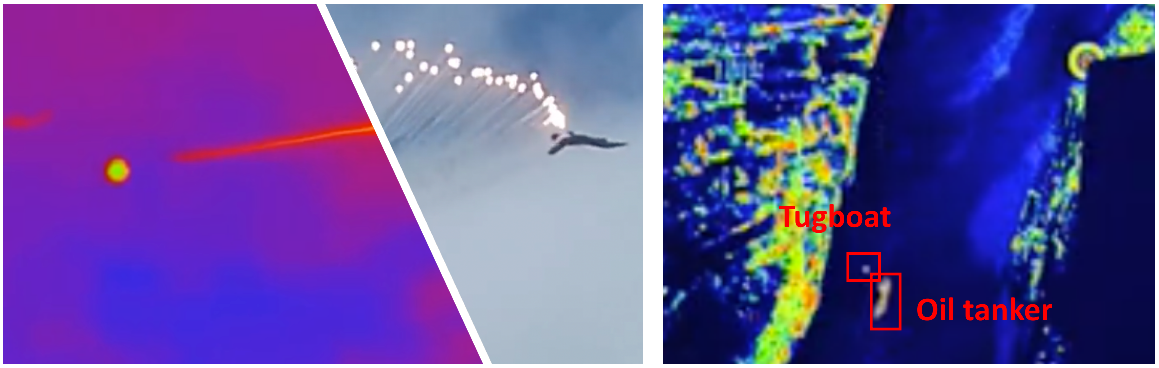

Fig. 2.1. Examples of distraction of amplitude-based target tracking system [28–30]

constant RCS as either constant or slowly varying parameters with respect to the target kinematic state because of a lack of information on the relation between the feature state and the kinematic state [25–27].

In this thesis, we attempt to exploit the feature state of a target depending on the target kinematics to improve the trajectory tracking performance of the data association filter. First, we propose two models to estimate the feature state (e.g., dimensions) of a target depending on the distance between the target and a radar, and the aspect-angle. To derive the first model, we consider the variation of the constant RCS corresponding to the distance in the near-field region while the RCS is assumed to be independent of the distance in the far-field region [31]. To derive the second model, we use the relationship between the RCS measured by a radar and the predicted RCS corresponding to the aspect-angle. We then integrate the feature state dependent on the kinematic state into the data association filter within the well-known JPDAF for tracking multiple targets in the presence of clutter [32]. We call the proposed data association filter as the JPDAF-TKSDFI. The feature state in the proposed JPDAF-TKSDFI can be estimated with state estimation algorithms (e.g., KF, EKF, or IMMF) with the proposed TKSD feature models [33–35]. With the estimated feature state, the proposed JPDAF-TKSDFI can select validated measurements more accurately by rejecting clutter which can cause track divergence, coalescence or swap problems. Then the probability that a target-originated measurement is associated to a track can be increased. The performance of the proposed data association algorithm is demonstrated with an illustrative simulation example in terms of track continuity, and further tested with real data collected from the surveillance radar in the vessel traffic tracking system.

2.2 System State Model

In this section, we introduce the target kinematic models and tractable feature models that account well for the feature state dependent on the kinematics of a target. For the target kinematic models, most target tracking algorithms treat a target as a point object. On the other hand, the target feature information comes from a rigid body model. To derive the target models, we consider the linear discrete-time state-space model as follows:

$$x_k = F_{k-1}x_{k-1} + w_{k-1} \tag{2.1}$$

$$z_k = H_k x_k + v_k \tag{2.2}$$

where $x_k = \begin{bmatrix} x_{m,k}^T & x_{f,k}^T \end{bmatrix}^T$ and $z_k = \begin{bmatrix} z_{m,k}^T & z_{f,k}^T \end{bmatrix}^T$ are the target state and measurement at time step k, respectively. The target state, x_k consists of the kinematic state, $x_{m,k}$ and the feature state, $x_{f,k}$. The measurement, z_k consists of the kinematic measurement, $z_{m,k}$ and the feature measurement, $z_{f,k}$. The process noise, w_{k-1} and the measurement noise, v_k are assumed to be uncorrelated zero mean, Gaussian noises, with known covariances, Q_{k-1} and R_k, respectively. The state transition and observation matrices are given by:

$$F_{k-1} = \begin{bmatrix} F_{m,k-1} & \mathbf{0} \\ \mathbf{0} & F_{f,k-1} \end{bmatrix}, \quad H_k = \begin{bmatrix} H_{m,k} \\ H_{f,k} \end{bmatrix} \tag{2.3}$$

where $F_{m,k-1}$ and $F_{f,k-1}$ are the kinematic and feature state transition matrices, respectively. $H_{m,k}$ and $H_{f,k}$ are the kinematic and feature observation matrices, respectively.

2.2.1 Models for Kinematic State

Many models for the kinematic state, $x_{m,k}$ have been proposed [36]. In this paper, we consider two models among those models: the constant velocity model for a non-maneuvering target and the coordinated turn model with a known turn rate for a maneuvering target. To describe the kinematic state of the target, we consider 2D horizontal motion $x_{m,k} = \begin{bmatrix} P_{x,k} & P_{y,k} & V_{x,k} & V_{y,k} \end{bmatrix}^T$ in the Cartesian coordinate system. We assume a radar can obtain the kinematic measurement which represents the position of a target, $z_{m,k} = \begin{bmatrix} z_{x,k} & z_{y,k} \end{bmatrix}^T$ in the Cartesian coordinate system.

Constant Velocity Model

This model assumes that a target moves with constant speed. The kinematic state transition matrix of the discrete-time CV model is given by [36]:

$$F_{m,k-1} = \begin{bmatrix} 1 & 0 & T & 0 \\ 0 & 1 & 0 & T \\ 0 & 0 & 1 & 0 \\ 0 & 0 & 0 & 1 \end{bmatrix} \tag{2.4}$$

where T is the sampling interval. The kinematic observation matrix of this model is:

$$H_{m,k} = \begin{bmatrix} 1 & 0 & 0 & 0 \\ 0 & 1 & 0 & 0 \end{bmatrix} \tag{2.5}$$

Coordinated Turn Model with Known Turn Rate

This model presumes that a target maneuvers with constant speed and constant angular (or turn) rate, ω_{k-1}. The kinematic state transition matrix of the discrete-time CT model is given by [36]:

$$F_{m,k-1} = \begin{bmatrix} 1 & 0 & \frac{\sin \omega_{k-1}T}{\omega_{k-1}} & -\frac{1-\cos \omega_{k-1}T}{\omega_{k-1}} \\ 0 & 1 & \frac{1-\cos \omega_{k-1}T}{\omega_{k-1}} & \frac{\sin \omega_{k-1}T}{\omega_{k-1}} \\ 0 & 0 & \cos \omega_{k-1}T & -\sin \omega_{k-1}T \\ 0 & 0 & \sin \omega_{k-1}T & \cos \omega_{k-1}T \end{bmatrix} \tag{2.6}$$

where the angular rate can be predefined by a constant value or calculated as follows:

$$\omega_{k-1} = \{ \tan^{-1} \frac{V_{y,k-1}}{V_{x,k-1}} - \tan^{-1} \frac{V_{y,k-2}}{V_{x,k-2}} \}/T \tag{2.7}$$

For this model, the kinematic observation matrix is the same as that of the CV model.

2.2.2 Models for Feature State

In this section, we propose two models to estimate the feature state of a target dependent on the distance between a target and a radar, and the aspect-angle. Although the feature state can include amplitude, dimensions, RCS, or other target signature information, in this paper, we consider target dimensions to describe the feature state. Without loss of generality, the following assumptions are used to derive two models for the feature state.

Assumption 1 *The dimensions of a target do not change.*

Assumption 2 *The heading of a target is the same as its velocity.*

Target Dimensions with Distance Model

The RCS is mostly defined in the far-field region, which is independent of the distance between a radar and a target. In the near-field region, however, this definition of the RCS cannot be used to estimate the feature state of a target since the RCS changes depending on the distance between the radar and the target [31, 37]. To accurately estimate the feature state of a target, we propose an elaborate feature model considering the distance between the target and the radar. In this section, we assume that a target's shape is approximated as a circle. Under Assumption 1, the feature state of the TDD model is the radius of a target, $\boldsymbol{x}_{f,k} = r_k$, and thus, the feature state transition matrix of the discrete-time TDD model is given by [27]:

$$F_{f,k-1} = 1 \tag{2.8}$$

In this section, we assume that the radar can obtain the RCS as the feature measurement. The radius of a target does not change under Assumption 1, but the constant RCS varies depending on the distance between the target and the radar when it is measured by the radar [31, 37]. To derive the feature observation matrix, we consider the non-linear discrete-time observation model for the RCS of a circular target as follows [31]:

$$z_{f,k} = 2\pi d_k^2 \Big\{ 1 - \cos\big(\frac{hr_k^2}{d_k}\big) \Big\} + v_{f,k} \tag{2.9}$$

where h is the wave number of the radar signal. d_k is the distance between the radar and the target. The feature measurement noise, $v_{f,k}$ is Gaussian noise with mean zero and covariance, $R_{f,k}$. Based on the observation model, the feature observation matrix of this model is obtained as:

$$H_{f,k} = \frac{\delta z_{f,k}}{\delta r_k} = 4\pi d_k h r_k \sin(\frac{hr_k^2}{d_k}) \tag{2.10}$$

Target Dimensions with Aspect-angle Model

In this section, we propose a model for the feature state of a target dependent on the aspect-angle between the heading and the line of sight of the target. A target is assumed to have an ellipsoidal shape. Under Assumption 1, the feature state of the TDA model is the dimensions of a target, $x_{f,k} = \begin{bmatrix} a_k & b_k \end{bmatrix}^T$ where a_k and b_k are the

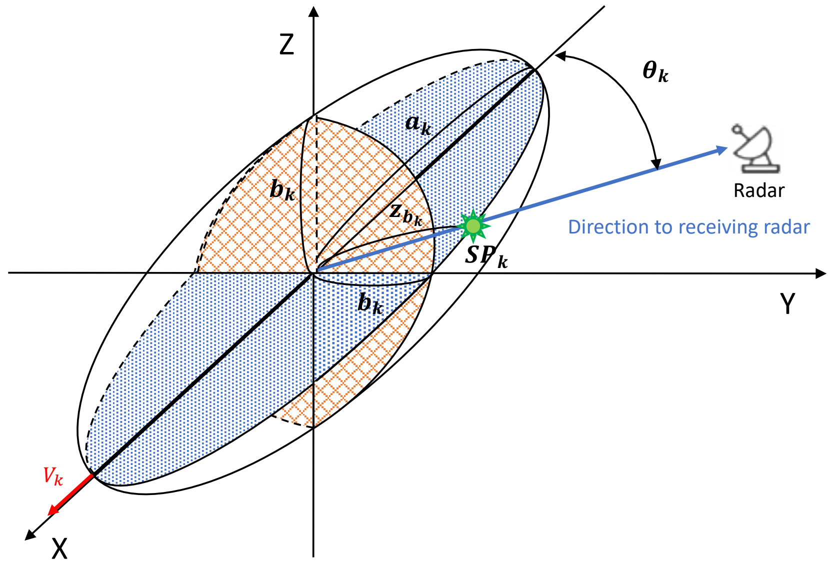

(a) a sensor and target

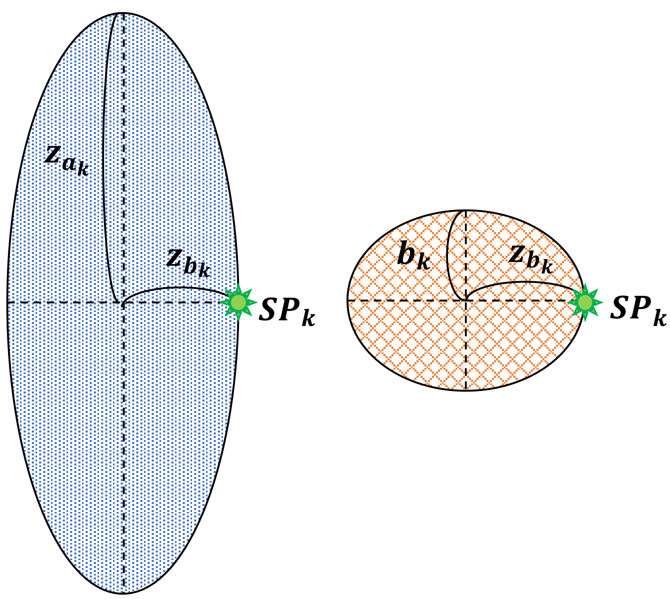

(b) Cross sections of a target

Fig. 2.2. Geometry of a sensor and a target, and target cross sections

semi-major and the semi-minor axes of a target, and thus, the feature state transition matrix of the discrete-time TDA model is given by:

$$F_{f,k-1} = \begin{bmatrix} 1 & 0 \\ 0 & 1 \end{bmatrix} \tag{2.11}$$

Under Assumption 2, Figure 2.2(a) shows the velocity, V_k, aspect-angle, θ_k and specular point, SP_k of an ellipsoidal target with X as the axis of symmetry. We assume that the radar can obtain the dimensions of the RCS as the feature measurement. Although the dimensions of a target do not change under Assumption 1, the semi-major and semi-minor axes of the RCS measured by a radar, z_{a_k} and z_{b_k} vary corresponding to the aspect-angle, respectively [19, 38]. To derive the feature observation matrix, we need to derive a formula for the semi-major and semi-minor axes of the measured RCS corresponding to the aspect-angle at the specular point. To derive the formula, we first consider the non-linear discrete-time RCS, σ_k of an ellipsoidal target as follows [38]:

$$\sigma_k \approx \pi r_{L,k} r_{S,k} \tag{2.12}$$

where $r_{L,k}$ and $r_{S,k}$ are the radii of curvature at the specular point in the direction of 0 and 90 degrees, respectively. Then, we derive the following Lemma 1 which will be used to compute the radii of curvature corresponding to the aspect-angle at a specular point.

Lemma 1 *Under Assumptions 1 and 2, the radii of curvature in the direction of 0 and 90 degree, $r_{L,k}(\theta_k)$ and $r_{S,k}(\theta_k)$ corresponding to the aspect-angle, θ_k at the specular point, SP_k are given by:*

$$r_{L,k}(\theta_k) = \frac{{a_k}^2}{b_k}\Big[1 + ((\frac{b_k}{a_k})^2 - 1)\frac{a_k^2\cos^2\theta_k}{a_k^2\cos^2\theta_k + b_k^2\sin^2\theta_k}\Big]^{3/2} \tag{2.13}$$

$$r_{S,k}(\theta_k) = b_k\sqrt{1 + ((\frac{b_k}{a_k})^2 - 1)\frac{a_k^2\cos^2\theta_k}{a_k^2\cos^2\theta_k + b_k^2\sin^2\theta_k}} \tag{2.14}$$

The proof of Lemma 1 is given in Appendix A.

Note that if the specular point is located at the intersection point between the red ellipse and the y axis in Figure 2.2(a) (i.e., the aspect-angle is 90 degrees), then the left principal cross section (blue ellipse) in Figure 2.2(b) can be expressed by the actual semi-major axis and semi-minor axis of the target, a_k and b_k, respectively. Also, the right principal cross section (red ellipse) in Figure 2.2(b) becomes a circle with its radius equal to the actual semi-minor axis of the target, b_k. However, as the aspect-angle changes, the major-axis and minor-axis of the left principal cross section in Figure 2.2(b) are changed to the semi-major axis and the semi-minor axis of the RCS measured by the radar, z_{a_k} and z_{b_k}. Also, the minor-axis of the right principal cross section in Figure 2.2(b) is changed to the semi-minor axis of the RCS measured by the radar, z_{b_k}. Hence, the radius of curvature of the left and right principal cross sections in Figure 2.2(b) are given by:

$$\bar{r}_{L,k} = \frac{z_{a_k}^2}{z_{b_k}} \tag{2.15}$$

$$\bar{r}_{S,k} = \frac{b_k^2}{z_{b_k}} \tag{2.16}$$

Since the RCS computed by the predicted radii of curvature in (2.13) and (2.14) is the same as the RCS computed by the radii of curvature in (2.15) and (2.16), the semi-major and semi-minor axes of the measured RCS, $z_{a_k}(\theta_k)$ and $z_{b_k}(\theta_k)$ dependent on the aspect-angle can be described as follows:

$$z_{a_k}(\theta_k) = a_k\Big(1 + ((\frac{b_k}{a_k})^2 - 1)\frac{a_k^2\cos^2\theta_k}{a_k^2\cos^2\theta_k + b_k^2\sin^2\theta_k}\Big)^{1/2} \tag{2.17}$$

$$z_{b_k}(\theta_k) = b_k\Big(1 + ((\frac{b_k}{a_k})^2 - 1)\frac{a_k^2\cos^2\theta_k}{a_k^2\cos^2\theta_k + b_k^2\sin^2\theta_k}\Big)^{-1/2} \tag{2.18}$$

With (2.17) and (2.18), we define the feature observation matrix of the discrete-time TDA model as follows:

$$H_{f,k} = \begin{bmatrix} \frac{\delta z_{a_k}(\theta_k)}{\delta a_k} & \frac{\delta z_{a_k}(\theta_k)}{\delta b_k} \\ \frac{\delta z_{b_k}(\theta_k)}{\delta a_k} & \frac{\delta z_{b_k}(\theta_k)}{\delta b_k} \end{bmatrix} \tag{2.19}$$

The elements of the matrix, $H_{f,k}$ are given in Appendix B.

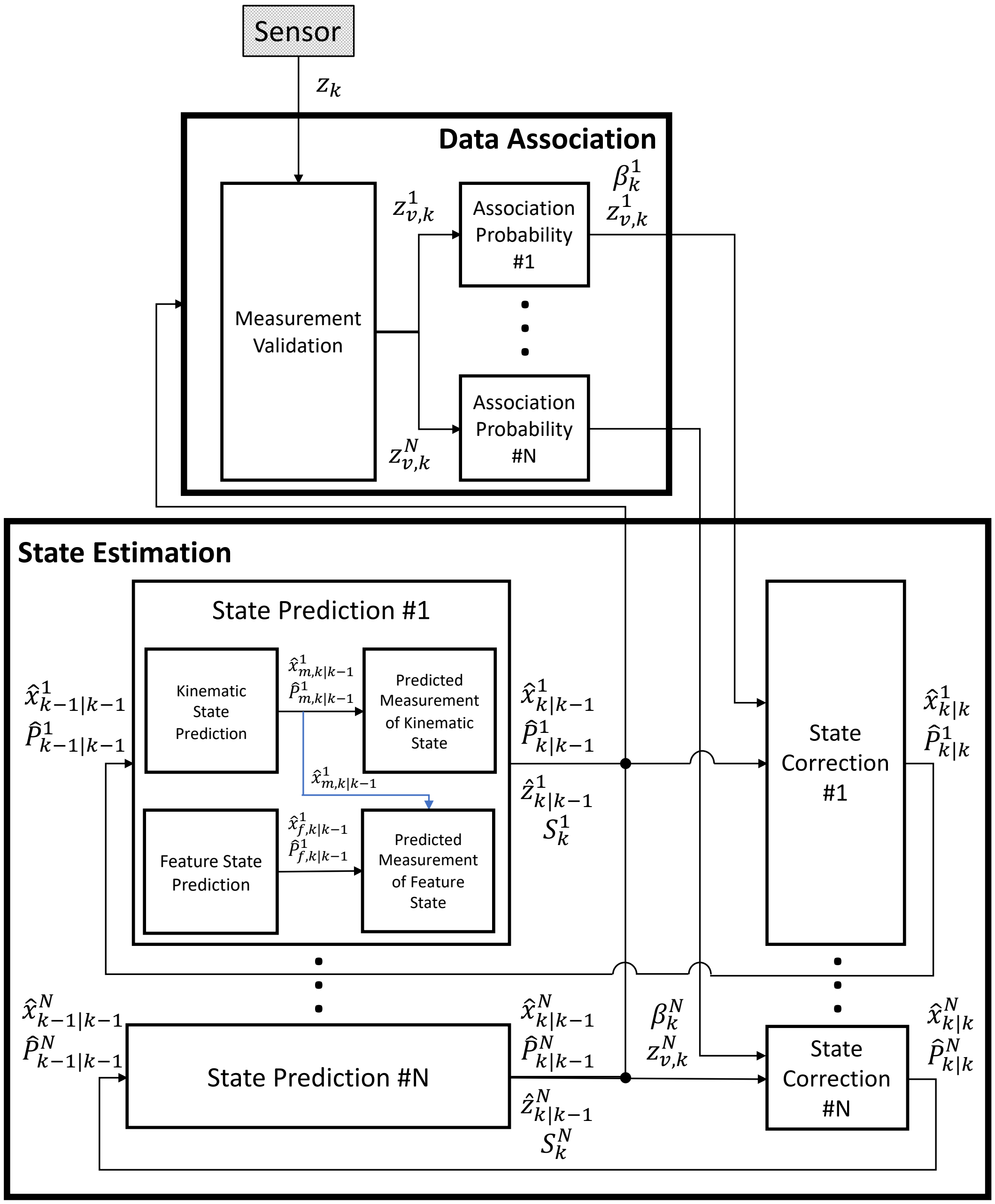

Fig. 2.3. Structure of proposed JPDAF-TKSDFI

2.3 Joint Probability Data Association Filter with Target Kinematic-State-Dependent Feature Information

In this section, we now present a new data association algorithm with TKSD feature information, based on the JPDAF for tracking multiple targets. Figure 2.3 shows the structure of the proposed JPDAF-TKSDFI. As illustrated, the kinematic state at time step $k-1$ is predicted, and then, the predicted kinematic state is used to predict the feature state since the feature state depends on the kinematic state (i.e., the distance between the target and the radar, or the aspect-angle between the heading and the line of sight of the target). Note that the propose the existing single target data association filters such as the NNF, PNNF and PDAF but also to the multi-target data association filters such as the MHT.

2.3.1 Data Association

Measurement Validation

This process selects validated measurements to reduce the processing load in the data association and increase the association probability that the true measurement can be associated to the target. To enhance the accuracy of the clutter-rejection, both the kinematic and feature states are used in the measurement validation process. Let z_k represent the set of measurements obtained by a radar at time step k, and $\{z_k^j\}_{j=1}^{T_k}$ where T_k denotes the number of measurements at time step k. We use superscript i to represent a track and possible target that track i may be following. Let $z_{v,k}^i$ be the set of validated measurements of the i-th track at time step k, and $z_{v,k}^i = \{z_{v,k}^{i,l}\}_{l=1}^{T_k^i}$ where T_k^i is the number of measurements in the validation region of the i-th track at time step k. To make the set of validated measurements for each track, we need to define the validation matrix as follows:

$$\Omega = [D_k^{i,j}] \qquad i = 1, ..., N, \quad j = 1, ..., T_k \tag{2.20}$$

where N denotes the number of tracks. The NDS, $D_k^{i,j}$ of the j-th measurement corresponding to the i-th track is defined as [32]:

$$\begin{aligned} D_k^{i,j} &= (z_k^j - \hat{z}_{k|k-1}^i)^T (S_k^i)^{-1} (z_k^j - \hat{z}_{k|k-1}^i) \\ &= (\nu_k^{i,j})^T (S_k^i)^{-1} \nu_k^{i,j} \end{aligned} \tag{2.21}$$

where S_k^i is the covariance of the residual, $\nu_k^{i,j}$ of the i-th track, and $\hat{z}_{k|k-1}^i$ is the predicted measurement. The validated measurement of the track corresponding to the column of Ω is one unit which has the smallest NDS that is less than the validation region after scanning Ω by a column (i.e., a measurement can be the validated measurement of one track). The validation region is identified as a region centered at the predicted measurement of a target where the measurement is expected to be for the target. The region is given by [32]:

$$\mathbf{R}_\gamma^i = \{z_{v,k}^{i,j} : D_k^{i,j} \leq \gamma\} \tag{2.22}$$

where $\sqrt{\gamma}$ is called the region size which depends on the variance of both the measurement noise and the predicted measurement.

Remark 1 *Most data association algorithms use only the position estimate to find the validated measurements via the measurement validation process. In this case, the measurements which are closely spaced could be assigned to a target or targets that are not related to the measurements even if they have different feature state values (e.g., RCS or dimensions). With both the kinematic and feature state estimates, the measurement validation process can more precisely remove measurements which are irrelevant to the target being tracked. Especially, the data association algorithms using the association probabilities of the validated measurements such as PNNF, PSNF, PDAF and JPDAF can have an accurate estimate since the association probability increases as the number of validated measurements decreases. Furthermore, in multi-target tracking, the feature state can help the data association algorithms to reject clutter and the measurements originated from other targets. Hence, the track coalescence or swap can be reduced.*

Association Probability

Denote association events as $\mathcal{H}_k^{i,l} = \{z_{v,k}^{i,l}$ is originated from the target being followed by the i-th track$\}$, $l = 1, 2, \ldots, T_k^i$ and $\mathcal{H}_k^{i,0} = \{$none of the measurements are originated from the target being followed by the i-th track$\}$. The association probability, $\beta_k^{i,l}$ of the l-th measurement originating from the target being followed by the i-th track is expressed as the likelihood that all of the measurements lie in the validation region [32]:

$$\beta_k^{i,l} = p\{\mathcal{H}_k^{i,l}|z_k\} = \begin{cases} \frac{e_k^{i,l}}{b_k + \sum_{j=1}^{T_k^i} e_k^{i,j}} & l = 1, \ldots, T_k^i \\ \frac{b_k}{b_k + \sum_{j=1}^{T_k^i} e_k^{i,j}} & l = 0 \end{cases} \tag{2.23}$$

where

$$e_k^{i,l} = \frac{P_D V_{D_k^l} \Lambda_k^{i,l}}{T_k^i} \tag{2.24}$$

$b_k = T_k^i \left(\frac{1 - P_D P_G}{P_D P_G V_{D_k^{i,l}}} \right)$ is the probability that none of the validated measurements are target-originated. P_D is the detection probability, and P_G is the probability that the target falls inside the validation region. The volume of the n-dimensional NDS, $D_k^{i,l}$ is given by:

$$V_{D_k^{i,l}} = C_n |S_k^i|^{\frac{1}{2}} (D_k^{i,l})^{\frac{n}{2}} \tag{2.25}$$

where C_n is the volume of the n-dimensional unit hypersphere given by [5]:

$$C_n = \frac{\pi^{n/2}}{\Gamma(n/2 + 1)} \tag{2.26}$$

$\Lambda_k^{i,l}$ is the measurement-to-track likelihood between the predicted measurement of the i-th track and the l-th measurement given by [32]:

$$\Lambda_k^{i,l} = \frac{1}{\sqrt{|2\pi S_k|}} \exp\Big(-\frac{1}{2} (\nu_k^{i,l})^T (S_k^i)^{-1} \nu_k^{i,l} \Big) \tag{2.27}$$

Note that the data association events are mutually exclusive and collectively exhaustive, i.e., $\sum_{l=0}^{T_k^i} \beta_k^{i,l} = 1$.

Remark 2 *To compute the likelihood of a measurement, the conventional data association algorithms assume that the feature measurement of a target is independent of its kinematic measurement, which implies that [11, 12, 24]:*

$$\Lambda_k = p(z_{m,k}|Z^{m,k})p(z_{f,k}|Z^{f,k}) \tag{2.28}$$

However, the proposed data association algorithm using the feature state dependent on the kinematic state does not need this assumption. Hence, the proposed algorithm can account for the more general case.

2.3.2 State Estimation

State Prediction

This process is to predict the states of targets at time step k. The prediction equations for the JPDAF-TKSDFI are given as follows [32]:

$$\hat{x}^i_{k|k-1} = F_{k-1}\hat{x}^i_{k-1|k-1} \tag{2.29}$$

$$\hat{P}^i_{k|k-1} = F_{k-1}\hat{P}^i_{k-1|k-1}F^T_{k-1} + Q_{k-1} \tag{2.30}$$

where $\hat{x}^i_{k-1|k-1}$ and $\hat{P}^i_{k-1|k-1}$ denote the state estimate and covariance of the state for the i-th track at time step $k-1$, respectively. $\hat{x}^i_{k|k-1}$ and $\hat{P}^i_{k|k-1}$ denote the predicted estimate and covariance of the estimate for the i-th track at time step k, respectively. We can compute the predicted measurement $\hat{z}^i_{k|k-1} = \begin{bmatrix} \hat{z}^i_{m,k|k-1} & \hat{z}^i_{f,k|k-1} \end{bmatrix}^T$ and residual covariance S^i_k as follows:

$$\hat{z}^i_{m,k|k-1} = H_{m,k}\hat{x}^i_{m,k|k-1} \tag{2.31}$$

$$\hat{z}^i_{f,k|k-1} = h_f(\hat{x}^i_{k|k-1}) \tag{2.32}$$

$$S^i_k = H_k\hat{P}^i_{k|k-1}H^T_k + R_k \tag{2.33}$$

where the measurement noise covariance R_k is given by:

$$R_k = diag([R_{m,k}, R_{f,k}]) \tag{2.34}$$

where $diag(\bullet)$ denotes the diagonal matrix whose diagonal elements are given by vector $\bullet$. $R_{m,k}$ and $R_{f,k}$ denote the kinematic and feature measurement noise covariances, respectively. The predicted measurement and the residual covariance are used to get the validated measurements and reject clutter in the measurement validation process.

State Correction

This process is to update the states of targets at time step k. With the association probabilities, the update equations for the JPDAF-TKSDFI are given by [32]:

$$\hat{x}^i_{k|k} = \hat{x}^i_{k|k-1} + K^i_k \Big(\sum_{l=1}^{T^i_k} \beta^{i,l}_k \nu^{i,l}_k \Big) \tag{2.35}$$

$$\hat{P}^i_{k|k} = \hat{P}^i_{k|k-1} \beta^{i,0}_k + [1 - \beta^{i,0}_k] \hat{P}^{i,c}_{k|k} + \tilde{P}^i_k \tag{2.36}$$

where $K^i_k = \hat{P}^i_{k|k-1} H^T_k (S^i_k)^{-1}$ is the Kalman gain. The covariance of the state with the correct measurement is given by [32]:

$$\hat{P}^{i,c}_{k|k} = [I_n - K^i_k H_k] \hat{P}^i_{k|k-1} \tag{2.37}$$

where I_n is the n-dimensional identity matrix. The spread of the residual term is given by [32]:

$$\tilde{P}^i_k = K^i_k \Big[\sum_{l=1}^{T^i_k} \beta^{i,l}_k \nu^{i,l}_k (\nu^{i,l}_k)^T - \nu^{i,l}_k (\nu^{i,l}_k)^T \Big] (K^i_k)^T \tag{2.38}$$

2.4 Simulation Results

In this section, the performance of the proposed feature models is demonstrated with the video of the real radar screen, in comparison to the feature model independent of the kinematic state. Furthermore, we compare the performance of the proposed data association algorithm using the proposed feature models with the well-known JPDAF and the JPDAF-AI.

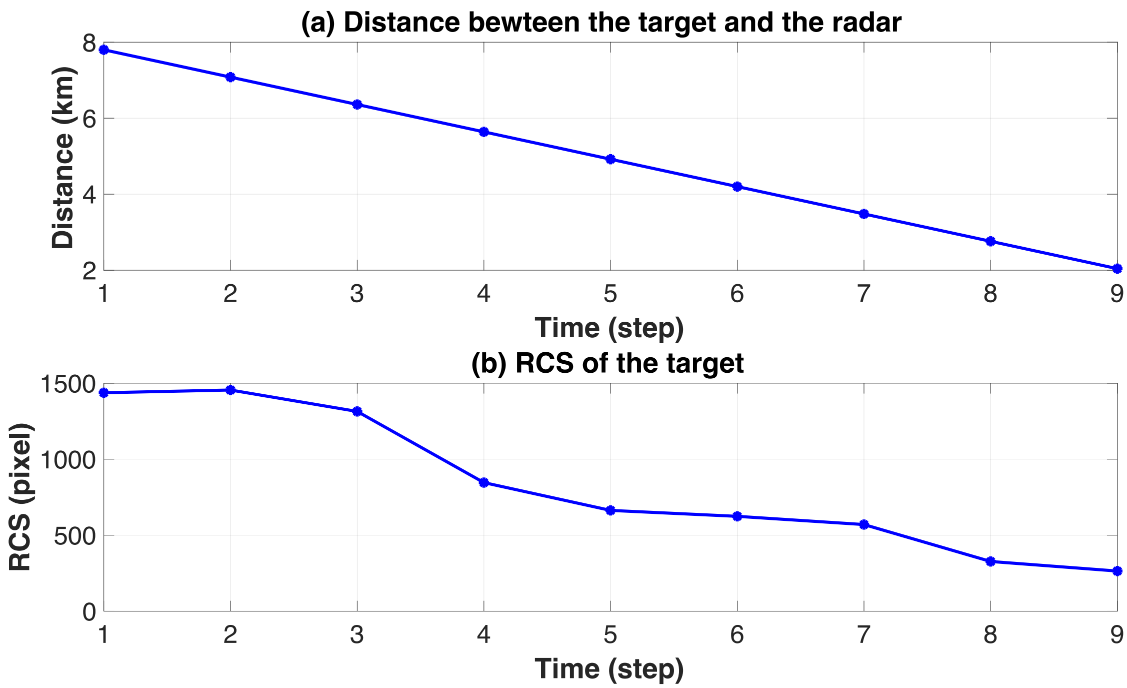

Fig. 2.4. Distance between the target and the radar, and RCS of the target [37]

2.4.1 Target Kinematic-State-Dependent Feature Models Results

To evaluate the performance of the proposed feature models, we compare the estimates of the tracking algorithms using the proposed feature models with that of the tracking algorithm using the feature model independent of the kinematic state. We utilize the videos of the radar screens of the ship and VTS system to evaluate the performance of the proposed TDD and TDA models, respectively.

Target Dimensions with Distance Model Results

We extract one target information from the video of the marine radar screen on the ship for 9 time steps [37]. Figure 2.4 shows the distance between the target and the radar, and the RCS of the target, which are extracted from the video of the radar. As illustrated in Figure 2.4, the RCS expressed in term of the number of pixels on screen decreases while the target moves toward the radar. To investigate the accuracy of the model, we compare the performance of the KF using the feature model independent of the distance and the EKF using the proposed TDD model. Note that the EKF is used for the TDD model since it is nonlinear. Let $x_{f,k} = r_k$ be the feature state. The discrete-time feature model independent of the distance and the TDD model are represented by:

$$x_{f,k} = x_{f,k-1} + \frac{T^2}{2} w_{f,k-1} \tag{2.39}$$

$$z_{f,k} = \begin{cases} x_{f,k} + v_{f,k} & \text{Feature model independent of distance} \\ \\ 2\pi d_k^2 \left\{ 1 - \cos\left(\frac{hr_k^2}{d_k}\right) \right\} + v_{f,k} & \text{TDD model} \end{cases} \tag{2.40}$$

where the sampling interval, T is 10 minutes. The process noise, $w_{f,k-1}$ is Gaussian with zero mean and 0.01 standard deviation. The feature measurement noise, $v_{f,k}$ is Gaussian with zero mean and the covariance $R_{f,k} = diag([10^2, 10^2])$.

Figure 2.5 illustrates the measurement and the estimates of the RCS computed by the KF using the feature model independent of the distance between the target and the radar, and the EKF using the proposed TDD model. The blue, red and green lines represent the measurement, the estimates of the RCS computed by the KF and the EKF, respectively. As illustrated in Figure 2.5, the estimate computed by the KF using the feature model independent of the distance is significantly deviated from the measurement as time goes by. This could severely degrade the performance of the target tracking system if the feature model without considering the distance is used in the data association algorithm. However, the estimate computed by the EKF using our proposed TDD model is close to the measurement, which demonstrates its superior performance.

Target Dimensions with Aspect-angle Model Results

In this section, the performance of the proposed TDA model is demonstrated with the ship surveillance data extracted from the radar screen of the VTS system [39].

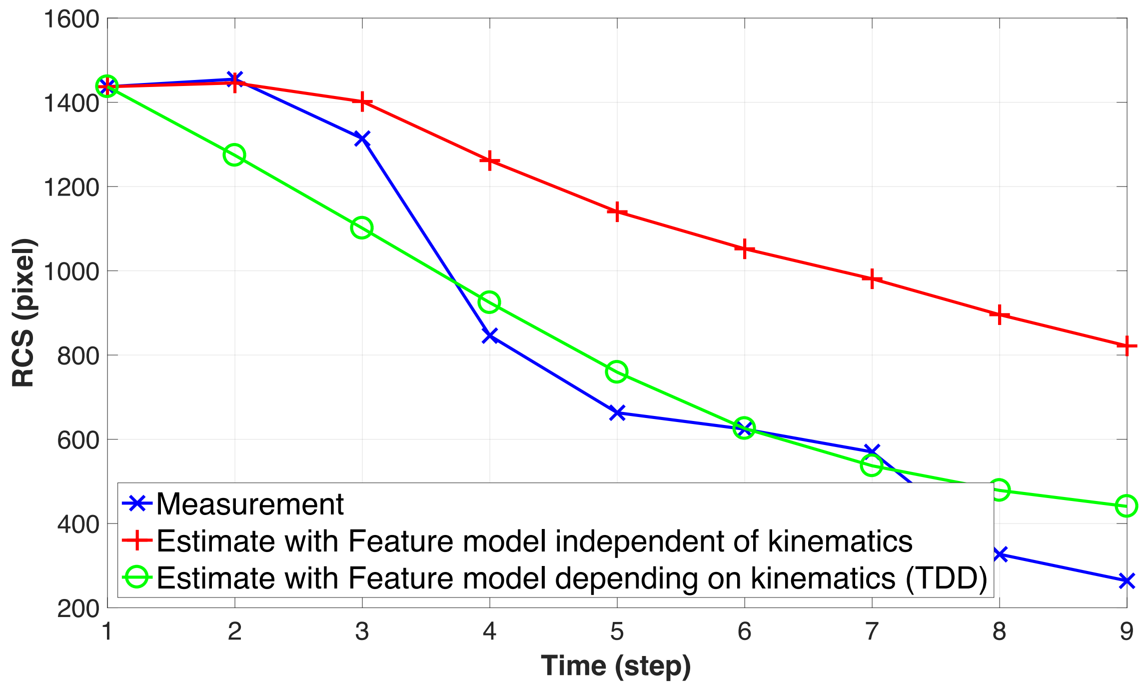

Fig. 2.5. Measurement and estimates computed by the KF using feature model independent of distance and the EKF using TDD model

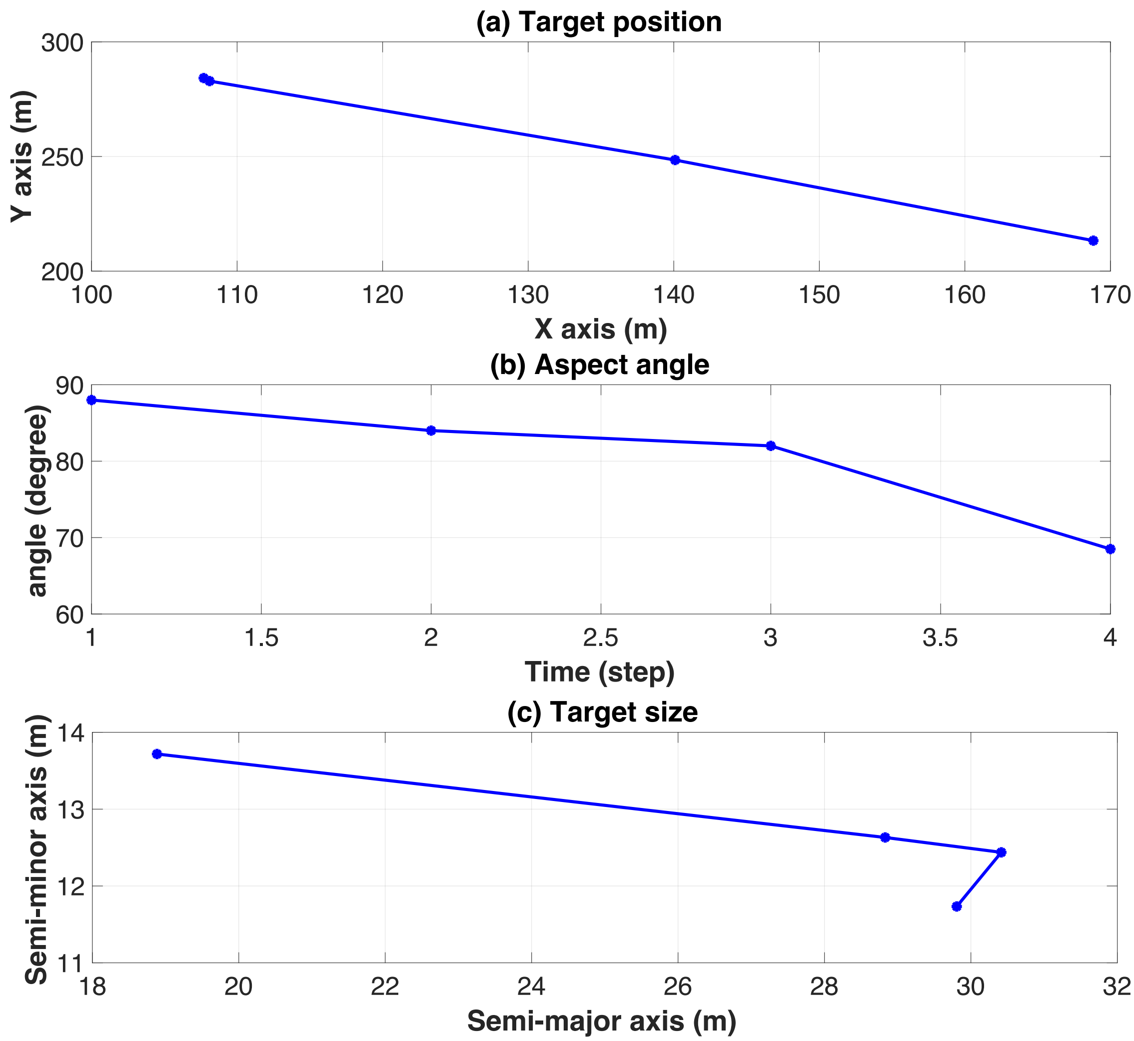

Fig. 2.6. Position, aspect-angle and dimensions of measurement [39]

Figure 2.6 shows the position, aspect-angle and dimensions of the measurement. From time step 3 to time step 4, the semi-major axis of the RCS changes rapidly from 29 meters to 19 meters since the aspect-angle suddenly changes from 82 degrees to 68 degrees. To investigate the accuracy of the proposed model, we compare the performance of the KF using the feature model without considering the aspect-angle and the EKF using the TDA model. Note that similarly, the EKF is used for the TDA model since it is nonlinear. Let $x_{f,k} = \begin{bmatrix} a_k & b_k \end{bmatrix}^T$ be the feature state. The discrete-time feature model independent of the aspect-angle and the TDA model are represented by:

$$x_{f,k} = \begin{bmatrix} 1 & 0 \\ 0 & 1 \end{bmatrix} x_{f,k-1} + \begin{bmatrix} \frac{T^2}{2} & 0 \\ 0 & \frac{T^2}{2} \end{bmatrix} w_{f,k-1} \tag{2.41}$$

where the sampling interval, T is 5 seconds. The process noise, $w_{f,k-1}$ is Gaussian with zero mean and 0.5 standard deviation. The feature measurement represents the dimensions of the target, $z_{f,k} = \begin{bmatrix} z_{a_k} & z_{b_k} \end{bmatrix}^T$. The observation models of the feature state are given by:

$$z_{f,k} = \begin{cases} \begin{bmatrix} 1 & 0 \\ 0 & 1 \end{bmatrix} x_{f,k} + v_{f,k} & \begin{array}{c}\text{Feature model} \\ \text{independent of aspect-angle}\end{array} \\ \\ \begin{bmatrix} a_k\left(1 + ((\frac{b_k}{a_k})^2 - 1)\frac{a_k^2 \cos^2\theta_k}{a_k^2\cos^2\theta_k + b_k^2\sin^2\theta_k}\right)^{1/2} \\ b_k\left(1 + ((\frac{b_k}{a_k})^2 - 1)\frac{a_k^2 \cos^2\theta_k}{a_k^2\cos^2\theta_k + b_k^2\sin^2\theta_k}\right)^{-1/2} \end{bmatrix} & \\ +v_{f,k} & \text{TDA model} \end{cases} \tag{2.42}$$

where the feature measurement noise $v_{f,k}$ is Gaussian with zero mean and the covariance $R_{f,k} = diag([0.3^2, 0.3^2])$.

Figure 2.7 shows the measurement and the estimates computed by the KF using the feature model independent of the aspect-angle and the EKF using the TDA model. As illustrated in Figure 2.7, the difference between the measurement and the estimate computed by the KF denoted as the red line is getting bigger as time goes by. However, the estimate computed by the EKF denoted as the green line is similar to

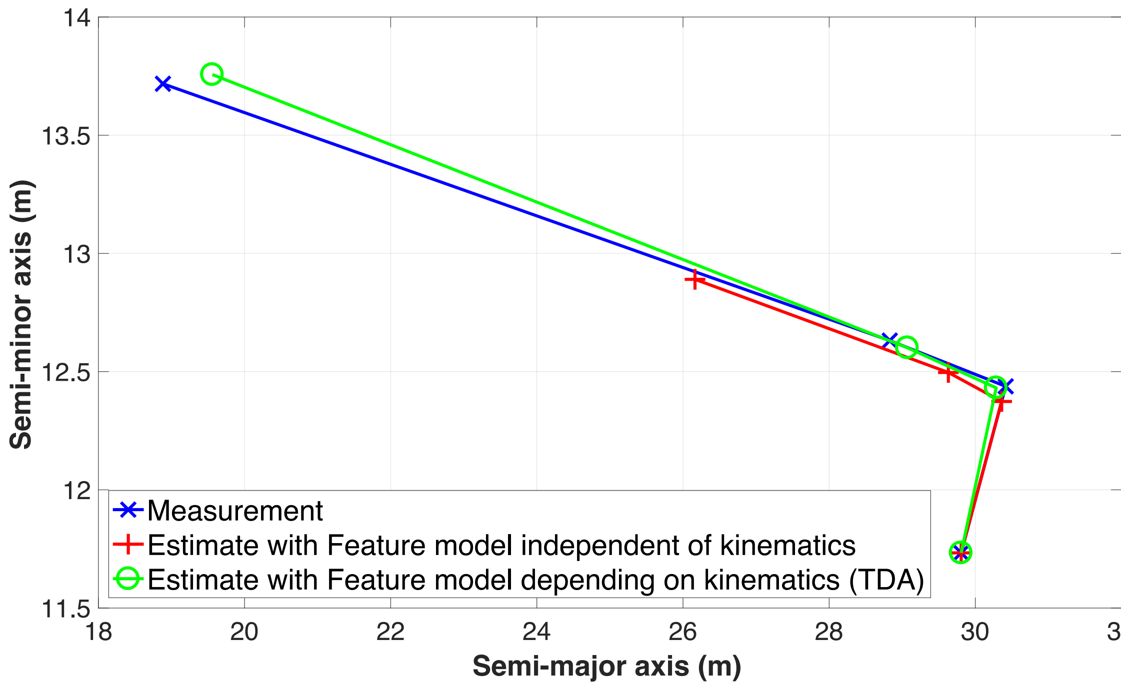

Fig. 2.7. Measurement and estimates computed by the KF using feature model independent of aspect-angle and the EKF using TDA model

the measurement since the TDA model explicitly accounts for the correlation between the target kinematic state and the feature state. As a result, improving the accuracy of the feature state estimates computed by the EKF using the proposed TDD or TDA model could reduce the track loss of the target in the presence of clutter if the models are implemented in the data association algorithms.

2.4.2 Joint Probabilistic Data Association Filter with Target Kinematic State-Dependent Feature Information Results

In this section, two scenarios are considered to demonstrate the performance of the proposed data association algorithm. In order to evaluate the performance of the proposed JPDA-TKSDFI versus the well-known JPDAF and JPDAF-AI in terms of the numbers of the track losses, the first scenario tests whether or not the three algorithms can correctly maintain the tracks for two targets in noisy environments with a range of the clutter density and the target detection probability. In the second scenario, the multi-target tracking ability of the JPDAF and proposed JPDAF-TKSDFI is tested by comparing the target state estimates computed by each filter with the data extracted from the radar screen of the VTS system.

Scenario 1

In this scenario, the performance of the proposed JPDAF-TKSDFI is demonstrated with an illustrative multi-target tracking example, in comparison to the original JPDAF and JPDAF-AI. To test the proposed algorithm in the case shown in Figure 2.1(b), the example considers that two ships with different sizes are crossing in the presence of clutter. The radii of target 1 and target 2 are 6 m and 50 m, respectively. The amplitudes of target 1 and target 2 are 8 dB and 30 dB, respectively. We generate clutter whose radius and amplitude are 5 m and 15 dB in the surveillance ares of $[-1500, 1500] \times [-500, 4000]$ m, respectively. Figure 2.8 shows the trajectories of the two targets and clutter (the average number of the clutter is 100 in the surveillance region) which are denoted as the black circle and the blue cross, respectively. The state of a target is composed of its position, velocity, and radius: $x_k = \begin{bmatrix} P_{x,k} & P_{y,k} & V_{x,k} & V_{y,k} & r_k \end{bmatrix}^T$. The discrete-time dynamic model of the target is represented by:

$$x_k = \begin{bmatrix} I_2 & TI_2 & 0_{2\times1} \\ 0_{2\times2} & I_2 & 0_{2\times1} \\ 0_{1\times2} & 0_{1\times2} & 1 \end{bmatrix} x_{k-1} + \begin{bmatrix} \frac{T^2}{2} I_2 & 0_{2\times1} \\ TI_2 & 0_{2\times1} \\ 0_{1\times2} & \frac{T^2}{2} \end{bmatrix} w_{k-1} \tag{2.43}$$

where the sampling interval, T is 1 second and the total simulation time is 400 seconds. The process noise, w_k denotes Gaussian with zero mean and 0.1 standard deviation. The measurement consists of the position and dimensions of the target,

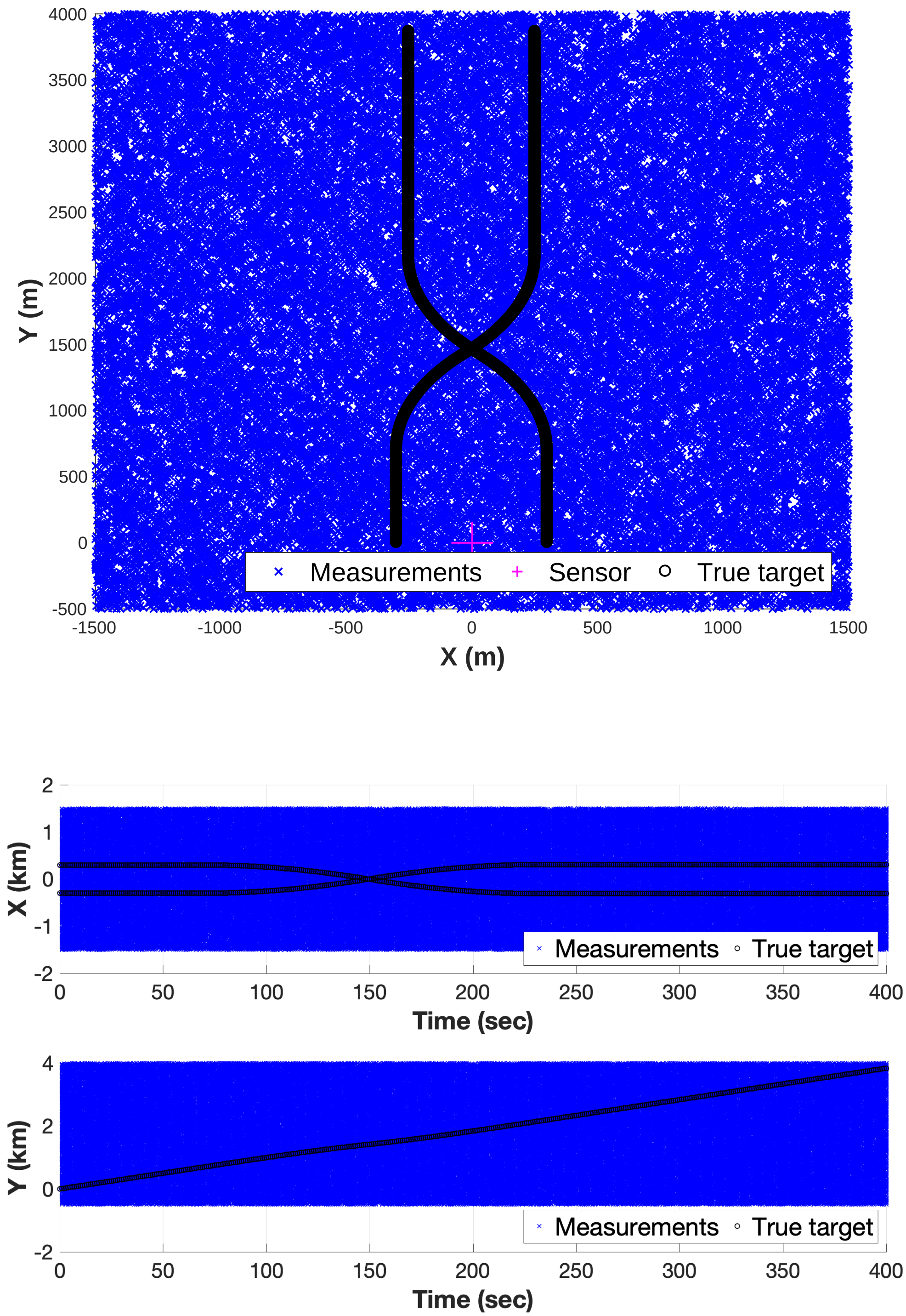

Fig. 2.8. Target trajectories and clutter (Average clutter = 100)

$z_k = \begin{bmatrix} z_{m,k} & z_{f,k} \end{bmatrix}^T = \begin{bmatrix} P_{z_x,k} & P_{z_y,k} & z_{RCS_k} \end{bmatrix}^T$. The observation model equation is represented by:

$$z_{m,k} = \begin{bmatrix} 1 & 0 & 0 & 0 & 0 \\ 0 & 1 & 0 & 0 & 0 \end{bmatrix} x_k + v_k$$

$$z_{f,k} = 2\pi d_k^2 \Big\{ 1 - \cos\big(\frac{hr_k^2}{d_k}\big) \Big\} + v_{f,k} \tag{2.44}$$

where the measurement noise, v_k is assumed to be Gaussian with zero mean and the following covariance, $R_k = diag([10^2, 10^2, 1])$.

In order to compare the performance of the track persistence between the three filters, we perform Monte Carlo simulation of 500 runs with the different detection probabilities and the average number of clutter values. Figures 2.9 and 2.10, and Table 1 show the number of track losses of three filters, which is defined as an event that the distance between the target and its track is longer than 50 m. The number of track losses is the sum of the numbers of track losses of target 1 and target 2. From Figures 2.9 and 2.10, and Table 1, the number of track losses of the JDAF and that of the JPDAF-AI are significantly high in the heavily cluttered and low detection probability environment since the filters cannot accurately distinguish the origin of the measurement when two targets are very close, and the amplitude of target 1 is less than that of clutter. However, the number of track losses of the proposed JPDAF-TKSDFI is very low even when the clutter density is high and/or the detection probability is low. On the whole, the proposed JPDAF-TKSDFI has much better performance than the JPDAF and JPDAF-AI in persistent target tracking, and thus is more robust than the JPDAF and JPDAF-AI for the closely spaced targets and in the heavily cluttered environment.

To show the computational complexity of the proposed algorithm, a Monte Carlo simulation with 500 runs was performed and average execution times of the proposed JPDAF-TKSDFI as well as JPDAF and JPDAF-AI were compared. For this simulation, we used a computer which has a 2.6 GHz Intel Core i5 processor and 8 GB 1600 MHz DDR3 memory. As shown in Figure 2.11, the execution time of the proposed

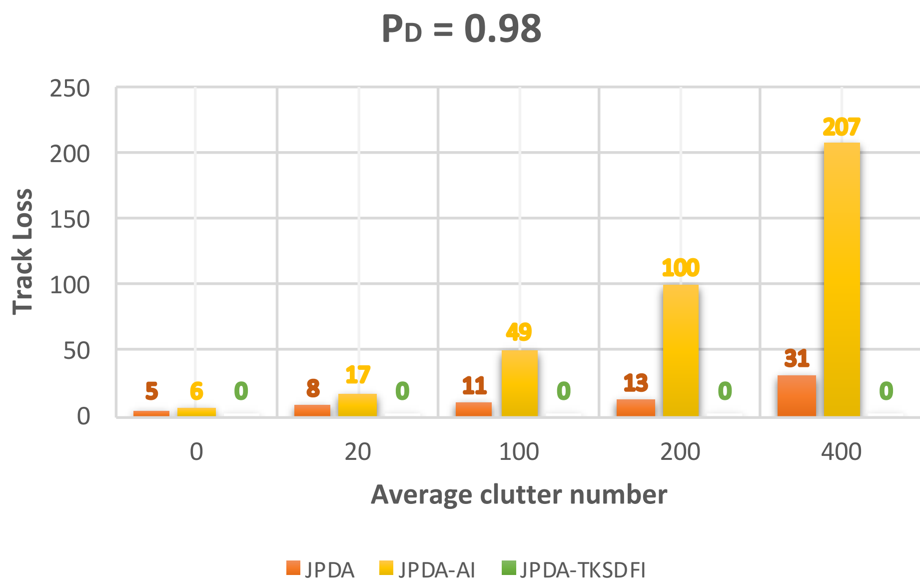

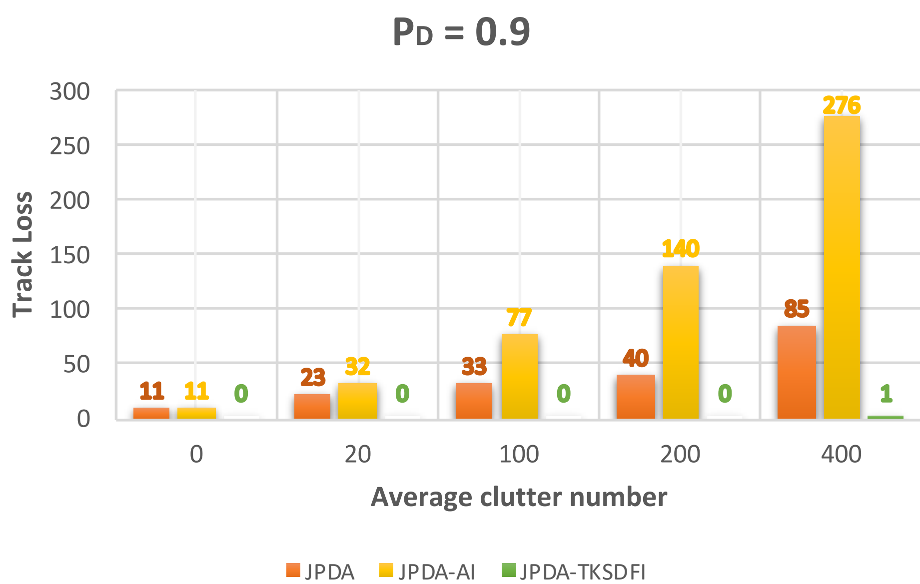

Fig. 2.9. Number of track losses of JPDAF, JPDAF-AI, and proposed JPDAF-TKSDFI ($P_D = 0.98$ and $P_D = 0.9$)

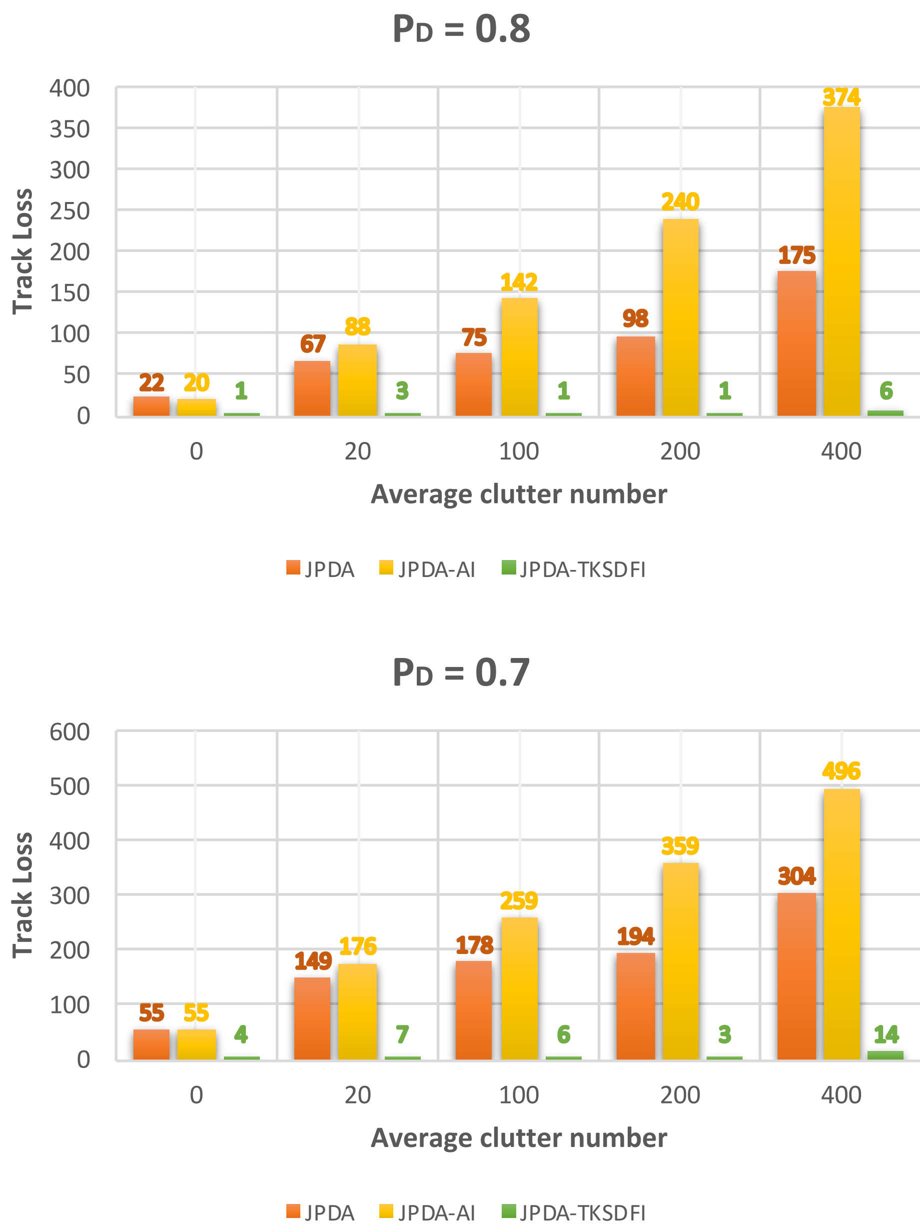

Fig. 2.10. Number of track losses of JPDAF, JPDAF-AI, and proposed JPDAF-TKSDFI ($P_D = 0.8$ and $P_D = 0.7$)

Table 2.1.
Number of track losses of JPDAF, JPDAF-AI, and proposed JPDAF-TKSDFI

	P_D											
Clutter density	0.98			0.9			0.8			0.7		
0	5	6	0	11	11	0	22	20	1	55	55	4
20	8	17	0	23	32	0	67	88	3	149	176	7
100	11	49	0	33	77	0	75	142	1	178	259	6
200	13	100	0	40	150	0	98	240	1	194	359	3
400	34	217	0	85	276	1	175	374	6	303	496	14

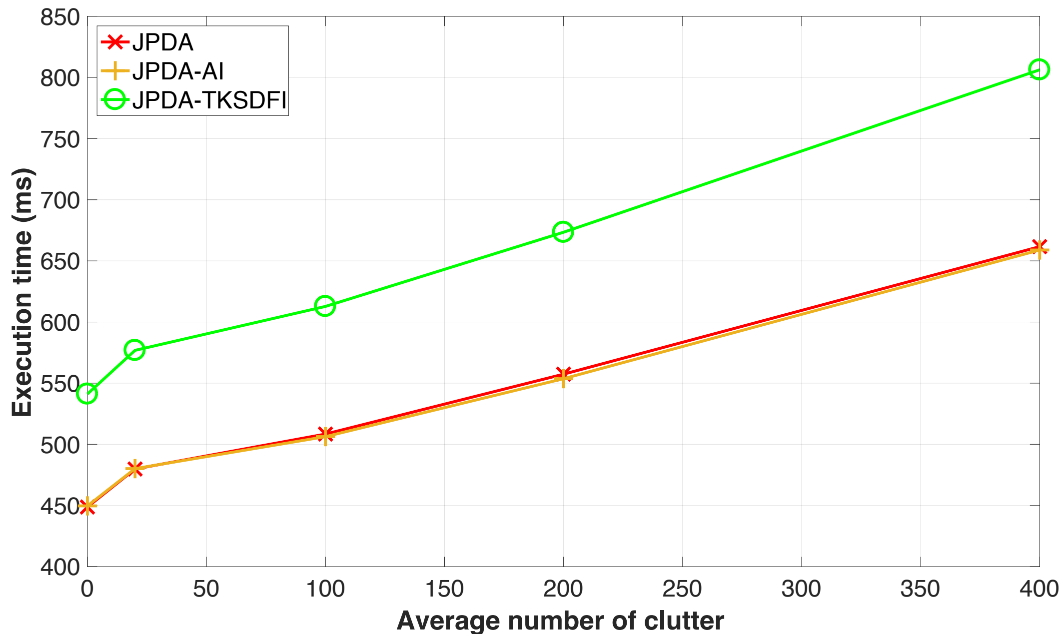

Fig. 2.11. Average execution time of JPDA, JPDA-AI, and JPDA-TKSDFI ($P_D = 0.98$)

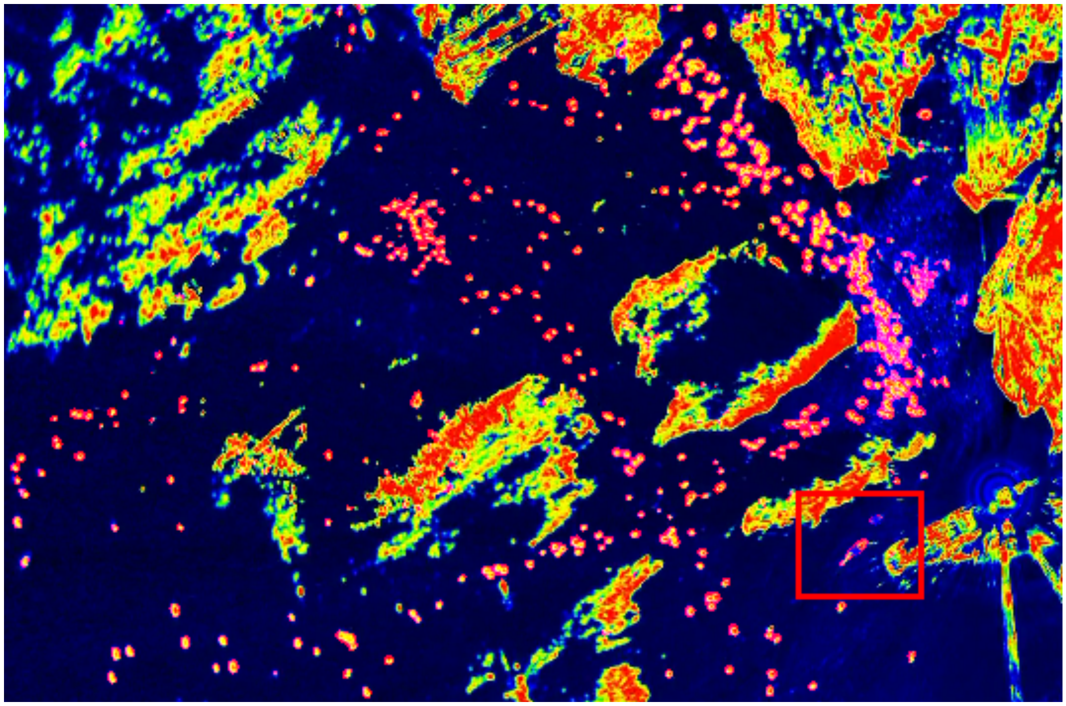

Fig. 2.12. Screen shot of the radar video of the Færder seilasen with C-Scope radar [40]

algorithm is higher than that of two other filters due to the augmented feature state of the proposed algorithm, but the growth rate of the proposed algorithm is similar to that of two other filters as the number of clutter increases.

Scenario 2

In comparison to the original JPDAF, the performance of the proposed JPDAF-TKSDFI is demonstrated with an illustrative multi-target tracking example in this scenario. Figure 2.12 shows a screen shot of the radar video of the Færder seilasen with C-Scope radar in Norway [40]. In the video, the total area is 5 km $\times$ 2.8 km and there are approximately 1,000 targets. For comparing the performance of the JPDAF and that of the proposed JPDAF-TKSDFI, we extract information on two targets from the area within the red box. The state of a target is composed of its position, velocity, and dimensions: $x_k = \begin{bmatrix} P_{x,k} & P_{y,k} & V_{x,k} & V_{y,k} & a_k & b_k \end{bmatrix}^T$. The discrete-time dynamic model of the target is represented by:

$$x_k = \begin{bmatrix} I_2 & TI_2 & 0_{2\times2} \\ 0_{2\times2} & I_2 & 0_{2\times2} \\ 0_{2\times2} & 0_{2\times2} & I_2 \end{bmatrix} x_{k-1} + \begin{bmatrix} \frac{T^2}{2} I_2 & 0_{2\times2} \\ TI_2 & 0_{2\times2} \\ 0_{2\times2} & \frac{T^2}{2} I_2 \end{bmatrix} w_{k-1} \tag{2.45}$$

where the sampling interval, T is 1 second. The process noise, w_k denotes Gaussian with zero mean and 0.1 standard deviation. The measurement consists of the position and dimensions of the target, $z_k = \begin{bmatrix} z_{m,k} & z_{f,k} \end{bmatrix}^T = \begin{bmatrix} P_{z_x,k} & P_{z_y,k} & z_{a_k} & z_{b_k} \end{bmatrix}^T$. The observation model equation is represented by:

$$\begin{aligned} z_{m,k} &= \begin{bmatrix} 1 & 0 & 0 & 0 & 0 & 0 \\ 0 & 1 & 0 & 0 & 0 & 0 \end{bmatrix} x_k + v_k \\ z_{f,k} &= \begin{bmatrix} a_k \left(1 + ((\frac{b_k}{a_k})^2 - 1)\frac{a_k^2 \cos^2\theta_k}{a_k^2\cos^2\theta_k + b_k^2 \sin^2\theta_k}\right)^{1/2} \\ b_k \left(1 + ((\frac{b_k}{a_k})^2 - 1)\frac{a_k^2 \cos^2\theta_k}{a_k^2\cos^2\theta_k + b_k^2 \sin^2\theta_k}\right)^{-1/2} \end{bmatrix} + v_k \end{aligned} \tag{2.46}$$

where the measurement noise, v_k is assumed to be Gaussian with zero mean and the following covariance, $R_k = diag([3^2, 3^2, 1, 1])$.

Figure 2.13 shows the estimates of the JPDAF and the proposed JPDAF-TKSDFI. For 18 time steps, the measurements denoted as the black crosses are originated from the two targets and clutter from the terrain in the lower right corner of Figure 2.13. Target 1 moves at a bearing of N45^{o}E from (861, 148) m, and target 2 moves at a bearing of S45^{o}W from (905, 193) m. The measurements of two targets extracted using the Fourier transform are merged when two targets are very close. When the two targets are closely spaced and the measurements are merged, the JPDAF uses the merged measurement to update the track 2 for target 2. Thus, the red asterisk trajectory (track 2) almost stay at the same place over time. Since there remains only the measurement from the terrain in the validation region of the track 1, the track 1 is likely to use the measurement which is deviated from the actual position of target 1. On the other hand, the proposed JPDAF-TKSDFI can identity the merged measurement and terrain measurement as clutter since the difference between the

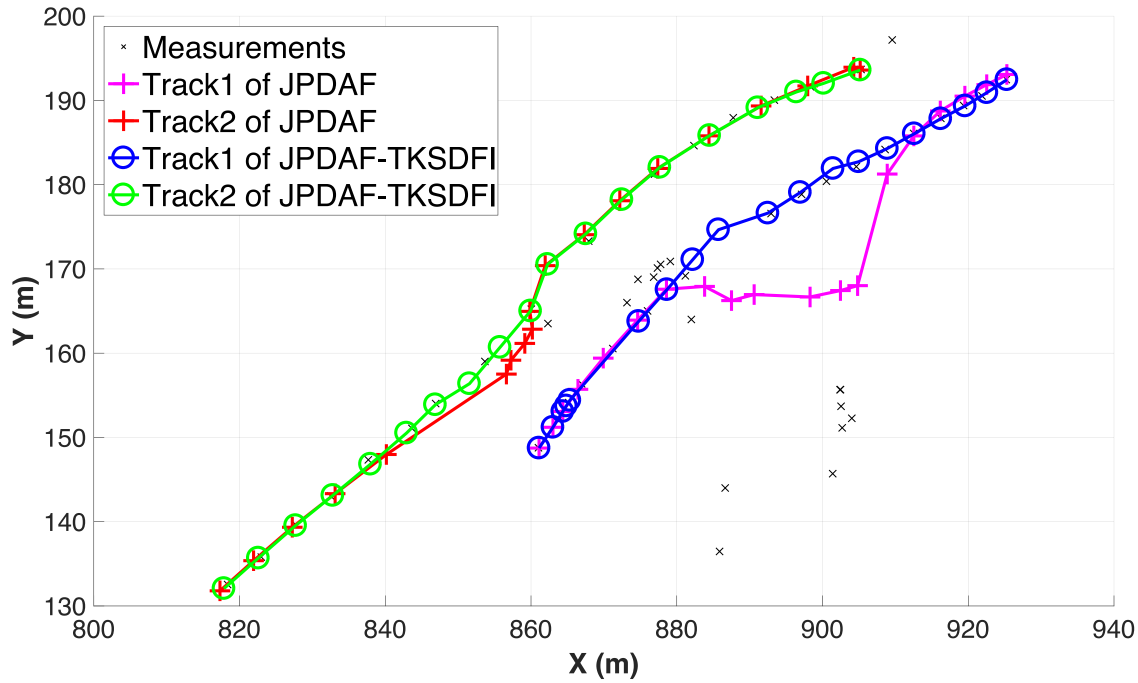

Fig. 2.13. Measurements and estimates computed by the JPDAF and the proposed JPDAF-TKSDFI

estimated target dimensions and the measured ones are large. Therefore, the proposed JPDA-TKSDFI can accurately keep track of both targets even in this difficult case where two targets get close to each other in the cluttered environment.

3. GAUSSIAN MIXTURE PROBABILITY HYPOTHESIS DENSITY FILTER AGAINST MEASUREMENT ORIGIN UNCERTAINTY

This chapter discusses a new GM-PHD filter which explicitly considers the uncertainty in the measurement origin. In Section 3.1, the motivation and literature review for this problem are presented. In Section 3.2, the models for multiple target tracking and the PHD filter are summarized. Section 3.3 presents a new GM-PHD filter that explicitly accounts for the measurement origin uncertainty. In Section 3.4, we demonstrate the performance of the proposed GM-PHD filter via comparison with the existing GM-PHD and its variant, N-scan GM-PHD filter.

3.1 Background and Motivation

MTT is the problem that assigns the measurements or identifications to tracks of targets and manages multiple tracks over time [1,3]. Initially, many MTT algorithms have been developed while considering the known and fixed number of targets [1, 2, 4, 41]. To further investigate MTT under the varying number of targets, Musicki et al. have proposed the JIPDA algorithm that simultaneously addresses the track initiation/termination along with each target track [13, 14]. To initiate, terminate, and update the tracks systematically, the JIPDA computes the probability of the individual track existence and extracts the valid sensor measurements for tracks out of clutter, called the JPDA [15, 32]. The JIPDA, however, is based on the restrictive assumptions that the target dynamics is linear and all the noises are assumed to be Gaussian [13, 14].

To eliminate the restrictive assumptions, Mahler has proposed an MTT algorithm using a point process theory, called the FISST [42, 43]. This method integrates the track initiation/termination and data association all together for MTT, while including practical considerations such as non-uniform distribution of clutter, intermittent transmission, etc. Despite its promising capability, the multi-target Bayesian filter based on the FISST framework is in general computationally demanding, making it difficult for practical implementation [44]. To address the computational complexity, the PHD filter has been proposed based on RFS theory and point process theory [44,45]. Vo et. al. have proposed the GM-PHD filter as a closed-form solution to the PHD filter [46,47]. Unlike the majority of the conventional data association filters [5,8,9,16], the GM-PHD (and PHD) filter does not have explicit data association (i.e., the measurement-to-track association) [44, 47]. Yazdian-Dehkordi et. al. have proposed the penalization scheme refining the weights of the Gaussian components due to the degradation of the estimation performance of the GM-PHD (and PHD) filter when targets are closely spaced [48]. However, this approach is prone to lose the estimates of targets when missed detection occurs consecutively over time. To improve the missed estimates problem, the RGM-PHD tracker was proposed which computes survival probability based on the state of a target and refines the weights of the closely spaced Gaussian components [49]; and the IPHD tracker has two auxiliary parameters in the standard target state, named the label and probability of existence [50]. However, these two improved approaches (RGM-PHD and IPHD) are based on *ad-hoc tuning* of some key parameters without explicit formulae, making it difficult to be implemented and generalized for other applications. To improve the accuracy of cardinality of the target estimates (i.e., more accurate estimate of the number of targets), the GM-CPHD filter has been proposed [51]. However, this approach suffers from not only heavy computational load in that it jointly propagates the target posterior intensity and cardinality distribution of targets, but also the missed estimates of targets, especially when the clutter density is high and/or the detection probability is low. To address the missed estimates of the targets in the GM-PHD filter, the N-scan GM-PHD filter was proposed which considers the history of weights of Gaussian components in the last N time steps, i.e., if the number of weights of individual Gaussian component in the last N time steps exceeds a predefined weight threshold (empirically chosen), then the Gaussian component will not be pruned [52]. However, the N-scan GM-PHD filter has its own problems such as defining the empirical parameters and delay in computing the estimates, when targets appear and/or disappear (since it needs N time steps to make a decision). Thus, to address the problem of the missed estimates of targets of the GM-PHD filter without suffering from the above-mentioned issues, we have proposed a new GM-PHD filter. Our approach explicitly considers the uncertainty in the measurement origin, i.e., whether 1) the measurement is clutter; 2) the measurement is originated from a target; and 3) there is no measurement [4]. To account for this uncertainty, a new error covariance update equation has been derived which computes the estimate error covariance of a newly generated Gaussian component corresponding to each measurement conditioned on the above three events. Hence, the new error covariance explicitly accounts for the uncertainty on whether a measurement is from a target or not analytically (i.e., not *ad-hoc tuning*); while the original GM-PHD filter computes the same estimate error covariances for all the newly generated Gaussian components. Different from the N-scan GM-PHD filter, our approach does not require to collect information over N time steps, and thus it does not suffer from time delay inherent in the N-scan GM-PHD filter.

In addition, if the proposed filter is implemented in the GM-PHD tracker, it can improve the trajectory tracking performance. This is because the GM-PHD tracker [53] (which is an extension of the GM-PHD filter) has a tendency to frequently lose the estimate of a target in heavily cluttered and/or low SNR environments [53, 54], while the proposed filter does not. Thus, the proposed GM-PHD filter can improve the trajectory tracking performance if it is implemented as a GM-PHD tracker. This thesis demonstrates the performance of the proposed filter via comparison with the original GM-PHD and N-scan GM-PHD filters with illustrative target tracking examples.

3.2 Models and Probability Hypothesis Density Filter

In this section, we introduce the state propagation and measurement models and the PHD filter to address MTT with the RFS in the Bayesian filtering framework.

Let X_k and Z_k denote the RFS of the multi-target states and the measurements at time step k, respectively.

$$X_k = \{x_k^1, \dots, x_k^{N_k}\} \tag{3.1}$$

$$Z_k = \{z_k^1, \dots, z_k^{T_k}\} \tag{3.2}$$

where $x_k^i \in \mathbb{R}^S$ and $z_k^j \in \mathbb{R}^O$ denote the state of the i-th target and the j-th measurement at time step k, respectively. N_k and T_k denote the number of targets and measurements at time step k, respectively. The spaces of RFSs of the multi-target states and measurements are Euclidean spaces $\mathbb{R}^S \times N_k$ and $\mathbb{R}^O \times T_k$, respectively. Since multiple targets can appear and disappear randomly in the surveillance area, the number of targets n_k can vary at each time step. Similarly, the number of measurements T_k can change over time due to false measurements.

Given the state and measurement RFSs, the discrete-time Bayesian recursive filtering equations for MTT are given by:

$$f(X_k|Z^{(k-1)}) = \int f(X_k|X_{k-1}) f(X_{k-1}|Z^{(k-1)}) \delta X_{k-1} \tag{3.3}$$

$$f(X_k|Z^{(k)}) = \frac{f(Z_k|X_k) f(X_k|Z^{(k-1)})}{\int f(Z_k|X_k) f(X_k|Z^{(k-1)}) \delta X_k} \tag{3.4}$$

where $Z^{(k)} = \{Z_1, \dots, Z_k\}$ is the measurement RFS sequence. $f(X_{k-1}|Z^{(k-1)})$ is the posterior distribution conditioned on the measurement RFS sequence $Z^{(k-1)}$ at time step $k-1$. $f(X_k|X_{k-1})$ is the multi-target Markov transition density. $f(X_k|Z^{(k-1)})$ is the prior distribution given the measurement RFS sequence $Z^{(k-1)}$ at time step k. $f(Z_k|X_k)$ is the multi-target likelihood function.

3.2.1 State Propagation and Measurement Models

In order to determine the multi-target Markov transition density $f(X_k|X_{k-1})$, we specify a multi-target state propagation model, i.e., a formula for the propagated random state set X_k in terms of the previous multi-target RFS $X_{k-1} = \{x_{k-1}^1, \ldots, x_{k-1}^{N_{k-1}}\}$ at time step k. The state RFS propagation can be described as follows [45]:

$$X_k = \varXi(X_{k-1}) \cup \varPsi(X_{k-1}) \cup \varPsi_{0,k} \tag{3.5}$$

where $\varXi(X_{k-1}) = \varXi(x_{k-1}^1) \cup \cdots \cup \varXi(x_{k-1}^{N_{k-1}})$ presents the state RFS of surviving targets propagated from the targets at the previous time step, $x_{k-1}^1, \ldots, x_{k-1}^{N_{k-1}}$, respectively. $\varXi(x_{k-1}^i) = \emptyset$ (target disappearance) with probability $1 - p_s(x_{k-1}^i)$ and $\varXi(x_{k-1}^i) = \{\mathbf{X}(x_{k-1}^i)\}$ with probability $p_s(x_{k-1}^i)$, where $p_s(x_{k-1}^i)$ is the probability that a target with state x_{k-1}^i will survive at time step k and $\mathbf{X}(x_{k-1}^i)$ is a random vector whose distribution is $f(x_k|x_{k-1}^i)$. $\varPsi(X_{k-1}) = \varPsi(x_{k-1}^1) \cup \cdots \cup \varPsi(x_{k-1}^{N_{k-1}})$ denotes the state RFS of newly spawned targets around the targets at the previous time step, $x_{k-1}^1, \ldots, x_{k-1}^{N_{k-1}}$, respectively. For instance, a target can be spawned when a fighter launches a missile or a tugboat finishes towing a ship and leaves the place. $\varPsi_{0,k}$ is the state RFS of born targets at time step k which are independent of the previous target states. This can happen when a target comes into the surveillance area of a sensor.

The RFS model of the measurements from the targets can be described as [45]:

$$Z_k = \varSigma(X_k) \cup C(X_k) \cup C_k \tag{3.6}$$

where $\varSigma(X_k) = \varSigma(x_k^1) \cup \cdots \cup \varSigma(x_k^{N_k})$ presents the measurement RFS produced by the targets whose states at current time step are $x_k^1, \ldots, x_k^{N_k}$, respectively. $\varSigma(x_k^i) = \emptyset$ (no measurement) with probability $1 - p_D(x_k^i)$ and $\varSigma(x_k^i) = \{\mathbf{Z}(x_k^i)\}$ with probability $p_D(x_k^i)$, where $\mathbf{Z}(x_k^i)$ is a random vector whose distribution is $f(z_k|x_k^i)$. $C(X_k)$ and C_k are the measurement RFSs of clutter which are dependent on and independent of the targets, respectively. In this thesis, the state-independent survival probability P_s and detection probability P_D, both of which are assumed to be constant are considered.

3.2.2 Probability Hypothesis Density Filter

To alleviate the computationally demanding problem in the multi-target Bayesian filter based on the FISST framework, the PHD filter has been proposed. The prior equation for the PHD filter is given as follows [45]:

$$I(x_k|Z^{(k-1)}) = b(x_k) + \int (P_s f(x_k|x_{k-1}) + sp(x_k|x_{k-1}))I(x_{k-1}|Z^{(k-1)})dx_{k-1} \quad (3.7)$$

If we assume that the prior probability distribution of multi-target is approximately Poisson, the posterior equation for the PHD filter can be derived as [45]:

$$I(x_k|Z^{(k)}) \backsimeq [1 - P_D]I(x_k|Z^{(k-1)}) + \sum_{z_k \in Z_k} \frac{P_D p(z_k|x_k)I(x_k|Z^{(k-1)})}{\lambda c(z_k) + \int P_D p(z_k|\eta_k)I(\eta_k|Z^{(k-1)})d\eta_k} \quad (3.8)$$

where $I(x_k|Z^{(k-1)})$ and $I(x_k|Z^{(k)})$ denote the intensities corresponding to the prior and posterior density functions of the multiple targets, respectively. $b(x_k)$ and $sp(x_k|x_{k-1})$ denote the intensities of birth and spawn RFSs, respectively. λ is the density of the Poisson clutter measurements. $c(z_k)$ is the pdf of the Poisson clutter process. Note that the GM-PHD filter has been proposed for an analytical solution to the PHD filter, which is explained in detail next.

3.3 Algorithm Development

In this section, the proposed GM-PHD filter is presented in detail. First, the filtering algorithm is presented in Section 3.1. Then, a new error covariance update equation for a Gaussian component is derived in Section 3.2.

3.3.1 Gaussian Mixture Hypothesis Density Filtering Algorithm

The GM-PHD filter interprets the prior and posterior intensities (3.7) and (3.8) as the Gaussian components, each can be presented as the propagation and update structures similar to the KF. In order to derive the propagation and update of the Gaussian components, the following assumptions are used.

Assumption 3 *The Markov density function and likelihood density function of a single target are assumed to be Gaussian.*

Assumption 4 *The intensities of the birth and spawn RFSs are Gaussian mixtures as follow [47]:*

$$b(x_k) = \sum_{j=1}^{J_{b,k}} w_{b,k}^j \mathcal{N}(x_k; x_{b,k}^j, P_{b,k}^j) \quad (3.9)$$

$$sp(x_k|x_{k-1}) = \sum_{j=1}^{J_{sp,k}} w_{sp,k}^j \mathcal{N}(x_k; F_{sp,k-1}^j x_{k-1} + d_{sp,k-1}^j, Q_{sp,k-1}^j) \quad (3.10)$$

where $\mathcal{N}(\cdot; m, P)$ denotes the Gaussian density function with mean m and covariance P. $J_{b,k}$ and $J_{sp,k}$ are the number of born and spawned Gaussian components at time step k, respectively. $w_{b,k}^j$ and $w_{sp,k}^j$ are the weights of the j-th Gaussian component born and spawned at time step k, respectively. $x_{b,k}^j$ and $P_{b,k}^j$ are the mean and covariance of the j-th born Gaussian component at time step k, respectively. $F_{sp,k-1}^j x_{k-1} + d_{sp,k-1}^j$ and $Q_{sp,k-1}^j$ are the mean and covariance of the j-th spawned Gaussian component at time step k, respectively.

With Assumption 3, the posterior intensity at time step $k-1$ is given by [47]:

$$I(x_{k-1}|Z^{(k-1)}) = \sum_{i=1}^{J_{k-1|k-1}} w_{k-1|k-1}^i \mathcal{N}(x_{k-1}; \hat{x}_{k-1|k-1}^i, \hat{P}_{k-1|k-1}^i) \quad (3.11)$$

where $J_{k-1|k-1}$ represents the number of posterior Gaussian components at time step $k-1$. $w_{k-1|k-1}^i$ is the posterior weight, and $\hat{x}_{k-1|k-1}^i$ and $\hat{P}_{k-1|k-1}^i$ denote the mean and covariance of the i-th Gaussian component at time step $k-1$. Based on Assumptions 3 and 4, the prior intensity can be derived with a Gaussian mixture function. Then, the prior intensity at time step k is given by [47]:

$$I(x_k|Z^{(k-1)}) = b(x_k) + I_{sp}(x_k|Z^{(k-1)}) + I_{sv}(x_k|Z^{(k-1)}) \quad (3.12)$$

where $I_{sp}(x_k|Z^{(k-1)})$ and $I_{sv}(x_k|Z^{(k-1)})$ are the intensities with the spawned and the survived Gaussian components, respectively. The intensity with the spawned Gaussian components can be written as [47]:

$$I_{sp}(x_k|Z^{(k-1)}) = \sum_{i=1}^{J_{k-1|k-1}} \sum_{j=1}^{J_{sp,k}} w^i_{k-1|k-1} w^j_{sp,k} \mathcal{N}(x_k; \hat{x}^{i,j}_{sp,k|k-1}, \hat{P}^{i,j}_{sp,k|k-1}) \tag{3.13}$$

where

$$\hat{x}^{i,j}_{sp,k|k-1} = F^j_{sp,k-1}\hat{x}^i_{k-1|k-1} + d^j_{sp,k-1} \tag{3.14}$$

$$\hat{P}^{i,j}_{sp,k|k-1} = F^j_{sp,k-1}\hat{P}^i_{k-1|k-1}\{F^j_{sp,k-1}\}^T + Q^j_{sp,k-1} \tag{3.15}$$

and $w^i_{k-1|k-1}$ denotes the posterior weight at time step $k-1$. The intensity with the surviving Gaussian components is given by [47]:

$$I_{sv}(x_k|Z^{(k-1)}) = P_s \sum_{i=1}^{J_{k-1|k-1}} w^i_{k-1|k-1}\mathcal{N}(x_k; \hat{x}^i_{sv,k|k-1}, \hat{P}^i_{sv,k|k-1}) \tag{3.16}$$

where

$$\hat{x}^i_{sv,k|k-1} = F_{k-1}\hat{x}^i_{k-1|k-1} \tag{3.17}$$

$$\hat{P}^i_{sv,k|k-1} = F_{k-1}\hat{P}^i_{k-1|k-1}F^T_{k-1} + Q_{k-1} \tag{3.18}$$

where F_{k-1} and Q_{k-1} are the transition matrix for the surviving Gaussian components and the covariance of the process noise, respectively. Based on the three intensities, the prior intensity can be represented as a Gaussian mixture function [47]:

$$I(x_k|Z^{(k-1)}) = \sum_{i=1}^{J_{k|k-1}} w^i_{k|k-1}\mathcal{N}(x_k; \hat{x}^i_{k|k-1}, \hat{P}^i_{k|k-1}) \tag{3.19}$$

where $w^i_{k|k-1} = P_s w^i_{k-1|k-1}$ denotes the prior weight from the posterior weight at time step $k-1$. $J_{k|k-1} = J_{b,k} + (J_{sp,k}+1) \times J_{k-1|k-1}$ represents the number of prior Gaussian components at time step k.

Then, the posterior intensity at time step k is given by [47]:

$$I(x_k|Z^{(k)}) \backsimeq [1-P_D]I(x_k|Z^{(k-1)}) + \sum_{l=1}^{T_k} \sum_{i=1}^{J_{k|k-1}} w^i_{k|k}(z^l_k)\mathcal{N}(x_k; \hat{x}^{i,l}_{k|k}, \hat{P}^i_{k|k}) \tag{3.20}$$

where

$$w^i_{k|k}(z^l_k) = \frac{P_D w^i_{k|k-1} p(z^l_k|\hat{x}^i_{k|k-1}, \hat{P}^i_{k|k-1})}{\lambda c(z^l_k) + P_D \sum_{j=1}^{J_{k|k-1}} w^j_{k|k-1} p(z^l_k|\hat{x}^j_{k|k-1}, \hat{P}^j_{k|k-1})} \tag{3.21}$$

$$K^i_k = \hat{P}^i_{k|k-1} H^T_k (H_k \hat{P}^i_{k|k-1} H^T_k + R_k)^{-1} \tag{3.22}$$

$$\hat{x}^{i,l}_{k|k} = \hat{x}^i_{k|k-1} + K^i_k (z^l_k - H_k \hat{x}^i_{k|k-1}) \tag{3.23}$$

$$\hat{P}^i_{k|k} = [I - K^i_k H_k] \hat{P}^i_{k|k-1} \tag{3.24}$$

where H_k is the measurement matrix, R_k is the measurement noise covariance matrix and I is the identity matrix. $J_{k|k} = (1 + T_k) J_{k|k-1}$ denotes the number of posterior Gaussian components at time step k. Note that equations (3.20) and (3.24) are rederived in Section 3.2 because the estimate error covariance does not explicitly account for the uncertainty on whether a measurement is from a target or not.

The prior and posterior numbers of targets are given by [47]:

$$\hat{N}_{k|k-1} = \hat{N}_{k-1|k-1} \left(P_s + \sum_{i=1}^{J_{sp,k}} w^i_{sp,k} \right) + \sum_{i=1}^{J_{b,k}} w^i_{b,k} \tag{3.25}$$

$$\hat{N}_{k|k} = \hat{N}_{k|k-1}[1 - P_D] + \sum_{l=1}^{T_k} \sum_{i=1}^{J_{k|k-1}} w^i_{k|k}(z^l_k) \tag{3.26}$$

Note that the pruning and extracting procedures of the proposed GM-PHD filter are the same as those used in the original GM-PHD filter in [47].

3.3.2 Modified Estimate Error Covariance

In this section, the uncertainty of whether the measurement used for the posterior process comes from a true target or false measurement is taken into account. Hence, the true/false uncertainty of the measurements used in the posterior process is mathematically derived and appropriately modified (3.20) and (3.24) based on uncertainty information. In particular, the estimate error covariances are derived corresponding to the three events that a measurement is a true target, clutter, and no measurement.

In the presence of clutter, the three events concerning a measurement can occur at any time.

- $M_{0,k}$ is the event that there is no measurement for updating the state at time step k.
- $M_{T,k}^{l}$ is the event that the l-th measurement is the true one at time step k.
- $M_{F,k}^{l}$ is the event that the l-th measurement is the false one at time step k.

The following assumption allows for analytically deriving the new estimate error covariance update equation while considering the uncertainty in the measurement origin.

Assumption 5 *The following statements hold:*

- *The targets are detected regardless of the false measurements. The detection of both targets and clutter are independent.*
- *The distribution of false measurements is the independent identically distributed (iid) uniform distribution.*
- *The location of a false measurement is independent of the true target and clutter measurements at all times.*
- *The number of false measurements m has a Poisson distribution with the density λ such that*

$$\mu_F(T) = \frac{(\lambda V_G)^T}{T!} e^{-\lambda V_G} \tag{3.27}$$

  where V_G is the volume of the surveillance region.

- *The discrete events $M_{T,k}^{l}$, $M_{F,k}^{l}$, and $M_{0,k}$ are independent of the previous events.*

Based on Assumption 5, the conditional pdfs under events $M_{T,k}^{l}$ and $M_{F,k}^{l}$ as well as the estimate error covariances corresponding to the three events are derived. The proposed algorithm uses both the distance information and ordering of all the measurements to evaluate the conditional probabilities that individual measurements are from the targets for the Gaussian component.

Probability Density Functions

In this section, the conditional probability that the l-th measurement is from a target for a i-th Gaussian component is described. To derive the conditional probability, we need to derive the pdfs of the NDS $D_k^{l,i}$ depending on the origin of the l-th measurement where the NSD of the l-th measurement z_k^l corresponding to the i-th Gaussian component is defined by [5]:

$$\begin{aligned} D_k^{i,l} &= (z_k^l - \hat{z}_{k|k-1}^i)^T (S_k^i)^{-1} (z_k^l - \hat{z}_{k|k-1}^i) \\ &= (\nu_k^{i,l})^T (S_k^i)^{-1} \nu_k^{i,l} \end{aligned} \tag{3.28}$$

where $\hat{z}_{k|k-1}^i = H_k \hat{x}_{k|k-1}^i$ denotes the predicted measurement and S_k^i is the covariance of the residual $\nu_k^{i,l}$ of the i-th Gaussian component, respectively. l is the order of the measurements from the predicted measurement of i-th Gaussian component. The probability functions derived in Lemmas 2 and 3 are used to calculate the conditional probability that the l-th measurement is from a target for the i-th Gaussian component.

Lemma 2 *With Assumption 5, the pdf of $D_k^{i,l}$ conditioned on the l-th measurement originated from a target among the T_k measurements is given by:*

$$\begin{aligned} f(D_k^{i,l} | M_{T,k}^l, T_k) = \frac{1}{Pr\{M_{T,k}^l, T_k\}} \binom{T_k - 1}{l-1} ((\frac{D_k^{i,l}}{\gamma})^{\frac{n}{2}})^{l-1} (1 - (\frac{D_k^{i,l}}{\gamma})^{\frac{n}{2}})^{T_k - l} \\ \cdot \mu_F(T_k - 1) \frac{n V_{D_k^{i,l}}}{2 D_k^{i,l}} \mathcal{N}(D_k^{i,l}) U(D_k^{i,l}; (0, \gamma]) P_D \end{aligned} \tag{3.29}$$

where $f(\cdot|\cdot)$ using a round bracket denotes a pdf and $Pr\{\cdot\}$ using a brace denotes a probability. $Pr\{M_{T,k}^l, T_k\}$ represents the probability that the l-th measurement among the T_k measurements is the true one. n is the dimension of the state. γ is the size of the surveillance region. The volume of the n-dimensional NDS $D_k^{i,l}$ is defined as [5]:

$$V_{D_k^{i,l}} = C_n |S_k^i|^{\frac{1}{2}} (D_k^{i,l})^{\frac{n}{2}} \tag{3.30}$$

The coefficient, C_n is given by:

$$C_n = \frac{\pi^{n/2}}{\Gamma(n/2+1)} \tag{3.31}$$

where the Gamma function, $\Gamma(n)$ is given by:

$$\Gamma(n) = \int_0^\infty x^{n-1} e^{-x} dx \tag{3.32}$$

To reduce the computational cost of the integral, in the thesis, we show the values of C_n in the 1, 2 and 3-dimensional cases such as $C_1 = 2$, $C_2 = \pi$ and $C_3 = \frac{4}{3}\pi$. $\binom{T_k}{l}$ is the combination of l selection of the T_k measurements at time step k. $\mathcal{N}(D_k^{i,l})$ denotes the multivariate Gaussian pdf of the target residual under event $M_{T,k}^l$, $\nu_k^{i,l} \sim \mathcal{N}(\nu_k^{i,l}; 0, S_k^i)$ obtained by replacing $\nu_k^{i,l}$ to $D_k^{i,l}$ such that

$$\mathcal{N}(D_k^{i,l}) = \frac{1}{\sqrt{(2\pi)^n |S_k^i|}} exp\{-\frac{D_k^{i,l}}{2}\} \tag{3.33}$$

$U(D_k^{i,l}; R)$ is a unit step function, defined by:

$$U(D_k^{i,l}; R) = \begin{cases} 1, & D_k^{i,l} \in R \\ 0, & elsewhere \end{cases} \tag{3.34}$$

Note that $(\frac{D_k^{i,l}}{\gamma})^{\frac{n}{2}}$ is the probability of the event that there is a false measurement closer to the i-th predicted measurement than the true one. Thus, $1 - (\frac{D_k^{i,l}}{\gamma})^{\frac{n}{2}}$ is the probability of the complement event. The proof of the Lemma 2 is given in Appendix C

For event $M_{F,k}^l$, the l-th measurement comes from a false measurement and has the distance information $D_k^{l,i}$. As illustrated in Figure 3.1, there are three cases under the assumption that the l-th measurement is a false measurement.

Case 1: The target is not detected.

Case 2: The target is detected but the NDS of the target is smaller than $D_k^{i,l}$.

Case 3: The target is detected but the NDS of the target is larger than $D_k^{i,l}$.

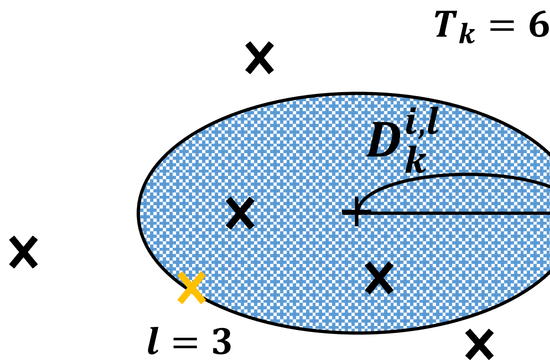

(a) Target is not detected

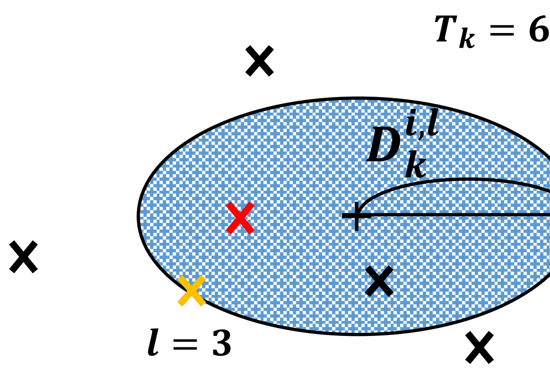

(b) NDS of target is smaller than $D_k^{i,l}$

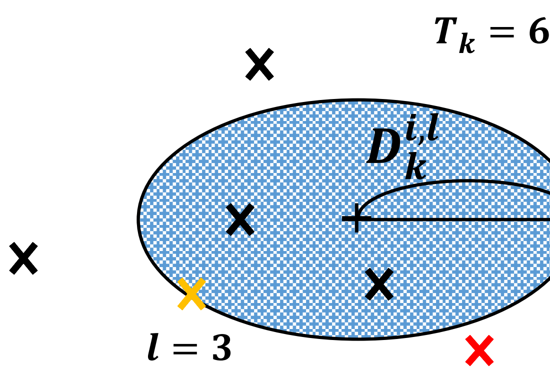

(c) NDS of target is larger than $D_k^{i,l}$

× : measurement × : Target × : selected l-th measurement

Fig. 3.1. An example of three cases conditioned on l-th measurement originated from clutter in 2-dimensional space

Lemma 3 *With Assumption 5 and the three cases, the pdf of $D_k^{i,l}$ conditioned on the l-th measurement originated from clutter among the T_k measurements is given by:*

$$
\begin{aligned}
f(D_k^{i,l}|M_{F,k}^l, T_k) = \frac{1}{Pr\{M_{F,k}^l T_k\}} \big(& (1-P_D) f_{c_l}(D_k^{i,l}|T_k)\mu_F(T_k) \\
& + P_D(1-P_R(D_k^{i,l})) f_{c_l}(D_k^{i,l}|T_k - 1)\mu_F(T_k - 1) \\
& + P_D P_R(D_k^{i,l}) f_{c_{l-1}}(D_k^{i,l}|T_k - 1)\mu_F(T_k - 1) \big)
\end{aligned} \tag{3.35}
$$

where $Pr\{M_{F,k}^l, T_k\}$ represents the probability that the l-th measurement among the T_k measurements is a false one. $f_{c_l}(D_k^{i,l}|T_k)$ is the conditional pdf of NDS $D_k^{i,l}$ of the l-th measurement under the assumptions that the l-th measurement comes from clutter and the number of false measurements is T_k. $P_R(D_k^{i,l})$ is the probability that the target exists in the region with size $\sqrt{D_k^{i,l}}$ such that [7]

$$
P_R(D_k^{i,l}) = \frac{1}{2^{\frac{n}{2}}\Gamma(\frac{n}{2})} \int_0^{D_k^{i,l}} q^{\frac{n}{2}-1} e^{-\frac{q}{2}} dq \tag{3.36}
$$

This result is proved in Appendix D.

The results of $Pr\{M_{T,k}^l, T_k\}$ and $Pr\{M_{F,k}^l, T_k\}$ are following:

$$
Pr\{M_{T,k}^l, T_k\} = \int_0^\infty f(D_k^{i,l}, M_{T,k}^l, T_k) dD_k^{i,l} \tag{3.37}
$$

$$
Pr\{M_{F,k}^l, T_k\} = \int_0^\infty f(D_k^{i,l}, M_{F,k}^l, T_k) dD_k^{i,l} \tag{3.38}
$$

It can be shown that

$$
Pr\{M_{T,k}^l, T_k\} + Pr\{M_{F,k}^l, T_k\} = (1-P_D)\mu_F(T_k) + P_D\mu_F(T_k - 1) \tag{3.39}
$$

This means the probability that the total number of measurements at time step k is T_k.

With the two pdfs of $D_k^{i,l}$, the conditional probability that the l-th measurement comes from the target for the i-th Gaussian component is denoted as $\beta_k^{i,l}$ and it can be derived as:

$$
\begin{aligned}
\beta_k^{i,l} &= Pr\{M_{T,k}^l | D_k^{i,l}, T_k\} \\
&= \frac{f(D_k^{i,l}, M_{T,k}^l, T_k)}{f(D_k^{i,l}, M_{T,k}^l, T_k) + f(D_k^{i,l}, M_{F,k}^l, T_k)}
\end{aligned} \tag{3.40}
$$

The conditional probability is used to calculate the estimate error covariance of the Gaussian component. The conditional probability that the l-th measurement is not target originated from target for the i-th Gaussian component becomes $1-\beta_k^{i,l}$.

Mean Square Error State Estimate

In this section, the error covariance of the state estimate for each Gaussian component is derived. Let the prior and posterior estimate errors of the i-th Gaussian component be defined as:

$$\bar{x}^i_{k|k-1} \triangleq x^i_k - \hat{x}^i_{k|k-1} \tag{3.41}$$

$$\tilde{x}^i_{k|k} \triangleq x^i_k - \hat{x}^i_{k|k} \tag{3.42}$$

First, under event M_0 where there is no measurement in the surveillance area, the estimate error covariance of the i-th Gaussian component for the target estimate $\hat{x}^i_{k|k}$ is equal to the prior estimate error covariance. However, the target is assumed to be perceivable [55], i.e, the target can be detected or not regardless of their existence. Owing to the target perceivability, the posterior estimate error covariance of the i-th Gaussian component under event M_0 is modified as [5]:

$$\hat{P}^i_{k|k,M_{o,k}} = \hat{P}^i_{k|k-1} + \frac{P_D(1-C_T)}{1-P_D} K^i_k S^i_k (K^i_k)^T \tag{3.43}$$

where $\hat{P}^i_{k|k-1}$ is the prior estimate error covariance of the i-th Gaussian component and C_T satisfies

$$C_T = \frac{\int_0^\gamma q^{\frac{n}{2}} e^{-\frac{q}{2}} dq}{n \int_0^\gamma q^{\frac{n}{2}-1} e^{-\frac{q}{2}} dq} \tag{3.44}$$

Note that the GM-PHD filter does not use the validation gate. In this case, the value of C_T is approximately 1 since γ is infinite value. Therefore, the estimate error covariance of the priori intensity in (3.20) is the same as (3.43). Second, the estimate error covariance of the i-th Gaussian component conditioned on event $M^l_{T,k}$ is equivalent to the estimate error covariance update equation of the KF,

$\hat{P}^i_{k|k,M^l_{T,k}} = \hat{P^i}_{k|k-1} - K^i_k S^i_k (K^i_k)^T$. Lastly, the estimate error covariance of the i-th Gaussian component conditioned on the number of total measurement T_k and the available NDS $D^{i,l}_k$ of the l-th measurement assumed to be originated from a clutter for event $M^l_{F,k}$ can be derived as follows.

Lemma 4 *With Assumption 5, the estimate error covariance of the i-th Gaussian component conditioned on event $M^l_{F,k}$ with the NDS, $D^{i,l}_k$, of the l-th measurement is given by:*

$$\hat{P}^{i,l}_{k|k,M^l_{F,k}} = \hat{P}^i_{k|k-1} - K^i_k S^i_k (K^i_k)^T + \alpha^{i,l}_k K^i_k S^i_k (K^i_k)^T \tag{3.45}$$

where

$$\begin{aligned}\alpha^{i,l}_k = & \frac{\lambda(1-P_D C_T)V_{D^{i,l}_k}(V_G - V_{D^{i,l}_k})}{\lambda(1-P_D)V_{D^{i,l}_k}(V_G - V_{D^{i,l}_k})} \\ & \frac{+P_D(C_T - P_R(D^{l,i}_k)C_T(D^{i,l}_k))(m-l)V_{D^{i,l}_k}}{+P_D(1-P_R(D^{i,l}_k))(m-l)V_{D^{i,l}_k}} \\ & \frac{+P_D P_R(D^{i,l}_k)C_T(D^{l,i}_k)(l-1)(V_G - V_{D^{i,l}_k})}{+P_D P_R(D^{i,l}_k)(l-1)(V_G - V_{D^{i,l}_k})}\end{aligned} \tag{3.46}$$

$$C_T(D^{i,l}_k) = \frac{\int_0^{D^{i,l}_k} q^{\frac{n}{2}} e^{-\frac{q}{2}} dq}{n\int_0^{D^{i,l}_k} q^{\frac{n}{2}-1} e^{-\frac{q}{2}} dq} \tag{3.47}$$

The estimate error covariance (3.45) can represent the actual measurement error by accounting for the uncertainty of a false measurement. The detailed proof is given in Appendix E. Note that the estimate error covariance of the i-th Gaussian component conditioned on event $M^l_{F,k}$ quantifies the increase of error in the state update from the state prediction due to the use of the l-th measurement which turns out to be the false measurement.

With $\hat{P}^i_{k|k,M_{o,k}}$, $\hat{P}^i_{k|k,M^l_{T,k}}$ and $\hat{P}_{k|k,M^l_F}(D^{i,l}_k)$, the posterior intensity at time step k of the proposed GM-PHD filter is given by:

$$I(x_k|Z^{(k)}) \backsimeq [1 - p_D(x_k)]I(x_k|Z^{(k-1)}) + \sum_{z^l_k \in Z_k} \sum_{i=1}^{J_{k|l-1}} w^i_k(z^l_k)\mathcal{N}(x_k; \hat{x}^{i,l}_{k|k}, \hat{P}^{i,l}_{k|k}) \tag{3.48}$$

where

$$\hat{P}_{k|k}^{i,l} = (1 - \beta_k^{i,l})\hat{P}_{k|k,M_F^l}^{i,l} + \beta_k^{i,l}\hat{P}_{k|k,M_{T,k}^l}^{i} + \beta_k^{i,l}(1 - \beta_k^{i,l})K_k^i \nu_k^{i,l}(\nu_k^{i,l})^T(K_k^i)^T \tag{3.49}$$

The posterior weight, Kalman gain and state equations of (3.48) are the same as (3.21), (3.22) and (3.23), respectively. Note that the proposed GM-PHD filter uses (3.48) for the posterior intensity instead of (3.20). The crucial part is the estimate error covariance (3.49), which is modified from (3.24) of the original GM-PHD filter, comprises three uncertainty. The first accounts for the uncertainty that the measurement might be clutter. It can be derived by $\hat{P}_{k|k,M_F}(D_k^{i,l})$ with weighting $1 - \beta_k^{i,l}$. The second represents the estimate error covariance when the measurement might be originated from a target. The third denotes the estimate error covariance reflecting the distance between the l-th measurement and the i-th propagated Gaussian component.

Remark 3 *Equation (3.49) can increase the covariance of the Gaussian component corresponding to the measurement originated from clutter. Due to the difference between the covariances of Gaussian components corresponding to the measurements from a target or clutter, the weight of the newly generated Gaussian component corresponding to the measurement originated from a target can be increased in the next time step. As a result, the proposed GM-PHD filter can provide the state estimate for the target which could have been lost in the original GM-PHD filter.*

3.4 Simulation Results

In this section, the performance of the proposed GM-PHD filter is demonstrated with illustrative target tracking examples, in comparison to the original GM-PHD and N-scan GM-PHD filters. The state vector of a target is composed of its position and velocity: $x_k = [P_{x,k}\ P_{y,k}\ V_{x,k}\ V_{y,k}]^T$. The discrete-time dynamic model of the target is represented by:

$$x_k = \begin{bmatrix} 1 & 0 & T & 0 \\ 0 & 1 & 0 & T \\ 0 & 0 & 1 & 0 \\ 0 & 0 & 0 & 1 \end{bmatrix} x_{k-1} + \begin{bmatrix} T^2/2 & 0 \\ 0 & T^2/2 \\ T & 0 \\ 0 & T \end{bmatrix} w_{k-1} \tag{3.50}$$

where the sampling interval T is 1 second and the total simulation time is 100 seconds. The process noise w_k of the surviving target is Gaussian with zero mean and 5 m/s^2 standard deviation. The process noise of the spawned target is Gaussian with zero mean and the following covariance

$$Q_{sp,k}^{(i)} = diag([100, 100, 400, 400]) \tag{3.51}$$

The weight of the spawned target is 0.05. The measurement vector represents the position of a target, $z_k = [P_{z_x,k}\ P_{z_y,k}]$. The observation model equation is given by:

$$z_k = \begin{bmatrix} 1 & 0 & 0 & 0 \\ 0 & 1 & 0 & 0 \end{bmatrix} x_k + v_k \tag{3.52}$$

where measurement noise v_k is assumed to be Gaussian with zero mean and 10 m standard deviation. In the Gaussian component pruning part, the truncation threshold of a Gaussian component is set to 10^{-5} and the merging threshold of Gaussian components is 4. The extraction threshold is set to 0.5. Note that all the noise and threshold values follow the simulation set-up in [47] for fair comparison of the proposed GM-PHD filter with the original GM-PHD filter.

The surveillance region is [-10000, -10000] $\times$ [10000, 10000] m^2. The possible maximum number of Gaussian components is set to be 400. Two scenarios demonstrate the performance of the proposed GM-PHD filter. In order to evaluate the performance of the proposed GM-PHD filter versus the original GM-PHD and N-scan GM-PHD filters in terms of the missed estimate of a target, the first scenario tests whether or not the three algorithms can correctly extract the estimate for a target while the

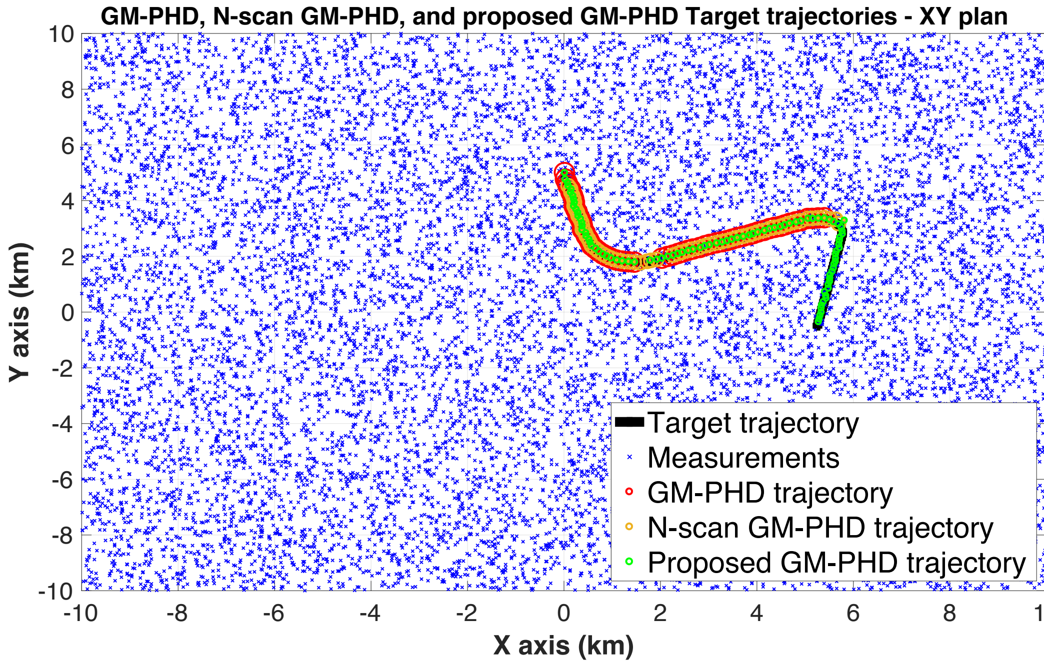

Fig. 3.2. Trajectory of a target, clutter, and target state estimates computed by GM-PHD, N-scan GM-PHD, and proposed GM-PHD filters

clutter density and P_D are varying. In the second scenario, the multi-target tracking ability of the three algorithms is tested by comparing the estimated number of targets computed by each algorithm with the true number of targets along when the number of targets varies over time. In the two scenarios, the clutter is uniformly distributed with respect to a Poisson distribution of the clutter density, λ, which is assumed to be known to the filters.

Scenario 1. In this scenario, only a single target is generated and maneuvers throughout the simulation, but the number of true target, i.e., $N_k = 1$, is unknown to the three algorithms. The intensity of the born target is set to be:

$$b(x_k) = 0.1\mathcal{N}(x_k; m_{b,k}^{(1)}, P_{b,k}^{(1)}) \tag{3.53}$$

where $m_{b,k}^{(1)} = [0, 5000, 25, -120]^T$ and $P_{b,k}^{(1)} = diag([100,\ 100,\ 25,\ 25])$ are the state vector and the error covariance of the each Gaussian component, respectively.

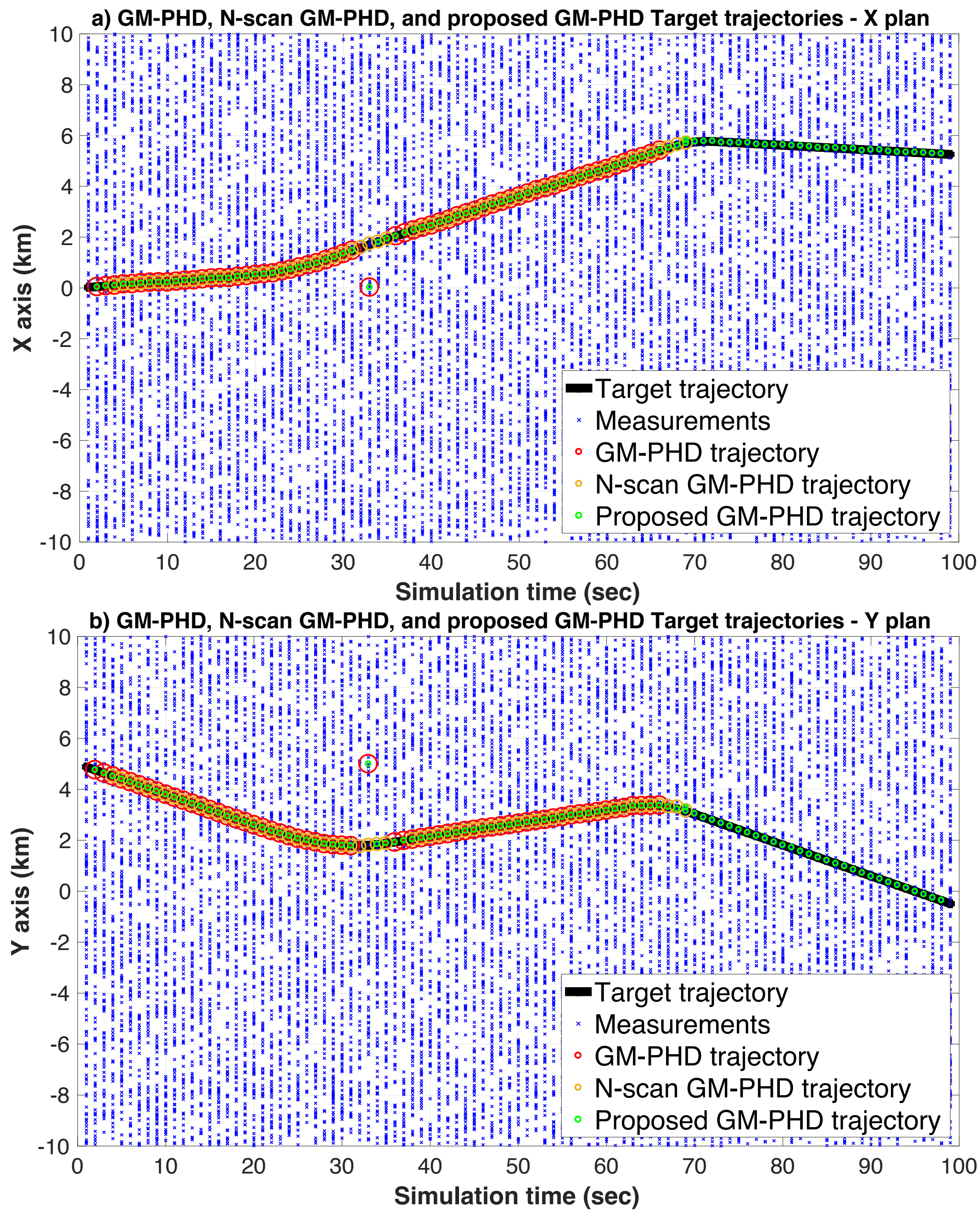

Fig. 3.3. Measurements, true target positions, and target state estimates computed by GM-PHD, N-scan GM-PHD, and proposed GM-PHD filters

Figure 3.2 shows the trajectory of the true target, the measurements obtained from a sensor, and the target state estimates computed by the GM-PHD, N-scan GM-PHD, and proposed GM-PHD filters, respectively, for the duration of 100 time steps. Figure 3.3 presents the filtering results separately along the X and Y axes so that the estimates of the three algorithms are clearly compared over time. The measurements include the position of the target along with the measurement noise and the false measurements coming from clutter. Specifically, the blue crosses indicate the measurements which consist of the target with noise as well as clutter. The black line indicates the position of the true target without the noise component. The red, gold, and green circles indicate the target state estimates computed by the GM-PHD, N-scan GM-PHD, and the proposed GM-PHD filters, respectively. In this case, the detection probability is set to 0.98 and the clutter density, λ, is 5×10^{-8} (i.e., an average of 200 clutter are generated in the surveillance area at each time step). Note that, at 65 and 69 seconds, the original GM-PHD and N-scan GM-PHD filters lose the estimate of the target and cannot provide the estimate for the target since after, while the proposed GM-PHD filter successfully regenerates the estimate of the target even after missing the estimate of the target for some time steps. This shows that the Gaussian component in the proposed GM-PHD filter is not eliminated by the pruning process but held by the extracting process since the weight of the Gaussian component is below 0.5. After several time steps, the weight of the Gaussian component in the proposed GM-PHD filter is increased by the measurement originated from the target. From these results, the proposed GM-PHD filter is able to keep the estimate of the target even though there are some missed state estimates for the target. The reason behind the intermittent missed estimate for the target depends on various factors such as the abrupt motion of the target, high clutter density, low signal-to-noise ratio, etc.

In order to compare the performance of the estimate persistence between the three algorithms, Monte Carlo simulation of 100 runs with different P_D and λ values is performed. Table 3.1 shows the number of the missed estimates of the target which is defined as an event that the estimate of the target does not exist successively in 3

Table 3.1.
Number of missed estimates of the target in GM-PHD, N-scan GM-PHD, and proposed GM-PHD filters

P_D	λ (Average number of clutter)	GM-PHD	N-scan GM-PHD	Proposed GM-PHD
0.9	5×10^{-10} (2)	54	19	35
	1×10^{-8} (40)	90	59	38
	5×10^{-8} (200)	100	79	63
0.95	5×10^{-10} (2)	31	14	17
	1×10^{-8} (40)	69	42	11
	5×10^{-8} (200)	95	85	26
0.98	5×10^{-10} (2)	13	9	2
	1×10^{-8} (40)	65	55	5
	5×10^{-8} (200)	92	85	18

scans or a distance between the target and its estimate is longer than 50 m. From Table 3.1 , the number of the missed estimates of the target in the GM-PHD and N-scan GM-PHD filters are similar to that in the proposed GM-PHD filter in the cases of high detection probability (e.g., $P_D = 0.98$) and low clutter density (e.g., $\lambda = 5 \times 10^{-11}$). However, the miss rate of the estimate of the target in the GM-PHD and N-scan GM-PHD filters significantly degrades when the detection probability is low and the clutter density is high. In cases when the detection probability and clutter density are both high, the number of the missed estimates of the target is still low for the proposed GM-PHD filter compared to the other two algorithms. Overall, the proposed GM-PHD filter has much better performance than the GM-PHD and N-scan GM-PHD filters in persistent target tracking under a large spectrum of P_D and λ values, and thus is more robust than the GM-PHD and N-scan GM-PHD filters in the presence of false measurements. Improving the missed estimate of the target by the proposed GM-PHD filter could also increase the trajectory tracking performance in the GM-PHD tracker if it is implemented in the GM-PHD tracker.

To evaluate the quality of the newly derived error covariance, we compare the credibility ratio of the proposed GM-PHD filter with those of the original GM-PHD and N-scan GM-PHD filters [56]. Since there are the multiple error covariance matrices of the Gaussian components in the proposed GM-PHD filter, we have computed the average of the credibility ratios of the error covariance matrices as follows:

$$
\begin{aligned}
ACR_k = &\frac{1}{J_{k|l-1} \times T_k} \\
&\sum_{z_k^l \in Z_k} \sum_{i=1}^{J_{k|l-1}} \frac{(x_k - \hat{x}_{k|k}^{i,l})^T (\hat{P}_{k|k}^{i,l})^{-1} (x_k - \hat{x}_{k|k}^{i,l})}{(x_k - \hat{x}_{k|k}^{i,l})^T (P_k^{i,l})^{-1} (x_k - \hat{x}_{k|k}^{i,l})}
\end{aligned}
\tag{3.54}
$$

Figure 3.4 depicts the average credibility ratio computed by the original GM-PHD, N-scan GM-PHD, and proposed GM- PHD filters when the average number of clutter per scan is 2 and the detection probability is 0.98. As illustrated in Figure 3.4, the average credibility ratio computed by the proposed GM-PHD filter is always lower

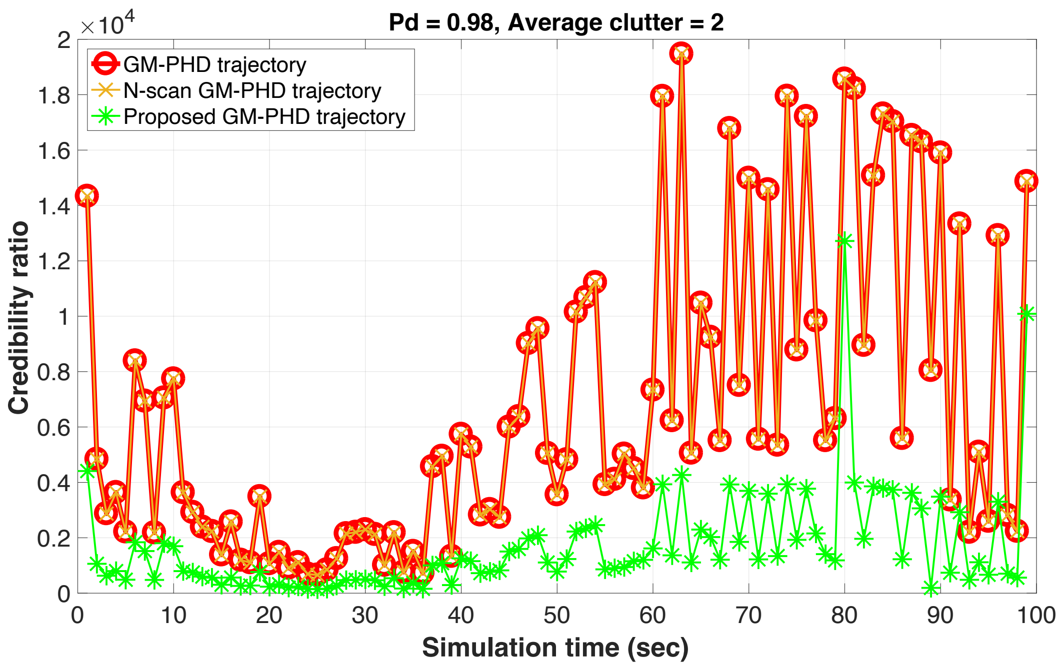

Fig. 3.4. Credibility ratio of GM-PHD, N-scan GM-PHD, and proposed GM-PHD filters ($P_D = 0.98$, average clutter $= 2$)

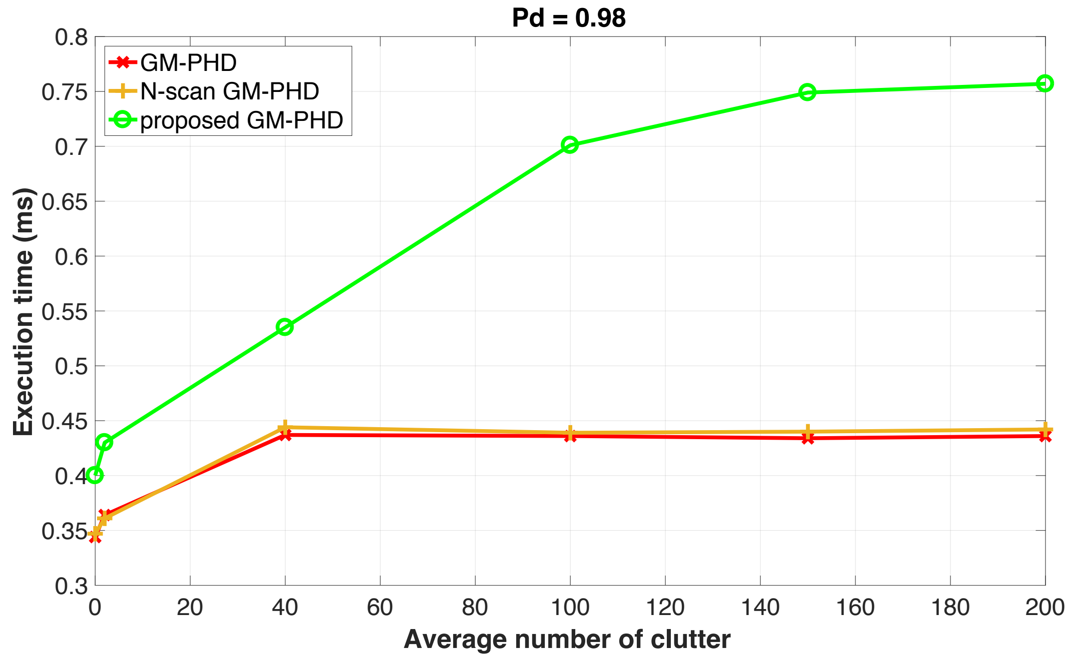

Fig. 3.5. Average execution time of GM-PHD, N-scan GM-PHD, and proposed GM-PHD filters ($P_D = 0.98$)

than the others, demonstrating the accuracy of the new covariance in the proposed algorithm outperforms others.

From Figure 3.5, a Monte Carlo simulation with 500 runs was performed and average execution times of the proposed GM-PHD filter as well as original GM-PHD filter and N-scan GM-PHD filter were compared. For this simulation, we used a laptop computer which has a 2.6 GHz Intel Core i5 processor and 8 GB 1600 MHz DDR3 memory. As shown in Figure 3.5, the execution time of the proposed algorithm is higher than that of two other filters due to the extra complexity of considering the measurement origin uncertainty, but the growth rate of the proposed algorithm is similar to that of two other filters as the number of clutter increases.

Scenario 2. This scenario emulates the terminal airspace area around an airport where there is high volume of air traffic. Here, multiple targets are generated at two possible locations and spawned from other targets. The maximum number of true

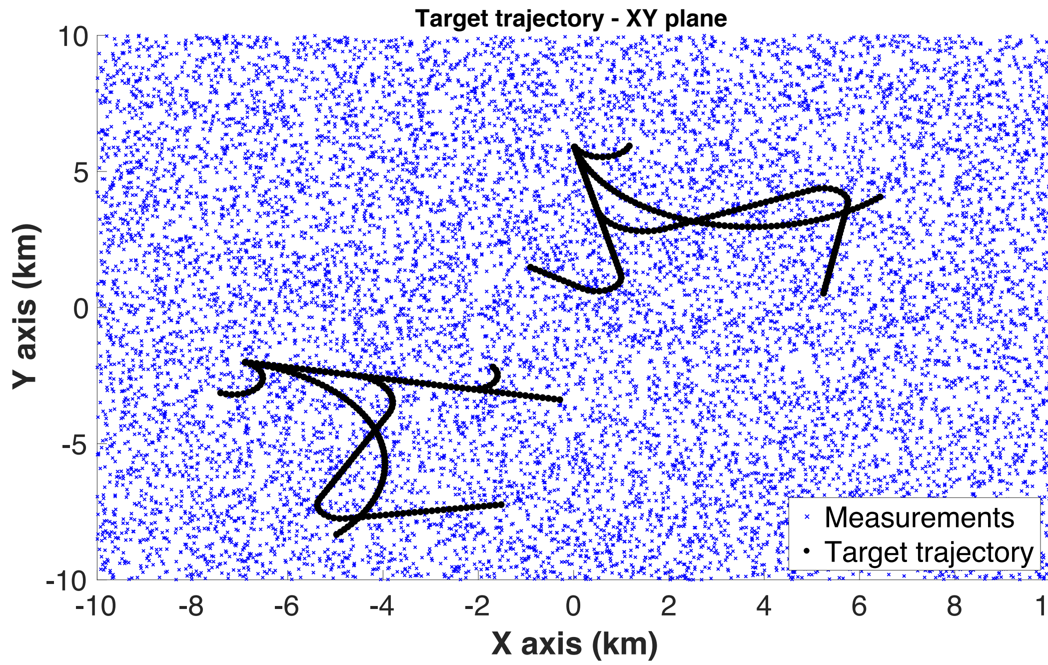

Fig. 3.6. Target trajectories and clutter

targets is 10 but the number varies over time since the targets appear and disappear randomly. The intensity of the born target is given by:

$$b(x_k) = 0.1\mathcal{N}(x_k; m_{b,k}^{(1)}, P_{b,k}^{(1)}) + 0.1\mathcal{N}(x_k; m_{b,k}^{(2)}, P_{b,k}^{(2)}) \tag{3.55}$$

where $m_{b,k}^{(1)} = [0, 5000, 25, -120]^T$ and $m_{b,k}^{(2)}$ =[-2500, 2000, 120, -25]^T are the state vectors of individual Gaussian components. The covariances are set to be the same as those used in Scenario 1.

Figure 3.6 shows the simulated multiple target tracking scenario with false measurements uniformly generated over 100 seconds. Here, the black dots are the trajectories of the true targets without the measurement noise and the blue crosses are the measurements that consist of the targets with measurement noise and clutter. The maneuvers of the targets vary randomly and the average number of clutter per scan is 200.

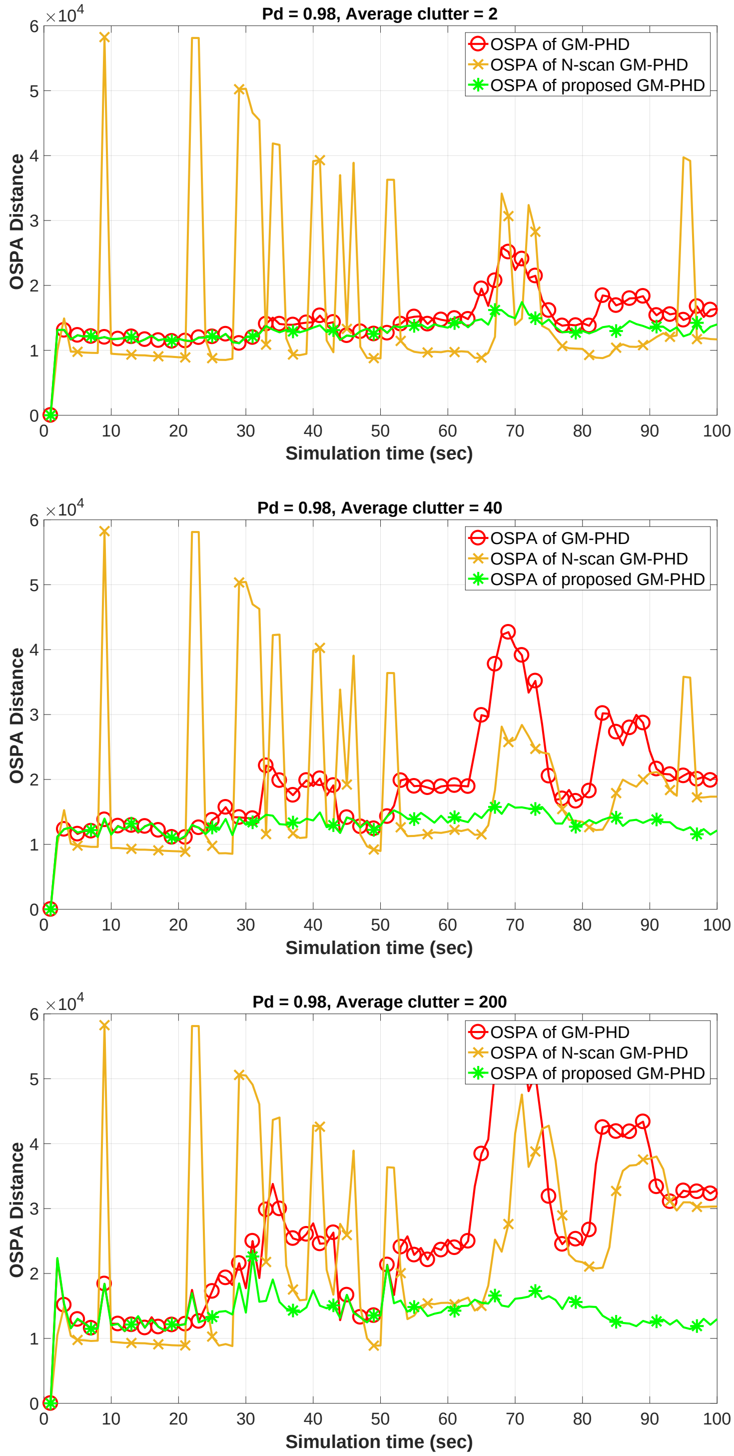

Fig. 3.7. Monte-Carlo results of mean OSPA distance of GM-PHD, N-scan GM-PHD, and proposed GM-PHD filters ($P_D = 0.98$)

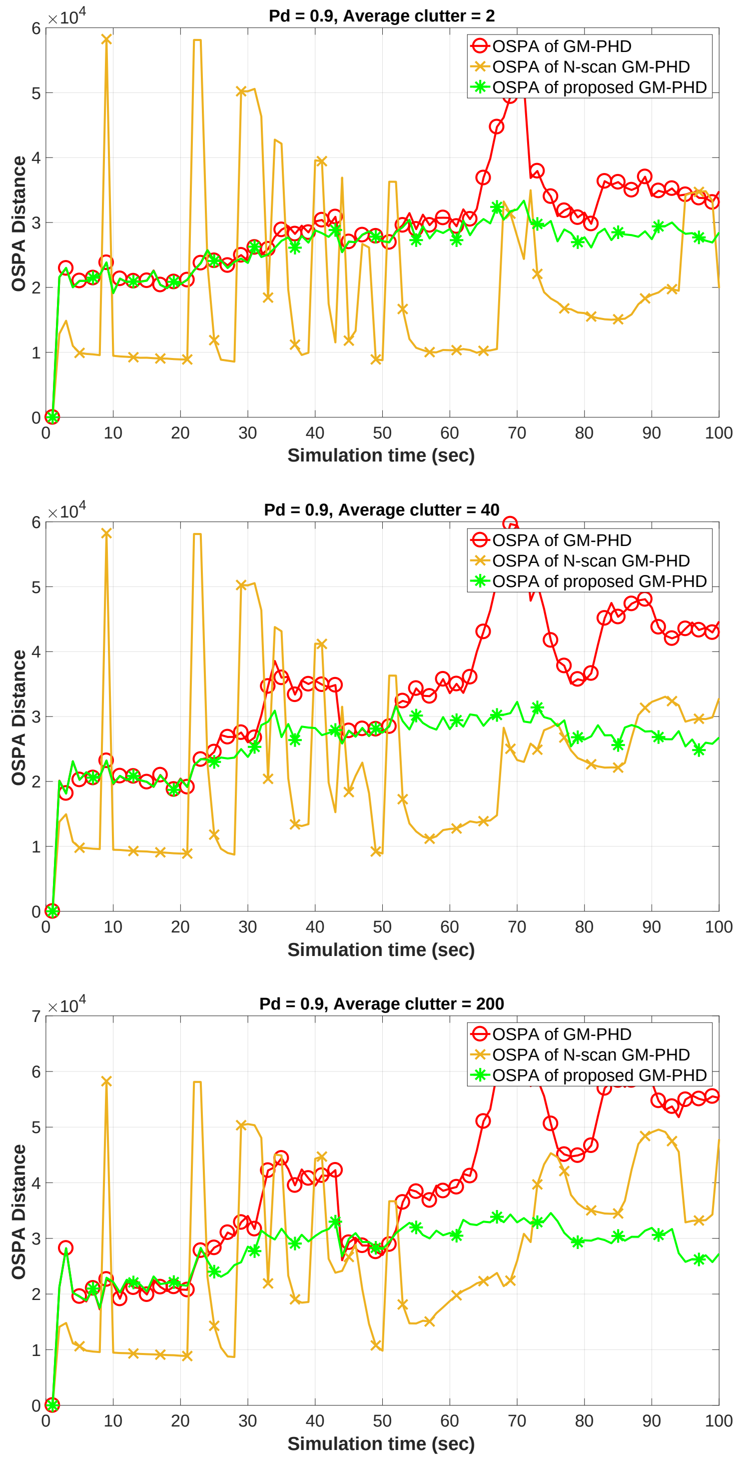

Fig. 3.8. Monte-Carlo results of mean OSPA distance of GM-PHD, N-scan GM-PHD, and proposed GM-PHD filters ($P_D = 0.9$)

In Figures 3.7 and 3.8, we consider the OSPA distance [57] as a metric to evaluate the performance of the proposed GM-PHD filter in comparison to the original GM-PHD, N-scan GM-PHD filters while varying the detection probability and the average number of clutter per scan. The OSPA distances (with order two and cutoff 10,000 m) are obtained via Monte-Carlo simulation with 100 runs. In this case, the OSPA distance predominantly reports a cardinality penalty (i.e. difference between the true number of targets and the estimated number of targets) because of a very high cutoff value relative to the magnitude of a typical localization error. As illustrated in Figures 3.7 and 3.8, both GM-PHD and N-scan GM-PHD filters have larger OSPA values than the proposed algorithm when the detection probability is high, which demonstrates the superior performance of the proposed algorithm in that the estimated number of targets computed by the proposed filter is more accurate than those of the other two filters. In case of the low detection probability, the OSPA distance of the N-scan GM-PHD filter is slightly lower than the proposed algorithm, but it has many high peaks due to the delay in Gaussian component initiation and termination as illustrated in Figure 3.9.

Figure 3.9 presents the true number of targets and the estimated number of targets computed by the GM-PHD, N-scan GM-PHD, and proposed GM-PHD filters when the number of average clutter per scan changes from 0 to 200. To demonstrate the multi-target tracking capability of the proposed GM-PHD filter, we perform the simulation subject to different densities of clutter. The black, red, gold, and green lines represent the true number of targets and the estimated numbers of targets computed by the GM-PHD, the N-scan GM-PHD, and the proposed GM-PHD filters, respectively. The estimated numbers of target are averaged over 100 Monte Carlo simulations. Note that the detection probability is set to 0.98 throughout the simulation, which is insignificant compared to the missed estimates of the targets.

At the Gaussian component initiation stage, when a new Gaussian component is generated, the initial covariance is large enough to account for the rapid maneuver of the target subject to heavy clutter. For that reason, the GM-PHD, N-scan GM-

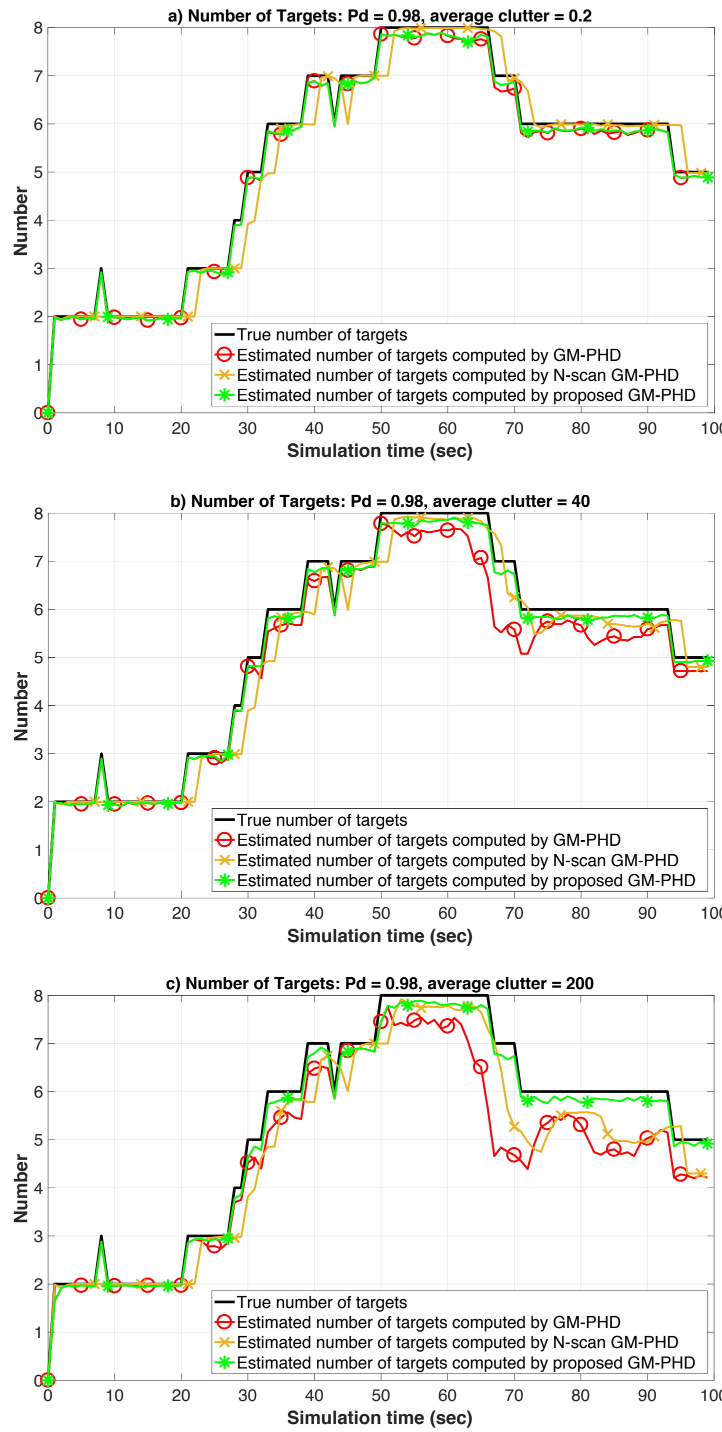

Fig. 3.9. True number of the targets and estimated numbers of targets computed by GM-PHD, N-scan GM-PHD, and proposed GM-PHD filters ($P_D = 0.98$)

PHD, and proposed GM-PHD filters all perform equally well up to 20 seconds in this simulation. However, the N-scan GM-PHD filter always shows the time delay when the targets appear and/or disappear as it requires at least N steps of weight history to determine whether or not extracting the estimate of the target. Furthermore, after 60 and 70 seconds, there are a large number of the missed estimates of targets observed in both the GM-PHD and N-scan GM-PHD filters due to their unreliable update of the error covariance without considering the uncertainty on whether a measurement is from a true target or not. This significantly degrades their tracking performance while our proposed GM-PHD filter maintains the estimated target number close to the true number. The difference between the true number target and the estimated numbers of targets computed by the GM-PHD, N-scan GM-PHD and the proposed GM-PHD filters is getting bigger as the number of false measurements (i.e., clutter density) increases.

Note that there are some parameters (i.e., model uncertainty, measurement noise, new birth target information, clutter density, detection probability, and packet loss/delay of a measurement, etc.) which need to be determined when the proposed target tracking filter is implemented in practical systems [58–64]; however, this is true for the original GM-PHD filter and its variants. Thus, further investigation addressing these practical concerns is needed for the proposed algorithm to be implemented in real-world applications.

4. GAUSSIAN MIXTURE PROBABILITY HYPOTHESIS DENSITY FILTER AND TRACKER WITH JUMP MARKOV SYSTEM MODELS

This chapter discusses a new GM-PHD filter with SD-JMS models and a GM-PHD tracker with JMS models to improve the performance of the existing GM-PHD filter with JMS models and to provide the identities of the target estimates, respectively. In Section 4.1, the motivation and literature review for this problem are presented. In Section 4.2, we summarize the system model for MTT with JMS models. Section 4.3 presents a new GM-PHD filter with SD-JMS models that can detect the state jumps depending on the state of a target. Section 4.4 presents a new GM-PHD tracker with JMS models which can provide the identities of target estimates. In Section 4.5, we demonstrate the performance of the proposed GM-PHD filter with SD-JMS models via comparison with the original GM-PHD filter and the GM-PHD filter with the JMS model. Additionally, we demonstrate the performance of the proposed GM-PHD tracker with JMS models via comparison with the GM-PHD tracker [65].

4.1 Background and Motivation

The GM-PHD filter could lose the estimates of maneuvering targets frequently due to the target's maneuver uncertainty. To address this issue, Pasha et al. proposed the GM-PHD filter which utilizes JMS models (or modes), each matched to a specific maneuver of the target, to address the maneuver uncertainty. The JMS models considered assume that mode transition probabilities are constant, irrespective of the target state [58]. However, this assumption is not valid in some applications where a target follows its planned trajectory. In this case, the mode transition probability is dependent on the target state. To address the state-dependent mode transition, Dong et al. considered a VS-MM algorithm which selects a subset of modes from the set of all possible modes depending on the target state [66]. However, the mode transition probabilities in each mode set are constant, as in the GM-PHD filter with JMS models. Due to the imprecise mode transition probabilities, the existing GM-PHD filter with JMS models could be likely to lose the estimates of the targets (e.g., aircraft, ships, ground vehicles or satellites) frequently in heavily cluttered and/or low SNR environments. Furthermore, the GM-PHD filter with JMS models does not provide temporal association of state estimates to targets over time, making it difficult for practical implementation in real target tracking systems that are interested in the trajectories of targets.

To address the missed estimates of the targets in the GM-PHD filter with JMS models, we propose a new GM-PHD filter with JMS models which have the state-dependent transitions, called the GM-PHD filter with the SD-JMS models. For example, in air traffic control, a target (aircraft) follows its planned trajectory which is composed of a series of waypoints. When the target reaches a waypoint, it takes a maneuver (i.e., changes its mode) to go to the next waypoint, thereby a mode transition occurs when the target state satisfies a condition (called as guard condition). A multiple-model based estimation algorithm for the JMS with state-dependent mode transitions was proposed in the authors' earlier work [67]. By integrating this algorithm with the GM-PHD filter, we develop the GM-PHD filter with SD-JMS models, which can address uncertainties in the number of targets to be tracked, clutter, and maneuvers. To provide both the state estimates of maneuvering targets at each time step and the labels of the state estimates for maneuvering targets over time, we propose a new GM-PHD tracker with JMS models. To determine the label of the state estimate for a maneuvering target, a new tag is assigned to newly generated Gaussian components for the target in the prior intensities. In the posterior intensities, the newly generated Gaussian components corresponding to measurements have the same tag as their associated Gaussian component in the prior intensities. After the pruning procedure, the unique label and state estimate for the target is extracted from the Gaussian components with the same tag.

4.2 System Model

In this section, we model a target as a discrete-time stochastic linear hybrid system whose mode transitions are dependent on the target state via a stochastic guard condition. A discrete-time stochastic linear hybrid system is given by

$$x_k = F_{k-1}(m_k)x_{k-1} + w_{k-1}(m_k) \tag{4.1}$$

$$z_k = H_k(m_k)x_k + v_k(m_k) \tag{4.2}$$

where $x_k \in \mathbb{R}^n$ and $z_k \in \mathbb{R}^p$ denote the target state and measurement at time k, respectively. $m_k \in \mathbb{M} = \{1, 2, \ldots, r\}$ is the mode and r denotes the number of modes (or models). $F_{k-1}(m_k)$ and $H_k(m_k)$ are the state transition and the measurement matrices corresponding to mode m_k. $w_{k-1}(m_k)$ and $v_k(m_k)$ are the process and measurement noises which are uncorrelated zero-mean, Gaussian sequences for mode m_k, respectively.

Then, the state transition probability density and the measurement likelihood are defined as

$$p(x_k|x_{k-1}, m_k) \tag{4.3}$$

$$p(z_k|x_k, m_k) \tag{4.4}$$

where $p(\cdot|\cdot)$ denotes a conditional probability density function (pdf). In addition, the mode evolution, $m_1, m_2, \ldots$ is a Markov chain described by a state-dependent mode transition matrix

$$\mathit{\Pi}(x_{k-1}) = \{\pi(i|j, x_{k-1})\}_{i,j=1,2,\ldots,r} \tag{4.5}$$

where $\pi(i|j, x_{k-1})$ is the conditional mode transition probability from mode j to mode i conditioned on the state x_{k-1},

$$\pi(i|j, x_{k-1}) := p(m_k = i|m_{k-1} = j, x_{k-1}). \tag{4.6}$$

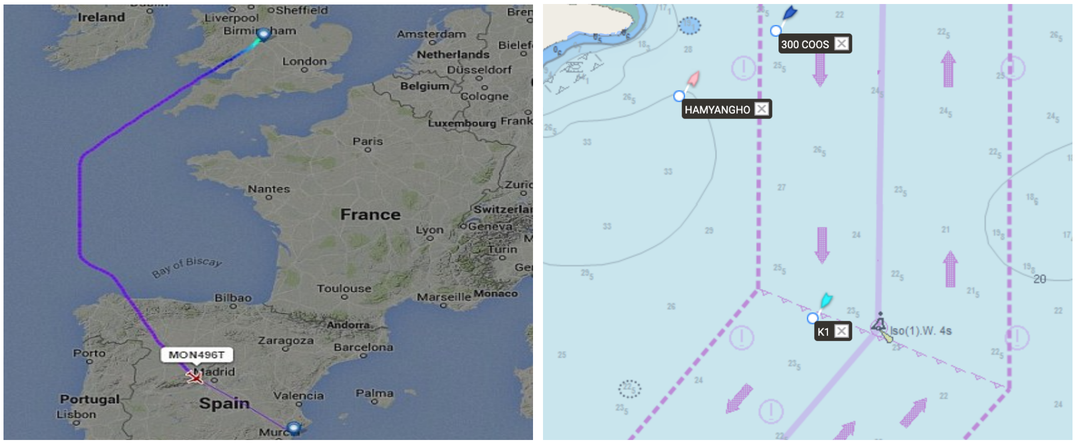

Fig. 4.1. Targets moving along planned trajectories [68, 69]

The transition of the augmented state vector $\xi_k = [x_k, m_k]^T \in \mathbb{X} = \mathbb{R}^n \times \mathbb{M}$ is governed by,

$$p(\xi_k|\xi_{k-1}) = p(x_k|x_{k-1}, m_k)\pi(i|j, x_{k-1}). \tag{4.7}$$

Then, a linear Gaussian JMS is a JMS with linear Gaussian models, i.e., conditioned on mode m_{k-1} the state transition density and measurement likelihood are given by

$$p(x_k|x_{k-1}, m_k) = \mathcal{N}(x_k; F_{k-1}(m_k)x_{k-1}, Q_{k-1}(m_k)) \tag{4.8}$$

$$p(z_k|x_k, m_k) = \mathcal{N}(z_k; H_k(m_k)x_k, R_k(m_k)) \tag{4.9}$$

where $Q_k(m_k)$ and $R_k(m_k)$ are covariance matrices of the process noise and measurement noise for mode m_k at time k, respectively. For brevity, we use the symbol, Ξ to represent the ordered pair of mean and covariance (x, P) of a Gaussian distribution as following,

$$\mathcal{N}(x, P) = \mathcal{N}(\Xi). \tag{4.10}$$

For the mode transition model, we consider a maneuvering target which follows the planned trajectory. As shown in Figure 4.1, aircraft or ships move along planned trajectories such as air routes or sea lanes. To track the target in the route, the dynamics of the target can be modeled as a stochastic linear hybrid system with multiple modes. In this scenario, a target is likely to take a maneuver when it gets close to its waypoints along the planned trajectory. Thus, the mode transition probability is dependent on the target state. In this thesis, we model the mode transition probability as a multivariate Gaussian pdf [67]

$$\begin{aligned}\pi(i|j, x_{k-1}) &= f(\mathbf{L}_{ij} x_{k-1} - \mu_{ij}) \\ &= a_{ij} + b_{ij} \mathcal{N}(\mathbf{L}_{ij} x_{k-1}; \mu_{ij}, \Sigma_{ij})\end{aligned} \tag{4.11}$$

where $\mathbf{L}_{ij}$ is a constant $q \times n$ matrix ($q \leq n$), and a_{ij} and b_{ij} are scalar constants such that $\pi(i|j, x_{k-1}) \geq 0$ for all $i, j = 1, \ldots, r$ and $\sum_{j=1}^{r} \pi(i|j, x_{k-1}) = 1$.

4.3 Gaussian Mixture Probability Hypothesis Density Filter with State-Dependent Jump Markov System Models

In this section, we present a closed-form PHD solution for linear Gaussian JMS models with state-dependent mode transition.

The posterior intensity at time $k-1$ is given by [58]:

$$I(x_{k-1}, m_{k-1}|Z^{(k-1)}) = \sum_{s=1}^{J_{k-1|k-1}^{m_{k-1}}} w_{k-1|k-1}^{s}(m_{k-1}) \mathcal{N}(x_{k-1}; \hat{\Xi}_{k-1|k-1}^{s}(m_{k-1})) \tag{4.12}$$

where $J_{k-1|k-1}^{m_{k-1}}$ represents the number of posterior Gaussian components for mode m_{k-1} at time $k-1$; $w_{k-1|k-1}^{s}(m_{k-1})$ is the weight of the s-th posterior Gaussian component for mode m_{k-1} at time $k-1$; $\hat{\Xi}_{k-1|k-1}^{s}(m_{k-1})$ is the ordered pair of mean, $\hat{x}_{k-1|k-1}^{s}(m_{k-1})$ and covariance, $\hat{P}_{k-1|k-1}^{s}(m_{k-1})$ of the s-th Gaussian component for mode m_{k-1} at time $k-1$. Then, the prior intensity at time k is given by [58]:

$$I(x_k, m_k|Z^{(k-1)}) = b(x_k, m_k) + I_{sp}(x_k, m_k|Z^{(k-1)}) + I_{sv}(x_k, m_k|Z^{(k-1)}) \tag{4.13}$$

where $I_{sp}(x_k, m_k|Z^{(k-1)})$ and $I_{sv}(x_k, m_k|Z^{(k-1)})$ are the intensities with the spawned and the survived Gaussian components for mode m_k, respectively. Each intensity can be derived by using the transition of the augmented state vector (4.7). The intensity of birth RFS for mode m_k at time k can be written as [58]:

$$b(x_k, m_k) = \sum_{t=1}^{J_{b,k}^{m_k}} \pi_b(m_k) w_{b,k}^t(m_k) \mathcal{N}(x_k; \hat{\Xi}_{b,k}^t(m_k)) \tag{4.14}$$

where $J_{b,k}^{m_k}$ is the number of newborn Gaussian components for mode m_k at time k; $\pi_b(m_k)$ is the mode probability that the target is operating in mode m_k at time k; $w_{b,k}^t(m_k)$ is the weight of born Gaussian components for mode m_k at time k; $\hat{\Xi}_{b,k}^t(m_k)$ denotes the pair of the mean, $(\hat{x}_{b,k}^t(m_k)$ and covariance, $\hat{P}_{b,k}^t(m_k))$ of the born Gaussian component. The intensity with the spawned Gaussian components can be written as [58]:

$$\begin{aligned} &I_{sp}(x_k, m_k | Z^{(k-1)}) \\ &\quad = \sum_{m_{k-1}} \sum_{s=1}^{J_{k-1|k-1}^{m_{k-1}}} \sum_{t=1}^{J_{sp,k}^{m_k, m_{k-1}}} w_{sp,k|k-1}^{s,t}(m_k, m_{k-1}) \mathcal{N}(x_k; \hat{\Xi}_{sp,k|k-1}^{s,t}(m_k, m_{k-1})) \end{aligned} \tag{4.15}$$

where $J_{sp,k}^{m_k, m_{k-1}}$ is the number of spawned Gaussian components for mode m_k from the Gaussian components for mode m_{k-1}; The weight of the spawned Gaussian components for mode m_k, $w_{sp,k|k-1}^{s,t}(m_k, m_{k-1})$ and the pair of the mean and covariance of the spawned Gaussian component, $\hat{\Xi}_{sp,k|k-1}^{s,t}(m_k, m_{k-1}) = (\hat{x}_{sp,k|k-1}^{s,t}(m_k, m_{k-1})$, $\hat{P}_{sp,k|k-1}^{s,t}(m_k, m_{k-1}))$ are given by [58]:

$$w_{sp,k|k-1}^{s,t}(m_k, m_{k-1}) = \pi_{sp}(m_k | m_{k-1}) w_{k-1|k-1}^s(m_{k-1}) w_{sp,k-1}^t(m_k, m_{k-1}) \tag{4.16}$$

$$\hat{x}_{sp,k|k-1}^{s,t}(m_k, m_{k-1}) = F_{sp,k-1}^t(m_k) \hat{x}_{k-1|k-1}^s(m_{k-1}) + d_{sp,k-1}^t \tag{4.17}$$

$$\hat{P}_{sp,k|k-1}^{s,t}(m_k, m_{k-1}) = F_{sp,k-1}^t(m_k) \hat{P}_{k-1|k-1}^s(m_{k-1}) \{F_{sp,k-1}^t(m_k)\}^T + Q_{sp,k-1}^t(m_k) \tag{4.18}$$

where $\pi_{sp}(m_k | m_{k-1})$ is the mode transition probability from mode m_{k-1} to mode m_k independent of the target state; $w_{sp,k-1}^t(m_k, m_{k-1})$ is the weight of the Gaussian component spawned at time k; $F_{sp,k-1}^t(m_k)$ and $Q_{sp,k-1}^t(m_k)$ are the transition matrix for the spawned Gaussian components and the covariance of the process noise for mode m_k, respectively. The intensity with the surviving Gaussian components is given by: [58]:

$$I_{sv}(x_k, m_k|Z^{(k-1)}) = \sum_{m_{k-1}} \sum_{s=1}^{J_{k-1|k-1}^{m_{k-1}}} w_{k|k-1}^{s}(m_k, m_{k-1})\mathcal{N}(x_k; \hat{\Xi}_{k|k-1}^{s}(m_k, m_{k-1})) \quad (4.19)$$

where the weight of surviving Gaussian components for mode m_k, $w_{k|k-1}^{s}(m_k, m_{k-1})$ and the pair of the mean and covariance, $\hat{\Xi}_{sv,k|k-1}^{s}(m_k, m_{k-1}) = (\hat{x}_{sv,k|k-1}^{s}(m_k, m_{k-1}),$ $\hat{P}_{sv,k|k-1}^{s}(m_k, m_{k-1}))$ are given by

$$w_{k|k-1}^{s}(m_k, m_{k-1}) = P_{sv}(m_{k-1})\pi(m_k|m_{k-1}, \hat{x}_{k-1|k-1}^{s}(m_{k-1}))w_{k-1|k-1}^{s}(m_{k-1}) \quad (4.20)$$

$$\hat{x}_{sv,k|k-1}^{s}(m_k, m_{k-1}) = F_{k-1}(m_k)\hat{x}_{k-1|k-1}^{s}(m_{k-1}) \quad (4.21)$$

$$\hat{P}_{sv,k|k-1}^{s}(m_k, m_{k-1}) = F_{k-1}(m_k)\hat{P}_{k-1|k-1}^{s}(m_{k-1})\{F_{k-1}(m_k)\}^T + Q_{k-1}(m_k) \quad (4.22)$$

where $\pi(m_k|m_{k-1}, \hat{x}_{k-1|k-1}^{s}(m_{k-1}))$ is the mode transition probability from mode m_{k-1} to mode m_k dependent on the target state estimate, $\hat{x}_{k-1|k-1}^{s}(m_{k-1})$. The mode transition probability is computed by (4.11). $P_{sv}(m_{k-1})$ is the probability of target survival which is assumed to be independent of the target state. $F_{k-1}(m_k)$ and $Q_{k-1}(m_k)$ are the transition matrix for the surviving Gaussian components and the covariance of the process noise for mode m_k, respectively. Based on these three intensities, the prior intensity can be represented as a Gaussian mixture function [58]:

$$I(x_k, m_k|Z^{(k-1)}) = \sum_{s=1}^{J_{k|k-1}^{m_k}} w_{k|k-1}^{s}(m_k)\mathcal{N}(x_k; \hat{\Xi}_{k|k-1}^{s}(m_k)) \quad (4.23)$$

where $J_{k|k-1}^{m_k}$ represents the number of prior Gaussian components for mode m_k at time k; $w_{k|k-1}^{s}(m_k)$ is the weight of the s-th prior Gaussian component for mode m_k at time k; $\hat{\Xi}_{k|k-1}^{s}(m_k)$ is the ordered pair of mean, $\hat{x}_{k|k-1}^{s}(m_k)$ and covariance, $\hat{P}_{k|k-1}^{s}(m_k)$ of the prior Gaussian component.

Then, the posterior intensity at time k is given by [58]:

$$\begin{aligned} I(x_k, m_k|Z^{(k)}) &= [1 - P_D(m_k)]I(x_k, m_k|Z^{(k-1)}) \\ &\quad + \sum_{t=1}^{T_k} \sum_{s=1}^{J_{k|k-1}^{m_k}} w_{k|k}^{s}(m_k; z_k^t)\mathcal{N}(x_k; \hat{\Xi}_{k|k}^{s,t}(m_k)) \end{aligned} \quad (4.24)$$

where the weight, $w^s_{k|k}(m_k; z^t_k)$, and the pair of the mean and covariance of the Gaussian component in the posterior intensity, $\hat{\Xi}^{s,t}_{k|k}(m_k) = (\hat{x}^{s,t}_{k|k}(m_k), \hat{P}^{s,t}_{k|k}(m_k))$ are given by [58]:

$$w^s_{k|k}(m_k; z^t_k) = \frac{P_D w^{s,m_k}_{k|k-1} p(z^t_k | \hat{x}^{s,m_k}_{k|k-1}, \hat{P}^{s,m_k}_{k|k-1})}{\kappa_k(z^t_k) + P_D \sum_{j=1}^{J^{m_k}_{k|k-1}} w^{j,m_k}_{k|k-1} p(z^t_k | \hat{x}^{j,m_k}_{k|k-1}, \hat{P}^{j,m_k}_{k|k-1})} \tag{4.25}$$

$$K^s_k(m_k) = \hat{P}^s_{k|k-1}(m_k)\{H_k(m_k)\}^T \left(H_k(m_k)\hat{P}^s_{k|k-1}(m_k)\{H_k(m_k)\}^T + R_k(m_k)\right)^{-1} \tag{4.26}$$

$$\hat{x}^{s,t}_{k|k}(m_k) = \hat{x}^s_{k|k-1}(m_k) + K^s_k(m_k)(z^t_k - H_k(m_k)\hat{x}^s_{k|k-1}(m_k)) \tag{4.27}$$

$$\hat{P}^s_{k|k}(m_k) = [I - K^s_k(m_k)H_k(m_k)]\hat{P}^s_{k|k-1}(m_k) \tag{4.28}$$

where I is the identity matrix; $J^{m_k}_{k|k} = (1 + T_k)J^{m_k}_{k|k-1}$ denotes the number of posterior Gaussian components for mode m_k at time k. Then, the expected number of predicted targets is given by [58]:

$$\hat{N}_{k|k-1} = \hat{N}_{b,k} + \hat{N}_{sp,k|k-1} + \hat{N}_{sv,k|k-1} \tag{4.29}$$

where

$$\hat{N}_{b,k} = \sum_{m_k} \sum_{t=1}^{J^{m_k}_{b,k}} \pi_b(m_k) w^t_{b,k}(m_k) \tag{4.30}$$

$$\hat{N}_{sp,k|k-1} = \sum_{m_k} \sum_{m_{k-1}} \sum_{s=1}^{J^{m_{k-1}}_{k-1|k-1}} \sum_{t=1}^{J^{m_k,m_{k-1}}_{sp,k}} \pi_{sp}(m_k|m_{k-1}) w^s_{k-1|k-1}(m_{k-1}) w^t_{sp,k-1}(m_k, m_{k-1}) \tag{4.31}$$

$$\hat{N}_{sv,k|k-1} = \sum_{m_k} \sum_{m_{k-1}} \sum_{s=1}^{J^{m_{k-1}}_{k-1|k-1}} P_{sv}(m_{k-1}) \pi(m_k | m_{k-1}, \hat{x}^s_{k-1|k-1}(m_{k-1})) w^s_{k-1|k-1}(m_{k-1}) \tag{4.32}$$

The expected number of targets is given by [58]:

$$\hat{N}_{k|k} = \sum_{m_k} [1 - P_D(m_k)] \sum_{s=1}^{J^{m_k}_{k|k-1}} w^s_{k|k-1}(m_k) + \sum_{t=1}^{T_k} \sum_{m_k} \sum_{s=1}^{J^{m_k}_{k|k-1}} w^s_{k|k}(m_k; z^t_k). \tag{4.33}$$

The pruning and extracting procedures of the proposed GM-PHD filter are the same as those used in the original GM-PHD filter in [47].

In summary, the pseudo-codes for the prior and posterior equations of the proposed GM-PHD filter with SD-JMS models are summarized in Algorithms 1 and 2.

Algorithm 1 Pseudo-code for the prior intensity of the GM-PHD filter with SD-JMS models

Input $\{\{w^s_{k-1|k-1}(m_{k-1}),\, \hat{x}^s_{k-1|k-1}(m_{k-1}), \hat{P}^s_{k-1|k-1}(m_{k-1})\}_{s=1}^{J^{m_{k-1}}_{k-1|k-1}}\}_{m_{k-1}=1}^{r}$

// Initiation of the number of prior Gaussian components
for $m_k = 1$ to r **do**
    $J^{m_k}_{k|k-1} = 0$
end for

// Prior intensity for born targets
for $m_k = 1$ to r **do**
    for $t = 1$ to $J_{b,k|k}$ **do**
        $J^{m_k}_{k|k-1} = J^{m_k}_{k|k-1} + 1,$
        $w^{J^{m_k}_{k|k-1}}_{k|k-1}(m_k) = \pi(m_k) w^t_{b,k}(m_k),$
        $\hat{x}^{J^{m_k}_{k|k-1}}_{k|k-1} = x^t_{b,k}(m_k),\ \hat{P}^{J^{m_k}_{k|k-1}}_{k|k-1} = P^t_{b,k}(m_k)$
    end for
end for

4.4 Gaussian Mixture Probability Hypothesis Density Tracker with Jump Markov System Models

In this section, we propose a GM-PHD tracker with JMS models which represents the prior and posterior intensities (3.7) and (3.8) with the Gaussian components, each

// Prior intensity for spawned targets

for $m_k = 1$ to r **do**

  for $m_{k-1} = 1$ to r **do**

    for $s = 1$ to $J_{k-1|k-1}^{m_{k-1}}$ **do**

      for $t = 1$ to $J_{sp,k}^{m_k,m_{k-1}}$ **do**

        $J_{k|k-1}^{m_k} = J_{k|k-1}^{m_k} + 1,$

        $w_{k|k-1}^{J_{k|k-1}^{m_k}}(m_k) = \pi(m_k|m_{k-1}) w_{k-1|k-1}^{s}(m_{k-1}) w_{sp,k-1}^{t}(m_k, m_{k-1})$

        $\hat{x}_{k|k-1}^{J_{k|k-1}^{m_k}}(m_k) = F_{sp,k-1}^{t}(m_k)\hat{x}_{k-1|k-1}^{s}(m_{k-1}) + d_{sp,k-1}^{t},$

        $\hat{P}_{k|k-1}^{J_{k|k-1}^{m_k}}(m_k) = F_{sp,k-1}^{t}(m_k)\hat{P}_{k-1|k-1}^{s}(m_{k-1})\{F_{sp,k-1}^{t}(m_k)\}^T$

          $+Q_{sp,k-1}^{t}(m_k)$

      end for

    end for

  end for

end for

// Prior intensity for existing targets
for $m_k = 1$ to r **do**
    for $m_{k-1} = 1$ to r **do**
        for $s = 1$ to $J_{k-1|k-1}^{m_{k-1}}$ **do**
            $J_{k|k-1}^{m_k} = J_{k|k-1}^{m_k} + 1,$
            $w_{k|k-1}^{J_{k|k-1}^{m_k}}(m_k) = P_{sv}(m_k)\pi(m_k|m_{k-1}\hat{x}_{k-1|k-1}^s(m_{k-1}))w_{k-1|k-1}^s(m_{k-1})$
            $\hat{x}_{k|k-1}^{J_{k|k-1}^{m_k}}(m_k) = F_{k-1}(m_k)\hat{x}_{k-1|k-1}^s(m_{k-1}),$
            $\hat{P}_{k|k-1}^{J_{k|k-1}^{m_k}}(m_k) = F_{k-1}(m_k)\hat{P}_{k-1|k-1}^s(m_{k-1})\{F_{k-1}(m_k)\}^T + Q_{k-1}(m_k)$
        end for
    end for
end for

// Calculation of Kalman gain
for $m_k = 1$ to r **do**
    for $s = 1$ to $J_{k|k-1}^{m_k}$ **do**
        $S_k^s(m_k) = H_k(m_k)\hat{P}_{k|k-1}^s(m_k)\{H_k(m_k)\}^T + R_k(m_k),$
        $K_k^s(m_k) = \hat{P}_{k|k-1}^s(m_k)\{H_k(m_k)\}^T\{S_k^s(m_k)\}^{-1}$
    end for
end for

Output $\{\{w_{k|k-1}^s(m_k), \hat{x}_{k|k-1}^s(m_k), \hat{P}_{k|k-1}^s(m_k)\}_{s=1}^{J_{k|k-1}^{m_k}}\}_{m_k=1}^r$

Algorithm 2 Pseudo-code for the posterior intensity of the GM-PHD filter with SD-JMS models

Input $\{\{w^s_{k|k-1}(m_k),\, \hat{x}^s_{k|k-1}(m_k), \hat{P}^s_{k|k-1}(m_k)\}_{s=1}^{J^{m_k}_{k|k-1}}\}_{m_k=1}^{r}, Z_k = \{z^t_k\}_{t=1}^{T_k}$

// Posterior intensity for the case that there is no measurement

for $m_k = 1$ to r **do**

    for $s = 1$ to $J^{m_k}_{k|k-1}$ **do**

        $w^s_{k|k}(m_k) = (1 - P_D) w^s_{k|k-1}(m_k),$

        $\hat{x}^s_{k|k}(m_k) = \hat{x}^s_{k|k-1}(m_k),$

        $\hat{P}^s_{k|k}(m_k) = \hat{P}^s_{k|k-1}(m_k)$

    end for

end for

// Posterior intensity for the existing Gaussian components and new Gaussian components

for $m_k = 1$ to r **do**

  for $t = 1$ to T_k **do**

    $SumWeight = 0$

    for $s = 1$ to $J_{k|k-1}^{m_k}$ **do**

      $ID = (t+1) \times J_{k|k-1}^{m_k} + s,$

      $w_{k|k}^{ID}(m_k) = P_D w_{k|k-1}^{s}(m_k)\mathcal{N}(z_k^t; H_k(m_k)\hat{x}_{k|k-1}^{s}(m_k)),$

      $SumWeight = SumWeight + w_{k|k}^{ID},$

      $\hat{x}_{k|k}^{ID}(m_k) = \hat{x}_{k|k-1}^{s}(m_k) + K_k^s(m_k)(z_k^t - H_k(m_k)\hat{x}_{k|k-1}^{s}(m_k)),$

      $\hat{P}_{k|k}^{ID}(m_k) = \hat{P}_{k|k}^{s}(m_k)$

    end for

    for $s = 1$ to $J_{k|k-1}^{m_k}$ **do**

      $ID = (t+1)J_{k|k-1}^{m_k} + s,$

      $w_{k|k}^{ID}(m_k) = \frac{w_{k|k}^{ID}(m_k)}{\kappa_k(z_k^t)+SumWeight}$

    end for

  end for

  $J_{k|k}^{m_k} = (T_k + 1)J_{k|k-1}^{m_k}$

end for

Output $\{\{w_{k|k}^{s}(m_k), \hat{x}_{k|k}^{s}(m_k), \hat{P}_{k|k}^{s}(m_k)\}_{s=1}^{J_{k|k}^{m_k}}\}_{m_k=1}^{r}$

of which can be expressed with the prior and the posterior structures similar to the KF [58].

The main idea of the GM-PHD tracker with JMS models is to assign tags to Gaussian components and update the assigned tags over time, and thus to provide the trajectories of targets. In the prior intensities, a new tag is assigned to the Gaussian components for a born target or a spawned target. In addition, the Gaussian components for a surviving target have the same tag as the Gaussian components in the posterior intensities at previous time. In the posterior intensities, newly generated Gaussian components corresponding to measurements have the same tag as the associated Gaussian component in the prior intensity. Based on this concept, the tag is managed over time without affecting the GM-PHD recursion with JMS models.

The posterior intensity for mode m_{k-1} at time $k-1$ is given by (4.12). The set of tags of the Gaussian components in the posterior intensity for mode m_{k-1} at time $k-1$ can be written as:

$$\mathcal{T}_{k-1|k-1}(m_{k-1}) = \left\{\tau^{1}_{k-1|k-1}(m_{k-1}), \cdots, \tau^{s}_{k-1|k-1}(m_{k-1}), \cdots, \tau^{J_{k-1|k-1}(m_{k-1})}_{k-1|k-1}(m_{k-1})\right\} \tag{4.34}$$

where $\tau^{s}_{k-1|k-1}(m_{k-1})$ is the tag of the s-th Gaussian component for mode m_{k-1} at time k. Then, the set of tags of the Gaussian components in the posterior intensities at time $k-1$ can be written as:

$$\mathcal{T}_{k-1|k-1} = \bigcup_{m_{k-1}=1}^{r} \mathcal{T}_{k-1|k-1}(m_{k-1}) \tag{4.35}$$

The prior intensity for mode m_k at time k can be decomposed into three terms as (4.13). With Assumption 4, the intensity of birth RFS for mode m_k at time k is given by (4.14). To identify the newborn Gaussian components for mode m_k at time k, new tags are assigned to the individual newborn Gaussian components. The set of tags of the newborn Gaussian components for mode m_k at time k can be written as:

$$\mathcal{T}_{b,k}(m_k) = \left\{\tau^{1}_{b,k}(m_k), \cdots, \tau^{t}_{b,k}(m_k), \cdots, \tau^{J_{b,k}(m_k)}_{b,k}(m_k)\right\} \tag{4.36}$$

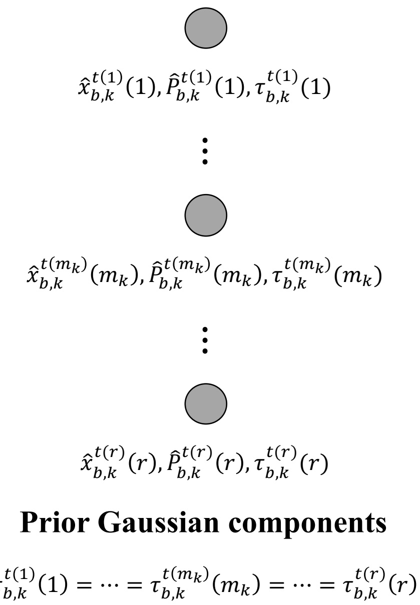

Fig. 4.2. Tree structures of the Gaussian components for a born target in the prior intensities

where $\tau_{b,k}^{t}(m_k)$ is the tag of the t-th newborn Gaussian components for mode m_k at time k. Then, the set of tags of the newborn Gaussian components at time k can be written as:

$$\mathcal{T}_{b,k} = \bigcup_{m_k=1}^{r} \mathcal{T}_{b,k}(m_k) \tag{4.37}$$

Note that the tag of the newborn Gaussian components for a born target is the same as those in all other modes, i.e., $\tau_{b,k}^{t(1)}(1) = \cdots = \tau_{b,k}^{t(m_k)}(m_k) = \cdots = \tau_{b,k}^{t(r)}(r)$ (see Figure 4.2 With Assumption 4, the intensity of the spawned Gaussian components for mode m_k at time k is given by (4.15). For the spawned Gaussian component for mode m_k at time k, a new tag which is different from that of the associated Gaussian component for mode m_{k-1} at time $k-1$ is assigned. The set of tags of the spawned Gaussian components for mode m_k at time k can be written as:

$$\mathcal{T}_{sp,k|k-1}(m_k) = \left\{\tau_{sp,k|k-1}^{1,1}(m_k), \cdots, \tau_{sp,k|k-1}^{s,t}(m_k), \cdots, \tau_{sp,k|k-1}^{J_{k-1|k-1}(m_{k-1}), J_{sp,k}(m_k, m_{k-1})}(m_k)\right\} \tag{4.38}$$

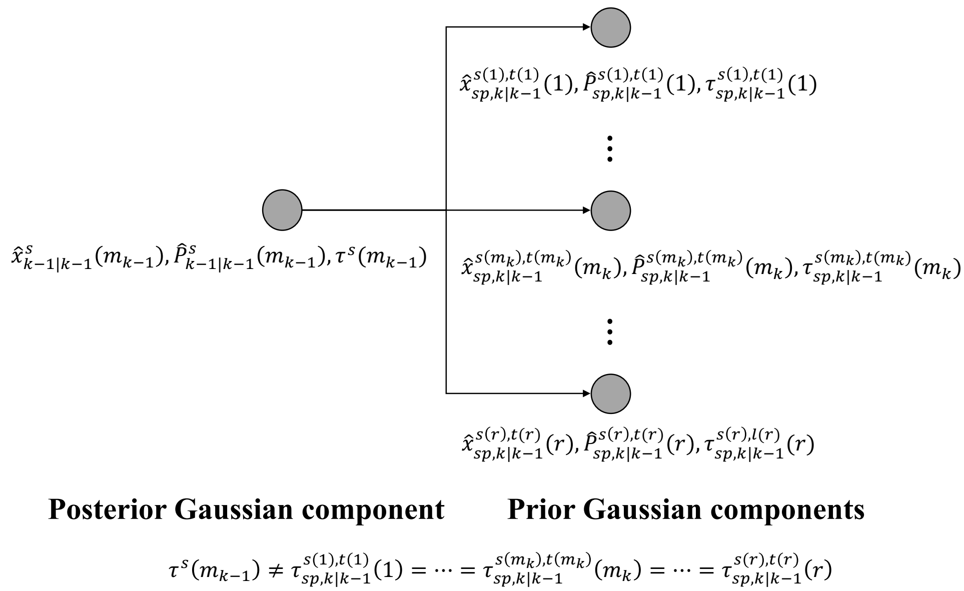

Fig. 4.3. Tree structures of the Gaussian components for a spawned target in the prior intensities

where $\tau^{s,t}_{sp,k|k-1}(m_k)$ is the tag of the spawned Gaussian component for mode m_k at time k. Then, the set of tags of the spawned Gaussian components at time k can be written as:

$$\mathcal{T}_{sp,k|k-1} = \bigcup_{m_k=1}^{r} \mathcal{T}_{sp,k|k-1}(m_k) \tag{4.39}$$

Note that the tag of the spawned Gaussian component for mode m_k from the posterior Gaussian component for mode m_{k-1} is the same as those in all other modes. However, the tag is different from that of the posterior Gaussian component for mode m_{k-1}, i.e., $\tau^{s}_{k-1|k-1}(m_{k-1}) \neq \tau^{s(1),t(1)}_{sp,k|k-1}(1) = \cdots = \tau^{s(m_k),t(m_k)}_{sp,k|k-1}(m_k) = \cdots = \tau^{s(r),t(r)}_{sp,k|k-1}(r)$ (see Figure 4.3 With Assumption 3, the intensity of the surviving Gaussian components is given by (4.19). The survived Gaussian component for mode m_k at time k has the same tag as that of the associated Gaussian component for mode m_{k-1}

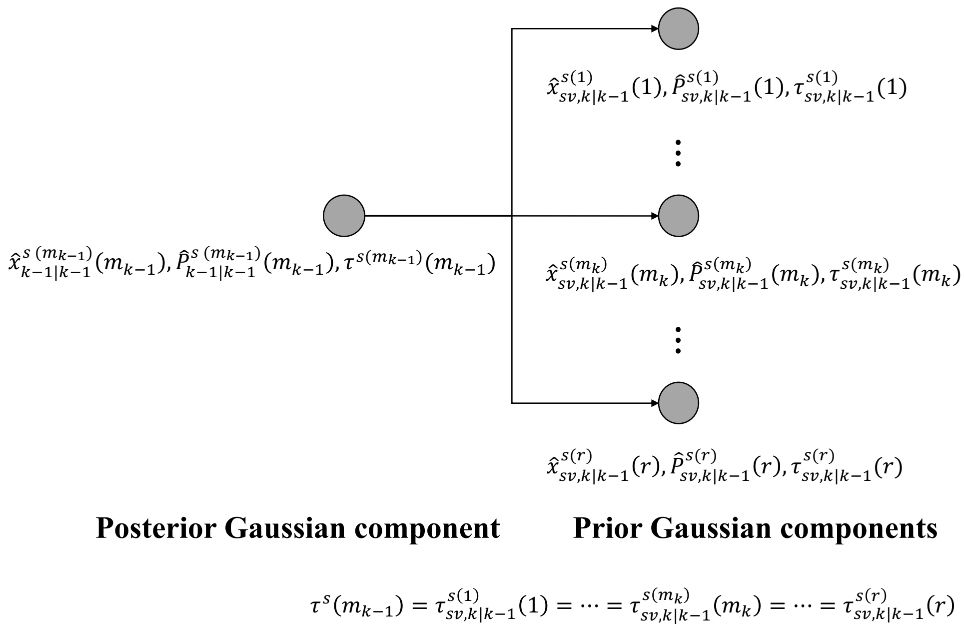

Fig. 4.4. Tree structures of the Gaussian components for a surviving target in the prior intensities

at time k. The set of tags of the survived Gaussian components for mode m_k at time k can be written as:

$$\mathcal{T}_{sv,k|k-1}(m_k) = \left\{\tau^1_{sv,k|k-1}(m_k), \cdots, \tau^s_{sv,k|k-1}(m_k), \cdots, \tau^{J_{k-1|k-1}(m_{k-1})}_{sv,k|k-1}(m_k)\right\} \tag{4.40}$$

where $\tau^s_{sv,k|k-1}(m_k)$ is the tag of the s-th survived Gaussian component for mode m_k at time k. Then, the set of tags of the survived Gaussian components at time k can be written as:

$$\mathcal{T}_{sv,k|k-1} = \bigcup_{m_k=1}^{r} \mathcal{T}_{sv,k|k-1}(m_k) \tag{4.41}$$

Note that the tag of the survived Gaussian component from the posterior Gaussian component for mode m_{k-1} at time $k-1$ is the same as those in all other modes as well as that of the posterior Gaussian component for mode m_{k-1} at time $k-1$, i.e., $\tau^s_{k-1|k-1}(m_{k-1}) = \tau^{s(1)}_{sv,k|k-1}(1) = \cdots = \tau^{s(m_k)}_{sv,k|k-1}(m_k) = \cdots = \tau^{s(r)}_{sv,k|k-1}(r)$ (see Figure 4.4 Based on these three intensities, the prior intensity at time k is given by (4.23).

Based on the sets of the tags corresponding to the individual modes in (4.37), (4.39) and (4.41), the set of tags of the Gaussian components in the prior intensities can be expressed as follows:

$$\mathcal{T}_{k|k-1} = \bigcup_{m_k=1}^{r} \mathcal{T}_{b,k}(m_k) \cup \mathcal{T}_{sp,k|k-1}(m_k) \cup \mathcal{T}_{sv,k|k-1}(m_k) \tag{4.42}$$

$$= \bigcup_{m_k=1}^{r} \left\{\tau^1_{k|k-1}(m_k), \cdots, \tau^s_{k|k-1}(m_k), \cdots, \tau^{J_{k|k-1}(m_k)}_{k|k-1}(m_k)\right\} \tag{4.43}$$

where $\tau^s_{k|k-1}(m_k)$ is the tag of the s-th Gaussian component of the prior intensity for mode m_k at time k. Figures 4.2, 4.3, and 4.4 show not only the tree structures of the Gaussian components in the posterior intensity at time $k-1$ and the prior intensities at time k but also the tags of the newborn, the spawned and the surviving Gaussian components at time k.

The posterior intensity at time k is given by (4.24). The newly generated Gaussian components corresponding to the measurements have the same tag of the associated the Gaussian component in the prior intensity. The set of tags of the Gaussian components in the posterior intensity for mode m_k can be written by:

$$\mathcal{T}_{k|k}(m_k) = \left\{\tau^1_{k|k}(m_k), \cdots, \tau^{s,t}_{k|k}(m_k), \cdots, \tau^{(1+T_k)J_{k|k-1}(m_k)}_{k|k}(m_k)\right\} \tag{4.44}$$

Based on the sets of the tags corresponding to the individual modes in (4.44), the set of tags of the Gaussian components in the posterior intensities can be expressed as follows:

$$\mathcal{T}_{k|k} = \bigcup_{m_k=1}^{r} \mathcal{T}_{k|k}(m_k) \tag{4.45}$$

Figure 4.5 illustrates the structure of the Gaussian components in the posterior intensity for mode m_k and their tags. Note that the tags of the generated Gaussian components corresponding to the measurements are the same as that of the associated Gaussian component in the prior intensity at time k, i.e., $\tau^{s(m_k)}_{k|k-1}(m_k) = \tau^{s(m_k)}_{k|k}(m_k) = \tau^{s_1(m_k)}_{k|k}(m_k) = \tau^{s_2(m_k)}_{k|k}(m_k) = \cdots = \tau^{s_{(1+T_k)}(m_k)}_{k|k}(m_k)$.

The expected number of predicted targets is given by (4.29). The expected number of targets is given by (4.33).

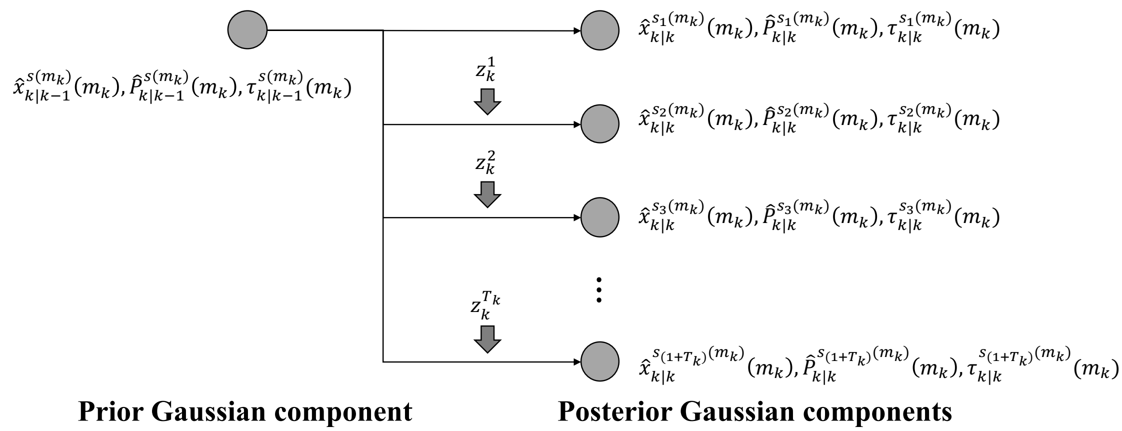

Fig. 4.5. Tree structure of the Gaussian components in the posterior intensity

The pruning procedure of the proposed GM-PHD tracker with JMS models is the same as that used in the GM-PHD filter with JMS models in [58]. In the extracting procedure of the proposed GM-PHD tracker with JMS models, the Gaussian components that have weights greater than a threshold are selected as the candidate Gaussian components. To extract the target's estimate and its label, there are two methods; The first is to merge the means of the candidate Gaussian components with the same tag based on their weights. The other is to pick the mean of the candidate Gaussian component with the largest weight among the components with the same tag. For simplicity, in this thesis we use the second approach.

In summary, the pseudo-codes for the prior equation, the posterior equation and the extracting procedure of the proposed GM-PHD tracker with JMS models are summarized in Algorithms 1, 2 and 3, respectively.

4.5 Simulation Results

In this section, the performance of the proposed GM-PHD filter and tracker are demonstrated with illustrative target tracking examples. For illustration purposes, we

Algorithm 3 Pseudo-code for the prior intensities of the GM-PHD tracker with JMS models

Input $\{\{w^s_{k-1|k-1}(m_{k-1}), \hat{x}^s_{k-1|k-1}(m_{k-1}),$

$\hat{P}^s_{k-1|k-1}(m_{k-1}), \tau^s_{k-1|k-1}(m_{k-1})\}_{s=1}^{J_{k-1|k-1}(m_{k-1})}\}_{m_{k-1}=1}^{r}$, tag

// Initiation the number of Gaussian components in the prior intensity

for $m_k = 1$ to r **do**

  $J_{k|k-1}(m_k) = 0$

end for

// Prior intensity for born targets

for $t = 1$ to $J_{b,k|k}$ **do**

  $tag = tag + 1$

  for $m_k = 1$ to r **do**

    $J_{k|k-1}(m_k) = J_{k|k-1}(m_k) + 1,$

    $w^{J_{k|k-1}(m_k)}_{k|k-1}(m_k) = \pi(m_k) w^t_{b,k}(m_k),$

    $\hat{x}^{J_{k|k-1}(m_k)}_{k|k-1} = x^t_{b,k}(m_k),$

    $\hat{P}^{J_{k|k-1}(m_k)}_{k|k-1} = P^t_{b,k}(m_k),$

    $\tau^{J_{k|k-1}(m_k)}_{k|k-1}(m_k) = tag$

  end for

end for

// Prior intensity for spawned targets

for $m_{k-1} = 1$ to r **do**

  for $s = 1$ to $J_{k-1|k-1}(m_{k-1})$ **do**

    for $t = 1$ to $J_{sp,k}(m_{k-1})$ **do**

      $tag = tag + 1$

      for $m_k = 1$ to r **do**

        $J_{k|k-1}(m_k) = J_{k|k-1}(m_k) + 1,$

        $w_{k|k-1}^{J_{k|k-1}(m_k)}(m_k) = \pi(m_k|m_{k-1}) w_{k-1|k-1}^{s}(m_{k-1}) w_{sp,k-1}^{t}(m_k, m_{k-1}),$

        $\hat{x}_{k|k-1}^{J_{k|k-1}(m_k)}(m_k) = F_{sp,k-1}^{t}(m_k) \hat{x}_{k-1|k-1}^{s}(m_{k-1}) + d_{sp,k-1}^{t},$

        $\hat{P}_{k|k-1}^{J_{k|k-1}(m_k)}(m_k) = F_{sp,k-1}^{t}(m_k) \hat{P}_{k-1|k-1}^{s}(m_{k-1}) \{F_{sp,k-1}^{t}(m_k)\}^T + Q_{sp,k-1}^{t}(m_k),$

        $\tau_{k|k-1}^{J_{k|k-1}(m_k)}(m_k) = tag$

      end for

    end for

  end for

end for

// Prior intensity for existing targets

for $m_{k-1} = 1$ to r **do**

  for $s = 1$ to $J_{k-1|k-1}(m_{k-1})$ **do**

    for $m_k = 1$ to r **do**

      $J_{k|k-1}(m_k) = J_{k|k-1}(m_k) + 1,$

      $w_{k|k-1}^{J_{k|k-1}(m_k)}(m_k) = P_{sv}(m_k) \pi(m_k|m_{k-1}, \hat{x}_{k-1|k-1}^{s}(m_{k-1})) w_{k-1|k-1}^{s}(m_{k-1}),$

      $\hat{x}_{k|k-1}^{J_{k|k-1}(m_k)}(m_k) = F_{k-1}(m_k) \hat{x}_{k-1|k-1}^{s}(m_{k-1}),$

      $\hat{P}_{k|k-1}^{J_{k|k-1}(m_k)}(m_k) = F_{k-1}(m_k) \hat{P}_{k-1|k-1}^{s}(m_{k-1}) \{F_{k-1}(m_k)\}^T + Q_{k-1}(m_k),$

      $\tau_{k|k-1}^{J_{k|k-1}(m_k)}(m_k) = \tau_{k-1|k-1}^{J_{k-1|k-1}(m_{k-1})}(m_{k-1})$

    end for

  end for

end for

// Calculation of Kalman gain
for $m_k = 1$ to r **do**
  for $s = 1$ to $J_{k|k-1}(m_k)$ **do**
    $S_k^s(m_k) = H_k \hat{P}^s_{k|k-1}(m_k) H_k^T + R_k,$
    $K_k^s(m_k) = \hat{P}^s_{k|k-1}(m_k) H_k^T (S_k^s(m_k))^{-1}$
  end for
end for

Output $\{\{w^s_{k|k-1}(m_k), \hat{x}^s_{k|k-1}(m_k), \hat{P}^s_{k|k-1}(m_k), \tau^s_{k|k-1}(m_k)\}_{s=1}^{J_{k|k-1}(m_k)}\}_{m_k=1}^{r}, tag$

Algorithm 4 Pseudo-code for the posterior intensities of the GM-PHD tracker with JMS models

Input $\{\{w^s_{k|k-1(m_k)}, \ \hat{x}^s_{k|k-1}(m_k), \ \hat{P}^s_{k|k-1}(m_k), \tau^s_{k|k-1}(m_k)\}_{s=1}^{J_{k|k-1}(m_k)}\}_{m_k=1}^{r}, Z_k = \{z_k^t\}_{t=1}^{T_k}$, tag

// Posterior intensity for the case that there is no measurement
for $m_k = 1$ to r **do**
  for $s = 1$ to $J_{k|k-1}(m_k)$ **do**
    $w^s_{k|k}(m_k) = (1 - P_D) w^s_{k|k-1}(m_k),$
    $\hat{x}^s_{k|k}(m_k) = \hat{x}^s_{k|k-1}(m_k),$
    $\hat{P}^s_{k|k}(m_k) = \hat{P}^s_{k|k-1}(m_k),$
    $\tau^s_{k|k}(m_k) = \tau^s_{k|k-1}(m_k)$
  end for
end for

// Posterior intensity for the existing Gaussian components and new Gaussian components

for $m_k = 1$ to r **do**

  for $t = 1$ to T_k **do**

    $SumWeight = 0$

    for $s = 1$ to $J_{k|k-1}(m_k)$ **do**

      $ID = (t+1) \times J_{k|k-1}(m_k) + s,$

      $w^{ID}_{k|k}(m_k) = P_D w^s_{k|k-1}(m_k)\mathcal{N}(z^t_k; H_k \hat{x}^s_{k|k-1}(m_k)),$

      $SumWeight = SumWeight + w^{ID}_{k|k},$

      $\hat{x}^{ID}_{k|k}(m_k) = \hat{x}^s_{k|k-1}(m_k) = +K^s_k(m_k)(z^t_k - H_k \hat{x}^s_{k|k-1}(m_k)),$

      $\hat{P}^{ID}_{k|k}(m_k) = \hat{P}^s_{k|k}(m_k),$

      $\tau^{ID}_{k|k}(m_k) = \tau^s_{k|k}(m_k)$

    end for

    for $s = 1$ to $J_{k|k-1}(m_k)$ **do**

      $ID = (t+1)J_{k|k-1}(m_k) + s,$

      $w^{ID}_{k|k}(m_k) = \frac{w^{ID}_{k|k}(m_k)}{\kappa_k(z^t_k) + SumWeight}$

    end for

  end for

  $J_{k|k}(m_k) = (T_k + 1)J_{k|k-1}(m_k)$

end for

Output $\{\{w^s_{k|k}(m_k), \hat{x}^s_{k|k}(m_k), \hat{P}^s_{k|k}(m_k), \tau^s_{k|k}(m_k)\}^{J_{k|k}(m_k)}_{s=1}\}^r_{m_k=1}$, tag

Algorithm 5 Pseudo-code for the state extraction of the GM-PHD tracker with JMS models

Input $\{\{w^s_{k|k}(m_k),\ \hat{x}^s_{k|k}(m_k),\ \hat{P}^s_{k|k}(m_k), \tau^s_{k|k}(m_k)\}_{s=1}^{J_{k|k-1}(m_k)}\}_{m_k=1}^{r}$

$i = 1$

Set $Candidate_{k|k} = \emptyset$.

for $m_k = 1$ to r **do**
    for $s = 1$ to $J_{k|k}(m_k)$ **do**
        if $w^s_{k|k}(m_k) > Th_e$ **then**
            $Candidate_{k|k}(i) = \left[w^s_{k|k}(m_k), \hat{x}^s_{k|k}(m_k), \hat{P}^s_{k|k}(m_k), \tau^s_{k|k}(m_k)\right]$,
            $i = i + 1$
        end if
    end for
end for

$l = 1$
while do $I = \emptyset$
    $j = \text{argmax}_{i \in I}$ weight of $Candidate_{k|k}(i)$,
    $L = \left\{i \in I |\ \text{tag of } Candidate_{k|k}(j) = \text{ tag of } Candidate_{k|k}(i)\right\}$,
    $I = I \backslash L$,
    $l = l + 1$
end while

Output $\{Candidate_{k|k}(i)\}_{i=1}^{l}$ as the state estimates of the GM-PHD tracker
with JMS model }

consider a two-dimensional scenario where two aircraft fly in the surveillance region of [-10000, -10000] $\times$ [10000, 10000] m^2. The state vector of a target (aircraft) is composed of its position and velocity: $x_k = [P_{x,k}\ P_{y,k}\ V_{x,k}\ V_{y,k}]^T$.

Three discrete-time dynamic models (or modes) of the surviving and spawned targets are described as follows: Model 1 ($m_k = 1$) is a constant velocity model given by:

$$F_{k-1}(m_k = 1) = F_{sp,k-1}(m_k = 1) = \begin{bmatrix} 1 & 0 & T & 0 \\ 0 & 1 & 0 & T \\ 0 & 0 & 1 & 0 \\ 0 & 0 & 0 & 1 \end{bmatrix} \tag{4.46}$$

where the sampling period T is 1 second. Models 2 ($m_k = 2$) and 3 ($m_k = 3$) are a coordinate turn model with known turn rates (ω) given by:

$$F_{k-1}(m_k = 2 \text{ or } 3) = F_{sp,k-1}(m_k = 2 \text{ or } 3) = \begin{bmatrix} 1 & 0 & \frac{\sin(\omega T)}{\omega} & -\frac{1-\cos(\omega T)}{\omega} \\ 0 & 1 & \frac{1-\cos(\omega T)}{\omega} & -\frac{\sin(\omega T)}{\omega} \\ 0 & 0 & \cos(\omega T) & 0 - \sin(\omega T) \\ 0 & 0 & \sin(\omega T) & \cos(\omega T) \end{bmatrix} \tag{4.47}$$

where Models 2 and 3 have a clockwise turn rate, $\omega = 4^o/s$ and a counterclockwise turn rate, $\omega = -4^o/s$, respectively. The process noises of the surviving and the spawned targets are Gaussian with zero means and the following covariances:

$$Q_{k-1}(m_k = 1, 2 \text{ or } 3) = \sigma^2(\omega) \begin{bmatrix} \frac{T^4}{4} & 0 & \frac{T^3}{2} & 0 \\ 0 & \frac{T^4}{4} & 0 & \frac{T^2}{2} \\ \frac{T^3}{2} & 0 & T^2 & 0 \\ 0 & \frac{T^3}{2} & 0 & T^2 \end{bmatrix} \tag{4.48}$$

$$Q^t_{sp,k-1}(m_k = 1, 2 \text{ or } 3) = diag([100, 100, 400, 400]) \tag{4.49}$$

The mode transition probabilities of the spawned target, the born target, and the surviving target in the GM-PHD filter with JMS models and the GM-PHD tracker are taken as [58]:

$$[\pi_{sp}(m_k|m_{k-1})] = \begin{bmatrix} 0.8 & 0.1 & 0.1 \\ 0.8 & 0.1 & 0.1 \\ 0.8 & 0.1 & 0.1 \end{bmatrix} \tag{4.50}$$

$$[\pi_b(m_k)] = \begin{bmatrix} 0.8 & 0.1 & 0.1 \end{bmatrix}^T \tag{4.51}$$

$$[\pi(m_k|m_{k-1})] = \begin{bmatrix} 0.8 & 0.1 & 0.1 \\ 0.1 & 0.8 & 0.1 \\ 0.1 & 0.1 & 0.8 \end{bmatrix}. \tag{4.52}$$

A sensor located at (0, 0) obtains the measurement vector which represents the position of a target, $z_k = [P_{z_x,k} \ P_{z_y,k}]^T$. The observation model is given by

$$z_k = \begin{bmatrix} 1 & 0 & 0 & 0 \\ 0 & 1 & 0 & 0 \end{bmatrix} x_k + v_k \tag{4.53}$$

where measurement noise v_k is assumed to be Gaussian with zero mean and 10 m standard deviation. Clutter is modeled as a Poisson RFS with intensity

$$\kappa_k(z_k) = \lambda V \mathcal{U}(z_k) \tag{4.54}$$

where λ and V are the clutter density and the surveillance region, respectively. $\mathcal{U}(\cdot)$ denotes a uniform density function. In the Gaussian component pruning part, the truncation threshold of a Gaussian component is set to 10^{-5} and the merging threshold of Gaussian components is 4. The extraction threshold is set to 0.5.

The intensity of the born target is given by

$$b(x_k) = 0.1\pi_b(m_k)[\mathcal{N}(x_k; m_{b,k}^{(1)}, P_{b,k}^{(1)}) + \mathcal{N}(x_k; m_{b,k}^{(2)}, P_{b,k}^{(2)})] \tag{4.55}$$

where $m_{b,k}^{(1)} = \begin{bmatrix} 0 & 6000 & 0 & -140 \end{bmatrix}^T$ and $m_{b,k}^{(2)} = \begin{bmatrix} -2500 & -1000 & 120 & -25 \end{bmatrix}^T$ are the state vectors of individual Gaussian components. $P_{b,k}^{(1,2)} = diag([100,\ 100,\ 25,\ 25])$ is

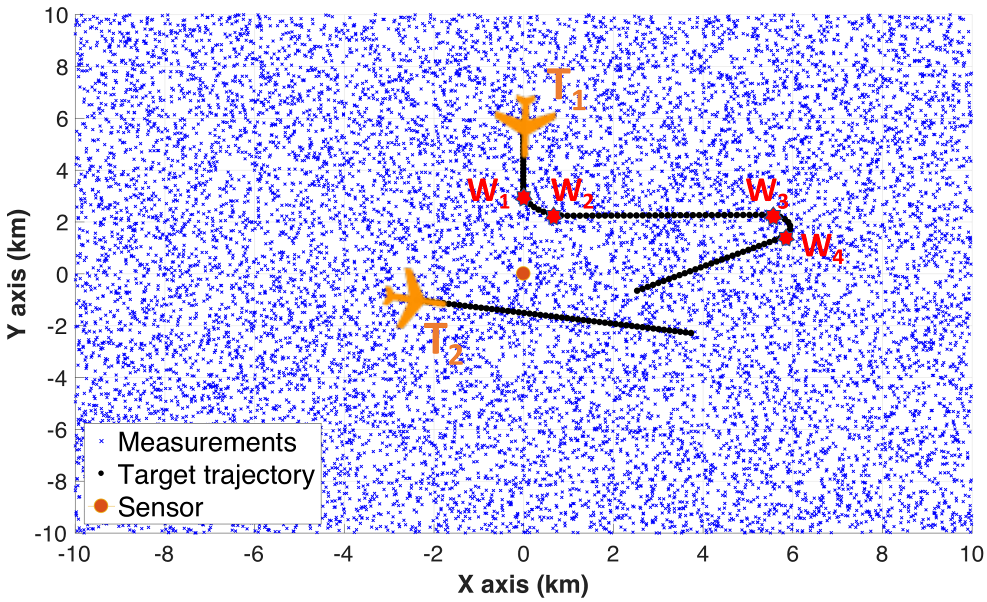

Fig. 4.6. Target trajectories, clutter, sensor and waypoints

the error covariance of the each Gaussian component. The weight of the spawned target is 0.05. In the Gaussian component pruning part, the truncation and the merging thresholds of a Gaussian component are set to 10^{-5} and 4, respectively. The extraction threshold is set to 0.5. Note that the remaining noise and threshold values follow the simulation set-up in [47, 58] for fair comparison. This scenario is used to demonstrate the performance of the proposed GM-PHD filter and tracker.

4.5.1 Simulation Results for Gaussian Mixture Probability Hypothesis Density filter with State-Dependent Jump Markov System Models

In this section, we present an illustrative numerical example to compare the proposed GM-PHD filter with SD-JMS models with the original GM-PHD filter and the GM-PHD filter with JMS models in terms of the performance of the target state estimate persistence.

Figure 4.6 shows a series of waypoints (w_1, w_2, w_3 and w_4), false measurements and trajectories of two aircraft flying along two air routes over 100 seconds. Target 1 (T_1) exists for the entire simulation but Target 2 (T_2) appears at time $k = 21$ second and disappears at time $k = 72$ second. To model the mode transitions, we define the guard condition of (4.11) where

$$\mathbf{L}_{ij} = \begin{bmatrix} 1 & 0 & 0 & 0 \\ 0 & 1 & 0 & 0 \end{bmatrix} \quad i, j = 1, 2, 3 \tag{4.56}$$

$$\begin{aligned} \mu_{21} &= w_1 = \begin{bmatrix} 0 & 3200 \end{bmatrix}^T, \mu_{12} = w_2 = \begin{bmatrix} 983 & 2224 \end{bmatrix}^T \\ \mu_{31} &= w_3 = \begin{bmatrix} 5462 & 2258 \end{bmatrix}^T, \mu_{13} = w_4 = \begin{bmatrix} 5728 & 1359 \end{bmatrix}^T \end{aligned} \tag{4.57}$$

$$\Sigma_{ij} = \begin{bmatrix} 100^2 & 0 \\ 0 & 100^2 \end{bmatrix} \quad i, j = 1, 2, 3 \tag{4.58}$$

Then, the conditional mode transition probabilities at the waypoints are modeled as,

$$\text{At } w_1, \ \ \pi(2|1, x_{k-1}) = \mathcal{N}(\mathbf{L}_{21} x_k; \mu_{21}, \Sigma_{21}) \tag{4.59}$$

$$\text{At } w_2, \ \ \pi(1|2, x_{k-1}) = \mathcal{N}(\mathbf{L}_{12} x_k; \mu_{12}, \Sigma_{12}) \tag{4.60}$$

$$\text{At } w_3, \ \ \pi(3|1, x_{k-1}) = \mathcal{N}(\mathbf{L}_{31} x_k; \mu_{31}, \Sigma_{31}) \tag{4.61}$$

$$\text{At } w_4, \ \ \pi(1|3, x_{k-1}) = \mathcal{N}(\mathbf{L}_{13} x_k; \mu_{13}, \Sigma_{13}) \tag{4.62}$$

In order to compare the performance of the target estimate persistence between the GM-PHD filter, the GM-PHD filter with JMS models and the proposed GM-PHD filter with SD-JMS models, we perform Monte Carlo simulation of 500 runs with different detection probabilities and clutter densities. Figure 4.7 presents the true number of targets and the estimated numbers of targets computed by the original GM-PHD filter, the GM-PHD filter with JMS models, and the proposed GM-PHD filter with SD-JMS models when the values of P_D and λ change from 0.8 to 0.98 and from 40 to 200, respectively. The black, red, purple, and green lines represent

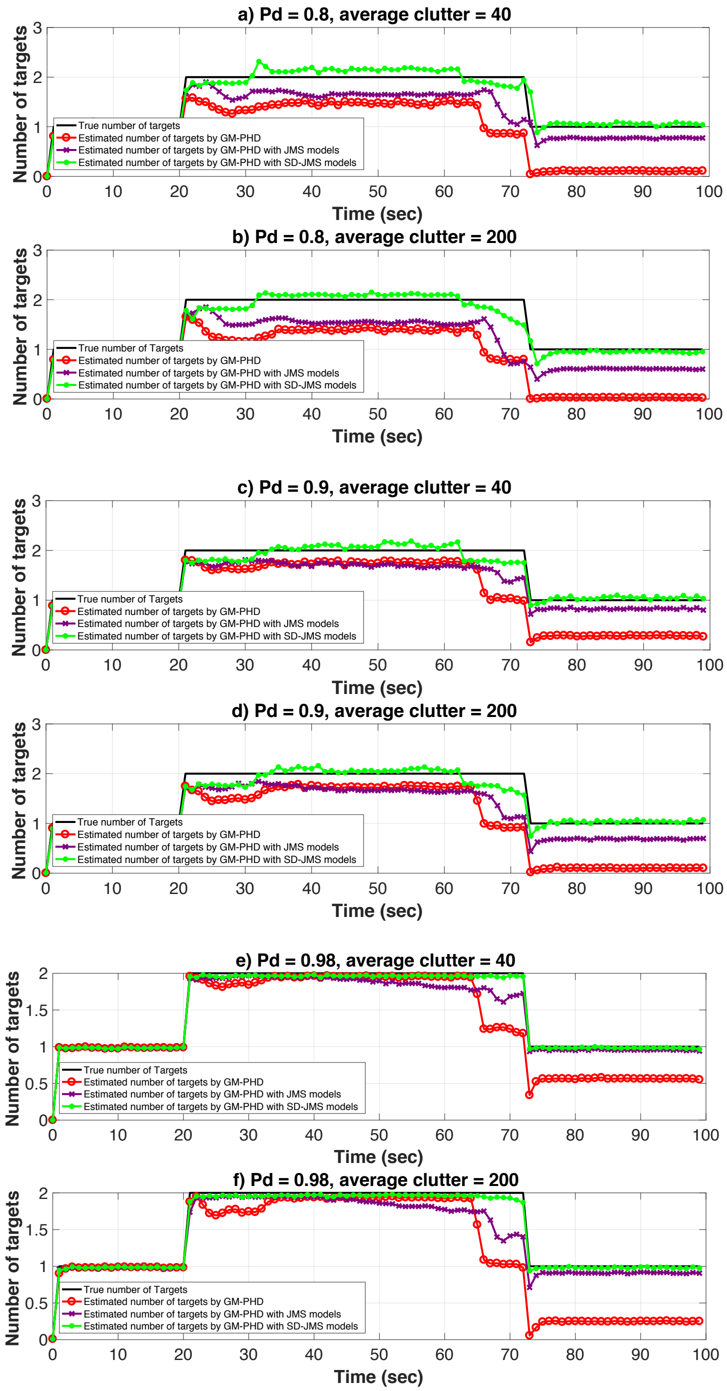

Fig. 4.7. The true number of targets and the estimated numbers of targets computed by GM-PHD filter, GM-PHD filter with JMS models, and proposed GM-PHD filter with SD-JMS models (average over 500 Monte Carlo runs)

the true number of targets and the estimated numbers of targets computed by the GM-PHD filter, the GM-PHD filter with JMS models, and the proposed GM-PHD filter with SD-JMS models, respectively. Note that, after 65 seconds, the estimated number of targets computed by the GM-PHD filter is significantly deviated from the true number of targets due to the rapid maneuver of Target 1. Furthermore, in the low detection probability and high clutter density environment, there are a number of missed estimates of the targets by the GM-PHD filter with JMS models because of the inaccurate constant mode transition probabilities. However, the estimated number of targets computed by the our proposed GM-PHD filter with SD-JMS is close to the true number of targets, which demonstrates its superior performance over the two existing filters.

4.5.2 Simulation Results for Gaussian Mixture Probability Hypothesis Density Tracker with Jump Markov System Models

In this section, an illustrative numerical example is considered to demonstrate the performance of the target state estimate persistence of the proposed GM-PHD tracker with JMS models. To evaluate its performance, we compare the proposed tracker with the GM-PHD tracker [65].

Figures 4.8 and 4.9 depict the trajectories of two aircraft, the measurements from a sensor and the target state estimates computed by the GM-PHD tracker and the proposed GM-PHD tracker with JMS models over 100 seconds. In this case, the detection probability is set to 0.98 and the clutter density is 5×10^{-8} (i.e., an average of 200 clutter are generated in the surveillance area at each time step). As shown in Figure 4.9, Target 1 exists for the entire simulation but Target 2 appears at time $k = 21$ second and disappears at time $k = 72$ second. The blue crosses indicate the measurements composed of the targets with noise and clutter. The red and the magenta circles indicate the state estimates of Target 1 and Target 2 computed by the GM-PHD tracker, respectively. Note that the red circle disappears at 65 seconds

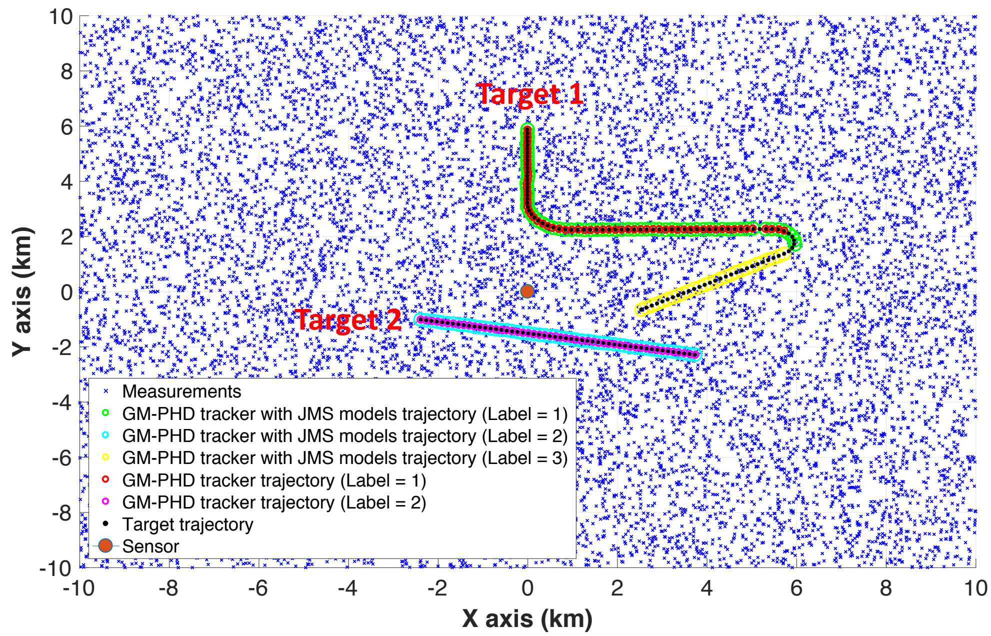

Fig. 4.8. Trajectories of targets, measurements, sensor position and target state estimates computed by the GM-PHD tracker and the GM-PHD tracker with JMS models

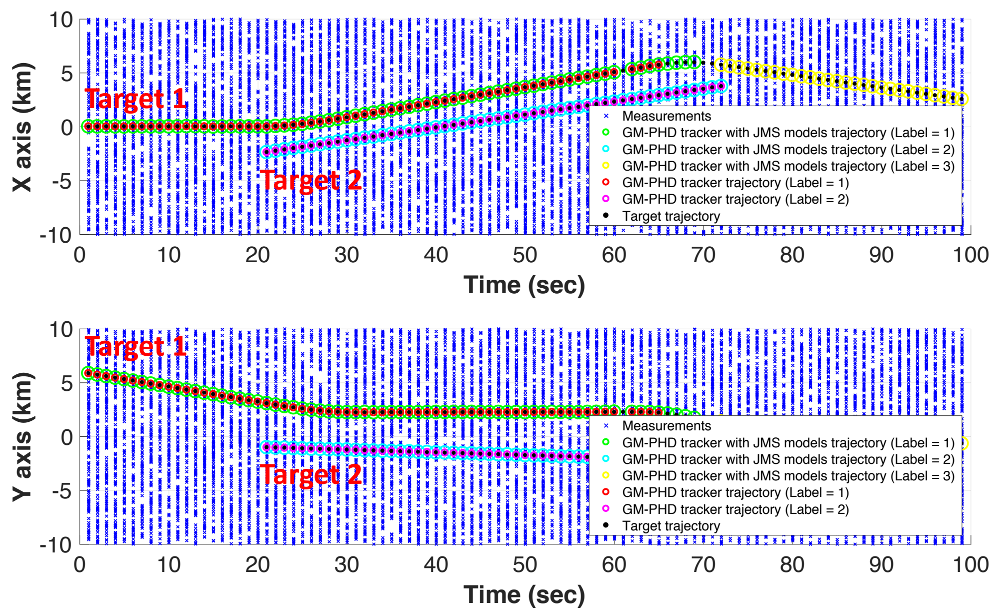

Fig. 4.9. True target positions, measurements, target state estimates of the GM-PHD tracker and the GM-PHD tracker with JMS models

due to a turning maneuver of Target 1. However, the state estimates for Target 1, indicated by the green and the yellow circles, can be produced by the proposed GM-PHD tracker with JMS models even though the label of the state estimate for Target 1 is changed from 1 to 3.

To compare the performance of the target estimate persistence between the GM-PHD tracker and the proposed GM-PHD tracker with JMS models, we perform Monte Carlo simulation of 500 runs with various values of detection probabilities, P_D and clutter densities, λ. Figure 4.10 presents the true number of targets and the estimated numbers of targets computed by the GM-PHD tracker and the proposed GM-PHD tracker with JMS models averaged over 500 Monte Carlo runs when the values of P_D and λ change from 0.8 to 0.98 and from 40 to 200, respectively. The black, red and green lines represent the true number of targets and the estimated numbers of targets computed by the GM-PHD tracker and the proposed GM-PHD tracker with JMS models, respectively. From 20 seconds to 34 seconds, the estimated number of targets computed by the GM-PHD tracker is less than that of the proposed GM-PHD tracker with JMS model due to the maneuver of Target 1. However, after 33 seconds, the estimated number of targets computed by the GM-PHD tracker becomes similar to that of the proposed GM-PHD tracker with JMS model since the Gaussian component might not be pruned or if it is pruned around 20 seconds, it is regenerated after a certain amount of time. Note that, after 65 seconds, the estimated number of targets computed by the GM-PHD tracker is significantly deviated from the true number of targets due to the rapid maneuver of Target 1. However, the estimated number of targets computed by the our proposed GM-PHD tracker with JMS models is close to the true number of targets, which demonstrates its superior performance over the existing tracker.

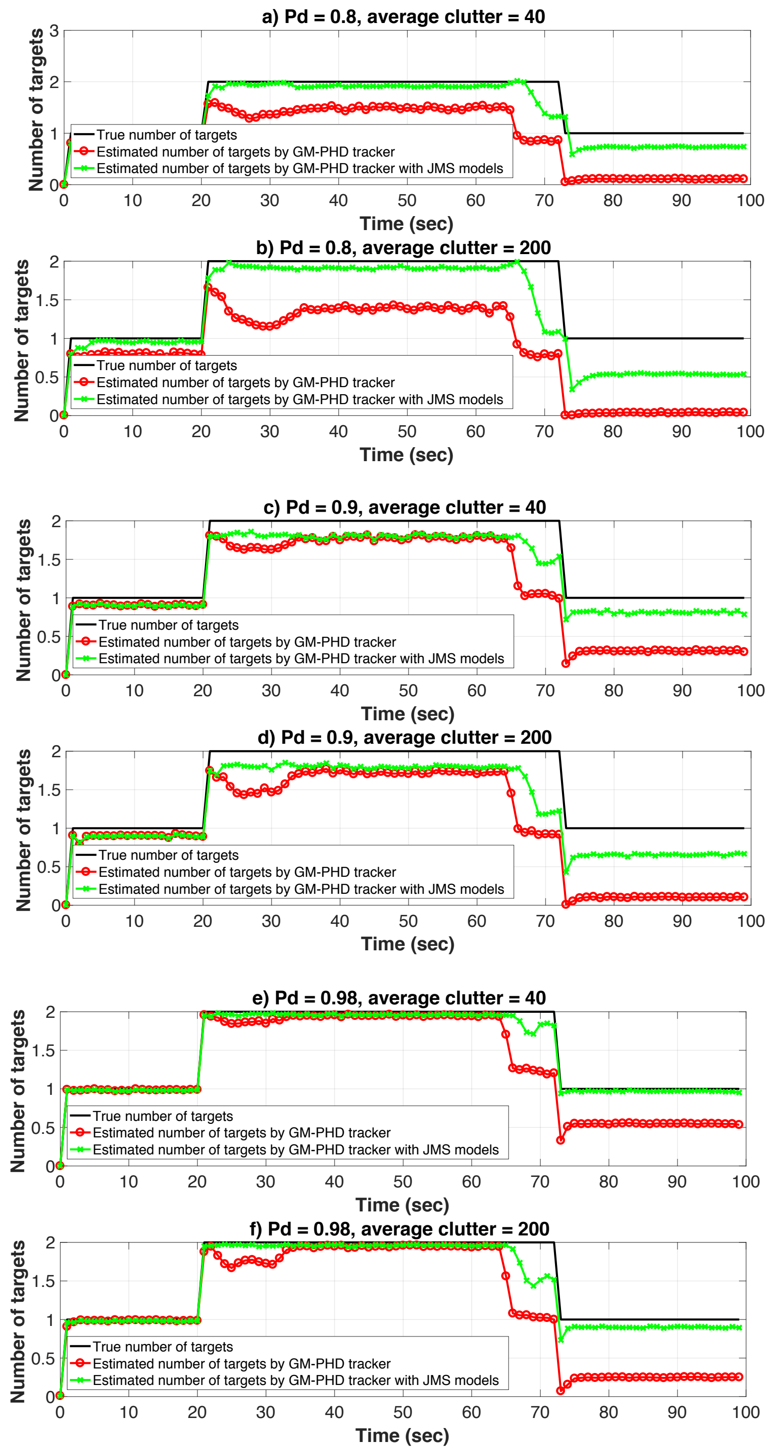

Fig. 4.10. The true number of targets and the estimated numbers of targets computed by GM-PHD tracker and proposed GM-PHD tracker with JMS models (averaged over 500 Monte Carlo runs)

5. SUMMARY

In this thesis, we discussed challenges of jointly estimating the number of targets and their states or trajectories in MTT, and developed new models and MTT algorithms that effectively overcome the challenges. The developed algorithms are demonstrated with illustrative simulation examples, and further tested with real data collected from the surveillance radar in the vessel traffic tracking system.

To improve the performance of the data association-based traditional filters, we have proposed a feature-aided data association filter for multi-target tracking. The proposed data association filter facilitates target kinematic state-dependent feature models which can explicitly account for the correlation between the kinematic and feature states of a target. Algorithmically, two feature models are derived based on the characteristics of the RCS. With the real data collected from the marine radar and the surveillance radar of a VTS system, the performance of the proposed target kinematic state-dependent feature models are validated via comparison with the existing feature model which is independent of the target kinematic state. The results have shown that the proposed models are more accurate than the feature model independent of the target's kinematic state. Furthermore, we have proposed a data association algorithm using the proposed feature models, which does not require the widely-used assumption that the kinematic state of the target is independent of its feature state. Illustrative multi-target tracking examples with simulated data and real data have been presented to demonstrate that the proposed data association filter outperforms the existing data algorithms in terms of the tracking continuity and the accuracy of estimate in heavily cluttered and/or low SNR environments.

To address the problem of the missed estimate of a target in the GM-PHD filter, we proposed a new GM-PHD filter which can explicitly account for the uncertainty in the measurement origin, i.e., whether 1) measurement is clutter; 2) measurement is originated from a target; and 3) there is no measurement. The conditional probabilities, whether the measurement is target-originated or not, have been derived algorithmically based on the measurement proximity information. A new estimate error covariance update equation was derived based on the conditional error covariances subject to the three different measurement origin events: true measurement, false measurement, and no measurement. With the new estimate error covariance update equation based on the conditional probability, proposed GM-PHD filter can adjust the filtering process to improve the reliability of updated Gaussian component against heavily cluttered and/or low SNR environments. Illustrative multi-target tracking examples demonstrated that the proposed GM-PHD filter has better performance than the original GM-PHD and N-scan GM-PHD filters in terms of the missed estimates of targets against the presence of false measurements. Simulation results showed that the number of the missed estimates of targets of the proposed method is significantly less than that of the original GM-PHD and N-scan GM-PHD filters as the clutter density increases and the detection probability decreases.

Finally, we proposed the GM-PHD filter with SD-JMS models to accurately account for maneuver uncertainty of a target moving along a planned trajectory. An illustrative multi-target tracking example demonstrates that the proposed GM-PHD filter with SD-JMS models outperforms the original GM-PHD filter and the GM-PHD filter with JMS models which assumes constant mode transition probabilities irrespective of the target state, in terms of the missed estimates of maneuvering targets. Simulation results showed that the number of the missed estimates of targets by the proposed method is significantly less than those of the original GM-PHD filter and the GM-PHD filter with JMS models, especially in harsh environments where the clutter density is high and the detection probability is low. Also, we have proposed the GM-PHD tracker with jump Markov system (JMS) models to estimate the trajectories of the maneuvering targets. An illustrative multi-target tracking example demonstrates that the proposed GM-PHD tracker with JMS models can persistently provide the state estimates of targets and their labels even though there are the some label changes. Through Monte Carlo simulations, we demonstrate that the proposed GM-PHD tracker with JMS models outperforms the original GM-PHD tracker which has a linear Gaussian target model, in terms of the missed estimates of maneuvering targets. Simulation results showed that the number of the missed estimates of targets by the proposed algorithm is significantly less than that of the GM-PHD tracker, especially in harsh environments where the clutter density is high and the detection probability is low.

In my future work, it is planned: i) to improve the proposed models and algorithm and apply them to various applications, including integration with other nonlinear filters and multiple model based tracking filters; ii) to generalize the target dimensions with aspect-angle model by relaxing the assumption, $\psi = 0$ and $b = c$; iii) to incorporate feature information of multiple targets to the proposed GM-PHD filters and tracker in order to further increase its accuracy and iv) to extend the problems to include practical factors such as unknown detection probability, and parameters for the new born targets and time varying clutter density.

REFERENCES

REFERENCES

[1] Y. Bar-Shalom and X. R. Li, *Multitarget-Multisensor Tracking: Principles and Techniques*. Storrs, CT: YBS Publishing, 1995.

[2] Y. Bar-Shalom, X. R. Li, and T. Kirubarajan, *Estimation with Applications to Tracking and Navigation*. New York, NY, USA: Wiley, 2001.

[3] D. Reid, "An algorithm for tracking multiple targets," *IEEE Transactions on Automatic Control*, vol. 24, no. 6, pp. 843–854, 1979.

[4] Y. Bar-Shalom and T. E. Fortmann, *MultitargetTracking and data association*. New York: Academic, 1988.

[5] X. R. Li and Y. Bar-Shalom, "Tracking in clutter with nearest neighbor filters: Analysis and performance," *IEEE Transactions on Aerospace and Electronic Systems*, vol. 32, no. 3, pp. 995–1010, 1996.

[6] T. L. Song, D. G. Lee, and J. Ryu, "A probabilistic nearest neighbor filter algorithm for tracking in a clutter environment," *Signal Processing*, vol. 85, no. 10, pp. 2044–2053, 2005.

[7] T. L. Song and D. G. Lee, "A probabilistic nearest neighbor filter algorithm for m validated measurements," *IEEE Transactions on Signal Processing*, vol. 54, no. 7, pp. 2797–2802, 2006.

[8] Y. Bar-Shalom, T. Kirubarajan, and X. Lin, "Probabilistic data association techniques for target tracking with applications to sonar, radar and eo sensors," *IEEE Transactions Aerospace and Electronic Systems Magazine*, vol. 20, no. 8, pp. 37–56, 2005.

[9] X. R. Li, "Tracking in clutter with strongest neighbor measurements - part i: Theoretical analysis," *IEEE Transactions on Automatic Control*, vol. 43, no. 11, pp. 1560–1578, 1998.

[10] X. R. Li and X. Zhi, "Psnf: A refined strongest neighbor filter for tracking in clutter," in *35th CDC, Kobe, Japan*, Dec. 1996, pp. 2557–2562.

[11] L. M. Ehrman and W. D. Blair, "Probabilistic data association with amplitude information versus the strongest neighbor filter," in *2007 IEEE Aerospace Conference, Big Sky, MT, USA*, Mar. 2007.

[12] F. Zhan, X. P. Zhou, and X. H. Chen, "Joint probabilistic data association particle filter algorithm based on amplitude information title," *Xi Tong Gong Cheng Yu Dian Zi Ji Shu/Systems Engineering and Electronics*, vol. 33, no. 2, pp. 453–457, 2011.

[13] D. Musicki and R. Evans, "Joint integrated probabilistic data association - jipda," in *Proceedings of the Fifth International Conference on Information Fusion*, Jul. 2002.

[14] ——, "Joint integrated probabilistic data association: Jipda," *IEEE Transactions on Aerospace and Electronic Systems*, vol. 40, no. 3, pp. 1093–1099, 2004.

[15] T. E. Fortmann, Y. Bar-Shalom, and M. Scheffe, "Multi-target tracking using joint probabilistic data association," in *Proceedings of the IEEE Conference on Decision and Control including the Symposium on Adaptive Processes*, Apr. 2007.

[16] Y. Bar-Shalom and E. Tse, "Tracking in a cluttered environment with probabilistic data association," *Automatica*, pp. 451–460, Sep. 1975.

[17] (2006, Feb.) Technical order 00-105e-9 and stang 3896 aerospace emergency rescue and mishap response information - chapters 8 - usaf fighter pt1 qf-4 thru f-16. [Online]. Available: https://0x4d.net/files/AF1/R11%20Segment%2011.pdf

[18] G. Stephens. (2017, Apr.) The difference between chaff & flare in a jet. [Online]. Available: https://ourpastimes.com/difference-between-chaff-flare-jet-8624626.html

[19] C. D. Papanicolopoulos, W. D. Blair, D. L. Sherman, and M. Brandt-Pearce, "Use of a rician distribution for modeling aspect-dependent rcs amplitude and scintillation," in *IEEE Radar Conference, Boston*, Apr. 2007.

[20] X. Song, W. D. Blair, P. Willett, and S. Zhou, "Dominant-plus-rayleigh models for rcs: Swerling iii/iv versus rician," *IEEE Transactions on Aerospace and Electronic Systems*, vol. 49, no. 3, pp. 2058–2064, 2013.

[21] O. E. Drummond, "Feature, attribute, and classification aided target tracking," in *SPIE, Conference on Signal and Data Processing of Small Targets, International Symposium on Optical Science and Technology*, Nov. 2001.

[22] ——, "Attribute in tracking and classification with incomplete data," in *SPIE, Conference on Signal and Data Processing of Small Targets, Defense and Security*, Aug. 2004.

[23] ——, "On features and attributes in multisensor, multitarget tracking," in *2nd International Conference on Information Fusion (FUSION'99)*, Jul. 1999.

[24] X. Wang, B. L. Scala, and R. Ellem, "Feature aided probabilistic data association for multi-target tracking," in *11th International Conference on Information Fusion*, Jun. 2008.

[25] D. H. Nguyen, J. H. Kay, B. J. Orchard, and R. H. Whiting, "Feature-aided tracking of moving ground vehicles," in *SPIE, Conference on Algorithms for Synthetic Aperture Radar Imagery IX, AeroSense 2002*, Aug. 2002.

[26] P. F. Singer and A. L. Coursey, "Feature aided tracking (fat)," in *SPIE, Signal and Data Processing of Small Targets*, Aug. 2004.

[27] B. J. Slocumb and M. E. Klusman, "A multiple model snr/rcs likelihood ratio score for radar-based feature-aided tracking," in *SPIE, Optics and Photonics 2005*, Sep. 2005.

[28] (2018, Oct.) Civil aircraft missile protection system. [Online]. Available: https://saab.com/air/electronic-warfare/self-protection-systems/camps/

[29] (2014, Jun.) F16 fighter jet shooting flares. [Online]. Available: https://www.youtube.com/watch?v=aYXkVOSUIy0

[30] (2008, Apr.) Radar video from knc c-scope extractor. [Online]. Available: https://www.youtube.com/watch?v=LKtNbCXuet0

[31] P. Pouliguen, R. Hmon, J. F. Damiens, and J. Saillard, "Analytical formulas for radar cross section of flat plates in near field and normal incidence," in *Progress In Electromagnetics Research B*, Jan. 2008.

[32] T. E. Fortmann, Y. Bar-Shalom, and M. Scheffe, "Sonar tracking of multiple targets using joint probabilistic data association," *IEEE Journal of Oceanic Engineering*, vol. 8, no. 3, pp. 173–184, 1983.

[33] R. E. Kalman, "A new approach to linear filtering and prediction problems," *Transactions of the ASME-Journal of Basic Engineering*, vol. 82 (Series D), pp. 35–45, 1960.

[34] S. J. Julier and J. K. Uhlmann, "New extension of the kalman filter to nonlinear systems," in *In Proceedings of the SPIE 3068, Signal Processing, Sensor Fusion, and Target Recognition VI*, Jul. 1997.

[35] H. Blom and Y. Bar-Shalom, "The interacting multiple model algorithm for systems with markovian switching coefficients," *IEEE Transactions on Automatic Control*, vol. 33, no. 8, pp. 780–783, 1988.

[36] X. R. Li and V. P. Jikov, "Survey of maneuvering target tracking. part i. dynamic models," *IEEE Transactions on Aerospace and Electronic Systems*, vol. 39, no. 4, pp. 1333–1364, 2003.

[37] (2017, Sep.) Vessel radar record - hangzhou wan & changjiang kou. [Online]. Available: https://www.youtube.com/watch?v=HICKCAFYwDE

[38] P. Rajyalakshmi and G. S. N. Raju, "Characteristics of radar cross section with different objects," *International Journal of Electronics and Communication Engineering*, vol. 4, no. 2, pp. 205–216, 2011.

[39] (2018, Nov.) Helge ingstad kollidiert mit der sola ts radar und funkdokumentation. [Online]. Available: https://www.youtube.com/watch?v=sjuKJfYmve8

[40] (2006, Jun.) Færder seilasen with the c-scope radar video extractor. [Online]. Available: https://www.youtube.com/watch?v=G7_dtOEZT7A

[41] B. Ristic, S. Arulampalam, and N. Gordon, *Beyond the Kalman Filter.* MA, USA: Artech House:Norwood, 2004.

[42] D. Daley and D. Vere-Jones, *An Introduction to the Theory of Point Processes, Volume 1: Elementary Theory and Methods.* New York: Springer-Verlag, 2003.

[43] R. Mahler, "An introduction to multisource-multitarget statistics and its applications," Lockheed Martin Technical Monograph, Tech. Rep., Mar. 2000.

[44] ——, *Statistical Multisource-Multitarget Information Fusion.* Artech House, 2007.

[45] ——, "Multi-target bayes filtering via first-order multi-target moments," *IEEE Transaction on Aerospace and Electronic Systems*, vol. 39, no. 4, pp. 1152–1178, 2003.

[46] B. N. Vo and W. K. Ma, "A closed-form solution for the probability hypothesis density filter," in *Information Fusion, 2005 8th International Conference on*, 2005, pp. 856–863.

[47] ——, "The gaussian mixture probability hypothesis density filter," *IEEE Transactions on Signal Processing*, vol. 54, no. 11, pp. 4091–4104, 2006.

[48] M. Yazdian-Dehkordi, Z. Azimifar, and M. AliMasnadi-Shirazi, "Penalized gaussian mixture probability hypothesis density filter for multiple target tracking," *Signal Processing*, vol. 92, 2012.

[49] M. Yazdian-Dehkordi and Z. Azimifar, "Refined gm-phd tracker for tracking targets in possible subsequent missed detections," *Signal Processing*, vol. 116, 2015.

[50] H. Zhang, L. Gao, M. Xu, and Y. Wang, "An improved probability hypothesis density filter for multi-target tracking," *Optik*, vol. 182, 2019.

[51] B. T. Vo, B. N. Vo, and A. Cantoni, "Analytic implementations of the cardinalized probability hypothesis density filter," *IEEE Transactions on Signal Processing*, vol. 55, no. 7, pp. 3553–3567, Jul. 2007.

[52] M. Yazdian-Dehkordi and Z. Azimifar, "Novel n-scan gm-phd-based approach for multi-target tracking," *IET Signal Processing*, vol. 10, no. 5, pp. 493–503, 2016.

[53] K. Panta, D. E. Clark, and B. N. Vo, "Data association and track management for the gaussian mixture probability hypothesis density filter," *IEEE Transactions on Aerospace and Electronic Systems*, vol. 45, no. 3, pp. 1003–1016, Jul. 2009.

[54] K. Panta, B. N. Vo, and S. Singh, "Novel data association schemes for the probability hypothesis density filter," *IEEE Transactions on Aerospace and Electronic Systems*, vol. 43, no. 2, Apr. 2007.

[55] N. Li and X. R. Li, "Target perceivability and its applications," *IEEE Transactions on Signal Processing*, vol. 49, no. 11, 2001.

[56] X. R. Li and Z. Zhao, "Measuring estimator's credibility: Noncredibility index," in *2006 9th International Conference on Information Fusion*, Oct. 2006.

[57] B. Ristic, B. N. Vo, D. Clark, and B. T. Vo, "A metric for performance evaluation of multi-target tracking algorithms," *IEEE Transactions on Signal Processing*, vol. 59, no. 7, pp. 3452–3457, 2008.

[58] S. A. Pasha, B. N. Vo, H. D. Tuan, and W. K. Ma, "A gaussian mixture phd filter for jump markov system models," *IEEE Transactions on Aerospace and Electronic Systems*, vol. 45, no. 3, pp. 919–936, Jul. 2009.

[59] P. Abbeel, A. Coates, M. Montemerlo, A. Y. Ng, and S. Thrun, "Discriminative training of kalman filters," in *In Proceeding Robitics: Science and Systems*, Jun. 2005.

[60] M. Beard, B. T. Vo, and B. N. Vo, "Multi-target filtering with unknown clutter density using a bootstrap gm-cphd filter," *IEEE Signal Processing Letters*, vol. 20, no. 4, pp. 323–326, 2013.

[61] R. Mahler, B. T. Vo, and B. N. Vo, "Cphd filtering with unknown clutter rate and detection profile," *IEEE Transaction on Signal Processing*, vol. 59, no. 8, pp. 3497–3513, 2011.

[62] M. Beard, B. T. Vo, B. N. Vo, and S. Arulampalam, "A partially uniform target birth model for gaussian mixture phd/cphd filtering," *IEEE Transactions on Aerospace and Electronic Systems*, vol. 49, no. 4, pp. 2835–2844, 2013.

[63] M. M. Rana, L. Li, and S. W. Su, "Distributed state estimation over unreliable communication networks with an application to smart grids," *IEEE Transactions on Green Communications and Networking*, vol. 1, no. 1, pp. 89–96, 2017.

[64] ——, "Distributed state estimation of smart grids with packet losses," *Asian Journal of Control*, vol. 19, no. 4, pp. 1306–1315, 2017.

[65] K. Panta, D. E. Clark, and B. N. Vo, "Data association and track management for the gaussian mixture probability hypothesis density filter," *IEEE Transactions on Aerospace and Electronic Systems*, vol. 45, no. 3, p. 1003–1016, 2009.

[66] P. Dong, Z. Jing, M. Li, and H. Pan, "The variable structure multiple model gm-phd filter based on likely-model set algorithm," in *19th International Conference on Information Fusion Heidelberg*, Jul. 2016.

[67] C. E. Seah and I. Hwang, "State estimation for stochastic linear hybrid systems with continuous-state-dependent transitions: An imm approach," *IEEE Transactions on Aerospace and Electronic Systems*, vol. 45, no. 1, p. 376–392, 2009.

[68] (2015, Apr.) Thousands of passengers have travel plans wrecked by french air traffic controller strike - and they're planning two more walkouts. [Online]. Available: https://www.dailymail.co.uk/news/article-3030019/Three-days-travel-chaos-begins-today-hundreds-flights-cancelled-French-air-traffic-controllers-walking-strike.html

[69] (2019, Apr.) Bigoceandata. [Online]. Available: https://app.bigoceandata.com/map/gmap.aspx

[70] D. J. Struik, *Lectures on Classical Differential Geometry.* MA: Addison-Wesley, 1957.

APPENDICES

A. PROOF OF LEMMA 1 IN CHAPTER 2

For deriving the semi-major and semi-minor axes, we need the equation of ellipsoid in the 3D coordinate, which is given by:

$$\frac{x^2}{a^2} + \frac{y^2}{b^2} + \frac{z^2}{c^2} = 1 \tag{A.1}$$

We can rewrite (A.1) as:

$$F(x, y, z) = \frac{x^2}{a^2} + \frac{y^2}{b^2} + \frac{z^2}{c^2} - 1 = 0 \tag{A.2}$$

The normal to the ellipsoid at (x, y, z) is given by:

$$\vec{N} = \frac{2x}{a^2}\hat{i} + \frac{2y}{b^2}\hat{j} + \frac{2z}{c^2}\hat{k} \tag{A.3}$$

so that the direction cosines of the normal are given by:

$$\cos\delta_x = \frac{x}{a^2 r},\ \cos\delta_y = \frac{y}{b^2 r},\ \cos\delta_z = \frac{z}{c^2 r} \tag{A.4}$$

where $r = \sqrt{\frac{x^2}{a^4} + \frac{y^2}{b^4} + \frac{z^2}{c^4}}$.

The direction cosines for the line of sight are given by:

$$\begin{aligned} \cos\delta_x &= \sin\theta\cos\psi \\ \cos\delta_y &= \sin\theta\sin\psi \\ \cos\delta_z &= \cos\theta \end{aligned} \tag{A.5}$$

where θ and ψ are the aspect-angle of the ellipsoid given in its own (or local) coordinate system. Then, the specular point (x_s, y_s, z_s) can be obtained (A.3):

$$\begin{aligned} x_s &= \frac{a^2}{p}\sin\theta\cos\psi \\ y_s &= \frac{b^2}{p}\sin\theta\cos\psi \\ z_s &= \frac{c^2}{p}\cos\theta \end{aligned} \tag{A.6}$$

where $p = \sqrt{a^2 \sin^2\theta \cos^2\psi + b^2 \sin^2\theta \sin^2\psi + c^2 \cos^2\theta}$. We can also rewrite (A.1) as:

$$x = f(y,z) = a\sqrt{1 - \frac{y^2}{b^2} - \frac{z^2}{c^2}} \tag{A.7}$$

where we take only the positive square root. Then, the vector form of (A.7) is given by:

$$\mathbf{x} = \left(a\sqrt{1 - \frac{y^2}{b^2} - \frac{z^2}{c^2}}, y, z\right) \tag{A.8}$$

The radii of curvature at a point are described by [70]:

$$r = \frac{\frac{\delta \mathbf{x}}{\delta y} \times \frac{\delta \mathbf{x}}{\delta z}}{d\mathbf{x} \bullet d\mathbf{x}} \tag{A.9}$$

where

$$d\mathbf{x} = \frac{\delta \mathbf{x}}{\delta y} dy + \frac{\delta \mathbf{x}}{\delta z} dz \tag{A.10}$$

The cross product and dot product are given by:

$$\frac{\delta \mathbf{x}}{\delta y} \times \frac{\delta \mathbf{x}}{\delta z} = \frac{\delta^2 \mathbf{x}}{\delta y^2} \bullet \hat{n} dy^2 + 2\frac{\delta^2 \mathbf{x}}{\delta y \delta z} \bullet \hat{n} dy dz + \frac{\delta^2 \mathbf{x}}{\delta z^2} \bullet \hat{n} dz^2 \tag{A.11}$$

$$d\mathbf{x} \bullet d\mathbf{x} = \frac{\delta \mathbf{x}}{\delta y} \bullet \frac{\delta \mathbf{x}}{\delta y} dy^2 + 2\frac{\delta \mathbf{x}}{\delta y} \bullet \frac{\delta \mathbf{x}}{\delta z} dy dz + \frac{\delta \mathbf{x}}{\delta z} \bullet \frac{\delta \mathbf{x}}{\delta z} dz^2 \tag{A.12}$$

where the unit normal vector at a point $\hat{n}$ is given by:

$$\hat{n} = \frac{\delta \mathbf{x}}{\delta y} \times \frac{\delta \mathbf{x}}{\delta z} = \left(1, \frac{a^2 y}{b^2 x}, \frac{a^2 z}{c^2 x}\right) \tag{A.13}$$

The inverse radii of curvature at a point are given by:

$$r(0) = \frac{b^2 \sqrt{1 + \left((\frac{a}{c})^2 - 1\right)\frac{z^2}{c^2}}}{a} \tag{A.14}$$

$$r(\pi/2) = \frac{c^2 \left[1 + \left((\frac{a}{c})^2 - 1\right)\frac{z^2}{c^2}\right]^{3/2}}{a} \tag{A.15}$$

The radii of curvature at the specular point are obtained from (A.6), (A.14), and (A.15) (assume $\psi = 0$, $b = c$)

$$r_{L,k}(\theta_k) = \frac{a^2}{b}\left[1 + ((\frac{b}{a})^2 - 1)\frac{a^2 \cos^2\theta_k}{a^2 \cos^2\theta_k + b^2 \sin^2\theta_k}\right]^{3/2} \tag{A.16}$$

$$r_{S,k}(\theta_k) = b\sqrt{1 + ((\frac{b}{a})^2 - 1)\frac{a^2 \cos^2\theta_k}{a^2 \cos^2\theta_k + b^2 \sin^2\theta_k}} \tag{A.17}$$

B. ELEMENTS OF OBSERVATION MATRIX OF TARGET DIMENSIONS WITH ASPECT-ANGLE MODEL IN CHAPTER 2

The feature observation matrix of he discrete-time TDA model as follows:

$$H_{f,k} = \begin{bmatrix} \frac{\delta z_{a_k}(\theta_k)}{\delta a_k} & \frac{\delta z_{a_k}(\theta_k)}{\delta b_k} \\ \frac{\delta z_{b_k}(\theta_k)}{\delta a_k} & \frac{\delta z_{b_k}(\theta_k)}{\delta b_k} \end{bmatrix} \tag{B.1}$$

The elements of the feature observation matrix, $H_{f,k}$ are calculated subsequently:

$$\begin{aligned} \frac{\delta z_{a_k}(\theta_k)}{\delta a_k} = &\sqrt{\frac{a_k^2(\frac{b_k^2}{a_k^2}-1)\cos^2\theta_k}{a_k^2\cos^2\theta_k + b_k^2\sin^2\theta_k}+1} - (a_k(\frac{2a_k^3(\frac{b_k^2}{a_k^2}-1)\cos^4\theta_k}{(a_k^2\cos^2\theta_k + b_k^2\sin^2\theta_k)^2} \\ &+\frac{2b_k^2\cos^2\theta_k}{a_k(a_k^2\cos^2\theta_k + b_k^2\sin^2\theta_k)} - \frac{2a_k(\frac{b_k^2}{a_k^2}-1)\cos^2\theta_k}{a_k^2\cos^2\theta_k + b_k^2\sin^2\theta_k})) \\ &/(2\sqrt{\frac{a_k^2(\frac{b_k^2}{a_k^2}-1)\cos^2\theta_k}{a_k^2\cos^2\theta_k + b_k^2\sin^2\theta_k}+1}) \end{aligned} \tag{B.2}$$

$$\begin{aligned} \frac{\delta z_{a_k}(\theta_k)}{\delta b_k} = &(a_k(\frac{2b_k\cos^2\theta_k}{a_k^2\cos^2\theta_k + b_k^2\sin^2\theta_k} - \frac{2a_k^2 b_k(\frac{b_k^2}{a_k^2}-1)\cos^2\theta_k\sin^2\theta_k}{(a_k^2\cos^2\theta_k + b_k^2\sin^2\theta_k)^2})) \\ &/(2\sqrt{\frac{a_k^2(\frac{b_k^2}{a_k^2}-1)\cos^2\theta_k}{a_k^2\cos^2\theta_k + b_k^2\sin^2\theta_k}+1}) \end{aligned} \tag{B.3}$$

$$\begin{aligned} \frac{\delta z_{b_k}(\theta_k)}{\delta a_k} = &(b_k(\frac{2a_k^3(\frac{b_k^2}{a_k^2}-1)\cos^4\theta_k}{(\cos^2\theta_k a_k^2 + \sin^2\theta_k b_k^2)^2} + \frac{2b_k^2\cos^2\theta_k}{a_k(a_k^2\cos^2\theta_k + b_k^2\sin^2\theta_k)} \\ &-\frac{2a_k(\frac{b_k^2}{a_k^2}-1)\cos^2\theta}{a_k^2\cos^2\theta_k + b_k^2\sin^2\theta_k}))/(2(\frac{a_k^2(\frac{b_k^2}{a_k^2}-1)\cos^2\theta_k}{a_k^2\cos^2\theta_k + b_k^2\sin^2\theta_k}+1)^{3/2}) \end{aligned} \tag{B.4}$$

$$\frac{\delta z_{b_k}(\theta_k)}{\delta b_k} = (\frac{a_k^2(\frac{b_k^2}{a_k^2}-1)\cos^2\theta_k}{a_k^2\cos^2\theta_k + b_k^2\sin^2\theta_k}+1)^{-1/2} - (b_k(\frac{2b_k\cos^2\theta_k}{a_k^2\cos^2\theta_k + b_k^2\sin^2\theta}$$
$$-\frac{2a_k^2b_k(\frac{b_k^2}{a_k^2}-1)\cos^2\theta_k\sin^2\theta_k}{(a_k^2\cos^2\theta_k + b_k^2\sin^2\theta)^2}))/(2(\frac{a_k^2(\frac{b_k^2}{a_k^2}-1)\cos^2\theta_k}{a_k^2\cos^2\theta_k + b_k^2\sin^2\theta}+1)^{3/2}) \tag{B.5}$$

C. PROOF OF LEMMA 2 IN CHAPTER 3

Define that A is the event that a target is detected. We assume the detection probability is a constant.

$$P\{A\} = P_D \tag{C.1}$$

Under event $M^l_{T,k}$, the l-th measurement with the NDS $D^{i,l}_k$ is considered as target originated, such that the numbers of true measurements and clutter within the surveillance area are 1 and $T_k - 1$, respectively. Therefore, $f(D^{i,l}_k M^l_{T,k}, T_k)$ can be rewritten as:

$$f(D^{i,l}_k, M^l_{T,k}, T_k) = f(D^{i,l}_k, M^l_{T,k}, T_k, A) \tag{C.2}$$

$$= Pr\{M^l_{T,k}|D^{i,l}_k, T_k, A\} f(D^{i,l}_k|T_k, A) Pr\{T_k|A\} Pr\{A\} \tag{C.3}$$

The first term of (C.2) represents that the $l-1$ false measurements among $T_k - 1$ measurements have the NDS smaller than $D^{i,l}_k$, and the remaining measurements have the larger one. With Assumption 5, we have

$$Pr\{M^l_{T,k}|D^{i,l}_k, T_k, A\} = \binom{T_k - 1}{l - 1}((\frac{D^{i,l}_k}{\gamma})^{\frac{n}{2}})^{l-1}(1 - (\frac{D^{i,l}_k}{\gamma})^{\frac{n}{2}})^{T_k - l} \tag{C.4}$$

From Assumption 5, the second term of (C.2) can be rewritten as follows:

$$f(D^{i,l}_k|T_k, A) = \frac{nV_{D^{i,l}_k}}{2D^{i,l}_k} \mathcal{N}(D^{i,l}_k) U(D^{i,l}_k; (0, \gamma]) \tag{C.5}$$

where V_D is the volume of the ellipsoid with the gate size of $\sqrt{D}$.

Then the third term of (C.2) becomes $Pr\{T_k|A\} = \mu_F(T_k\ -1)$. Thus, we can rewrite the pdf $f(D_k^{i,l}M_{T,k}^l, T_k)$ as follows:

$$f(D_k^{i,l}, M_{T,k}^l, T_k) = \binom{T_k - 1}{l - 1}((\frac{D_k^{i,l}}{\gamma})^{\frac{n}{2}})^{l-1}(1 - (\frac{D_k^{i,l}}{\gamma})^{\frac{n}{2}})^{T_k - l}$$
$$\cdot \mu_F(T_k - 1)\frac{nV_{D_k^{i,l}}}{2D_k^{i,l}}\mathcal{N}(D_k^{i,l})U(D_k^{i,l}; (0, \gamma])P_D \quad \text{(C.6)}$$

D. PROOF OF LEMMA 3 IN CHAPTER 3

Under event $M_{F,k}^l$, the l-th measurement with the NDS $D_k^{i,l}$ is considered as a false measurement. Therefore, $f(D_k^{i,l},\, M_{F,k}^l, T_k)$ can be written as:

$$f(D_k^{i,l}, M_{F,k}^l, T_k) = Pr\{M_{F,k}^l|T_k, D_k^{i,l}\}f(D_k^{i,l}|T_k)Pr\{T_k\} \tag{D.1}$$

Under the three cases and Assumption 5, the first factor of (D.1) can be written as:

$$\begin{aligned} Pr\{M_{F,k}^l|T_k, D_k^{i,l}\} &= Pr\{\text{target is not detected}\} \\ &\quad +Pr\{\text{target is detected but it is not the } l\text{-th measurement}\} \\ &= (1-P_D)f_{c_l}(D_k^{i,l}|T_k) + P_D(1-P_R(D_k^{i,l}))f_{c_l}(D_k^{i,l}|T_k-1) \\ &\quad +P_DP_R(D_k^{i,l})f_{c_{l-1}}(D_k^{i,l}|T_k-1) \end{aligned} \tag{D.2}$$

where

$$f_{c_l}(D_k^{i,l}|T_k) = T_k\binom{T_k-1}{l-1}((\frac{D_k^{i,l}}{\gamma})^{\frac{n}{2}})^{l-1}\frac{n}{2D_k^{i,l}}(\frac{D_k^{i,l}}{\gamma})^{\frac{n}{2}}(1-(\frac{D_k^{i,l}}{\gamma})^{\frac{n}{2}})^{T_k-l} \tag{D.3}$$

Thus, we can rewrite the pdf $f(D_k^{i,l}M_{F,k}^l, T_k)$ as follows:

$$\begin{aligned} f(D_k^{i,l}, M_{F,k}^l, T_k) &= Pr\{\text{target is not detected}\}f(D_k^{i,l}|T_k)Pr\{T_k\} \\ &\quad +Pr\{\text{target is detected but it is not the } l\text{-th measurement}\} \\ &\quad \cdot f(D_k^{i,l}|T_k-1)Pr\{T_k\} \\ &= (1-P_D)f_{c_l}(D_k^{i,l}|T_k)\mu_F(T_k) \\ &\quad +P_D(1-P_R(D_k^{i,l}))f_{c_l}(D_k^{i,l}|T_k-1)\mu_F(T_k-1) \\ &\quad +P_DP_R(D_k^{i,l})f_{c_{l-1}}(D_k^{i,l}|T_k-1)\mu_F(T_k-1) \end{aligned} \tag{D.4}$$

E. PROOF OF LEMMA 4 IN CHAPTER 3

The prior error covariance of the i-th Gaussian component conditioned on event $M^l_{F,k}$ is given by:

$$\begin{aligned}
\hat{P}^{i,l}_{k|k-1,M^l_{F,k}} &\triangleq E[\bar{x}^i_{k|k-1}(\bar{x}^i_{k|k-1})^T|Z^{k-1}, M^l_{F,k}] \\
&= \int \bar{x}^i_{k|k-1}(\bar{x}^i_{k|k-1})^T p(\bar{x}^i_{k|k-1}|M^l_{F,k})d\bar{x}^i_{k|k-1} \\
&= \int [\int \bar{x}^i_{k|k-1}(\bar{x}^i_{k|k-1})^T \mathcal{N}(\bar{x}^i_{k|k-1}; K^i_k\nu^{i,l}_k, P^{i,*}_k)d\bar{x}^i_{k|k-1}] \\
&\qquad\qquad \cdot p(\nu^{i,l}_k|M^l_{F,k})d\nu^{i,l}_k \\
&= P^{i,*}_k + K^i_k[\int \nu^{i,l}_k(\nu^{i,l}_k)^T p(\nu^{i,l}_k|M^l_{F,k})d\nu^{i,l}_k](K^i_k)^T
\end{aligned} \tag{E.1}$$

The last equation in (E.1) is based on Assumption 5 that $\nu^{i,l}_k$ is uniformly distributed in the surveillance region and independent of the state of the true target. Under event $M^l_{F,k}$, the l-th measurement with the NDS $D^{i,l}_k$ is not target-originated. The pdf of

$D_k^{i,t}$, the NDS of the target-originated measurement conditioned on event $M_{F,k}^l$ and T_k are needed. In order to derive $p(\nu_k^{i,l}|M_{F,k}^l)$, we first compute

$$\begin{aligned} p(D_k^{i,t}|D_k^{i,l}, M_{F,k}^l, T_k) = \frac{p(D_k^{i,t}, D_k^{i,l}, M_{F,k}^l, T_k)}{p(D_k^{i,l}, M_{F,k}^l, T_k)} \\ = \frac{(1-P_D U(\gamma - D_k^{i,t}))f_{c_l}(D_k^{i,l}|T_k)}{(1-P_D)f_{c_l}(D_k^{i,l}|T_k)} \\ \frac{nV_{D_k^{i,t}}\mathcal{N}(D_k^{i,t})\mu_F(T_k)U(D_k^{i,l})U(\gamma - D_k^{i,l})}{2D_k^{i,t}\mu_F(T_k)} \\ \frac{+P_D(U(\gamma - D_k^{i,t}) - U(D_k^{i,l} - D_k^{i,t}))f_{c_l}(D_k^{i,l}|T_k - 1)}{+P_D(1-P_R(D_k^{i,l}))f_{c_l}(D_k^{i,l}|T_k - 1)} \\ \frac{\mu_F(T_k - 1)U(D_k^{i,l})}{\mu_F(T_k - 1)} \\ \frac{+P_D U(D_k^{i,l} - D_k^{i,t})f_{c_{l-1}}(D_k^{i,l}|T_k - 1)}{+P_D P_R(D_k^{i,l})f_{c_{l-1}}(D_k^{i,l}|T_k - 1)} \\ \frac{\mu_F(T_k - 1)U(\gamma - D_k^{i,l})}{\mu_F(T_k - 1)} \end{aligned} \tag{E.2}$$

With this pdf, we can rewrite the error covariance as follows:

$$\begin{aligned} &\hat{P}_{k|k-1,M_{F,k}^l}^{i,l} \\ &= P_k^{i,*} + K_k^i \int \nu_k^{i,l}(\nu_k^{i,l})^T p(\nu_k^{i,l}|M_{F,k})d\nu_k^{i,l}(K_k^i)^T \\ &= P_k^{i,*} + K_k^i \int D_k^{i,t}(D_k^{i,t})^T p(D_k^{i,t}|M_{F,k})\frac{2D_k^{i,t}}{nV_{D_k^{i,t}}}dD_k^{i,t}(K_k^i)^T \\ &= P_k^{i,*} + K_k^i \int D_k^{i,t}(D_k^{i,t})^T p(D_k^{i,t}|D_k^{i,t}, M_{F,k}, m)\frac{2D_k^{i,t}}{nV_{D_k^{i,t}}}dD_k^{i,t}(K_k^i)^T \\ &= \hat{P}_{k|k-1}^i + \alpha_k^{i,l}K_k^i S_k^i (K_k^i)^T \end{aligned} \tag{E.3}$$

Here, $\alpha_k^{i,l}$ is computed as:

$$\begin{aligned} \alpha_k^{i,l} = \frac{\lambda(1-P_D C_T)V_{D_k^{i,l}}(V_G - V_{D_k^{i,l}})}{\lambda(1-P_D)V_{D_k^{i,l}}(V_G - V_{D_k^{i,l}})} \\ \frac{+P_D(C_T - P_R(D_k^{i,l})C_T(D_k^{i,l}))(T_k - l)V_{D_k^{i,l}}}{+P_D(1-P_R(D_k^{i,l}))(T_k - l)V_{D_k^{i,l}}} \\ \frac{+P_D P_R(D^{i,l})C_T(D_k^{i,l})(l-1)(V_G - V_{D_k^{i,l}})}{+P_D P_R(D_k^{i,l})(l-1)(V_G - V_{D_k^{i,l}})} \end{aligned} \tag{E.4}$$

Based on the prior covariance conditioned on event $M^l_{F,k}$, the posterior covariance conditioned on event $M^l_{F,k}$ can be derived as:

$$\begin{aligned}
\hat{P}^{i,l}_{k|k,M^l_{F,k}} &= E[\tilde{x}^i_{k|k}(\tilde{x}^i_{k|k})^T|M^l_{F,k},T_k,Z^k] \\
&= E[(\bar{x}^i_{k|k-1} - K^i_k\nu^{i,l}_k)(\bar{x}^i_{k|k-1} - K^i_k\nu^{i,l}_k)^T|M^l_{F,k},T_k,Z^k,\nu^{i,l}_k] \\
&= E[\bar{x}^i_{k|k-1}(\bar{x}^i_{k|k-1})^T|M^l_{F,k},T_k,\nu^{i,l}_k] - K^i_k\nu_k E[(\bar{x}^i_{k|k-1})^T|M^l_{F,k},\nu^{i,l}_k] \\
&\qquad -E[\bar{x}^i_{k|k-1}|M^l_{F,k},\nu^{i,l}_k](\nu^{i,l}_k)^T(K^i_k)^T + K^i_k\nu^{i,l}_k(\nu^{i,l}_k)^T(K^i_k)^T \\
&= \hat{P}^i_{k|k-1,M^l_{F,k}} - K^i_k\nu^{i,l}_k(\nu^{i,l}_k)^T(K^i_k)^T
\end{aligned} \tag{E.5}$$

VITA

VITA

Dohyeung Kim received the B.S. and M.S. degree in Electrical and Electronic engineering from Hanyang University, Korea, in 2004 and 2006, respectively. He was with LIGNex1, Youngin, Korea, where from 2007 to 2009 he worked as a research engineer. From 2011 to 2014, he was a senior research engineer at Electronics and Telecommunications Research Institute, Daejeon, Korea, where from 2007 to 2009. He is currently a Ph.D. student in the School of Aeronautics and Astronautics at Purdue University, West Lafayette, IN. His research interests are signal processing, multi-target tracking, and data fusion.